

Stanford S. and Beverly P. Penner Lecture
Department of Mechanical and Aerospace Engineering
University of California, San Diego
16 January 2015

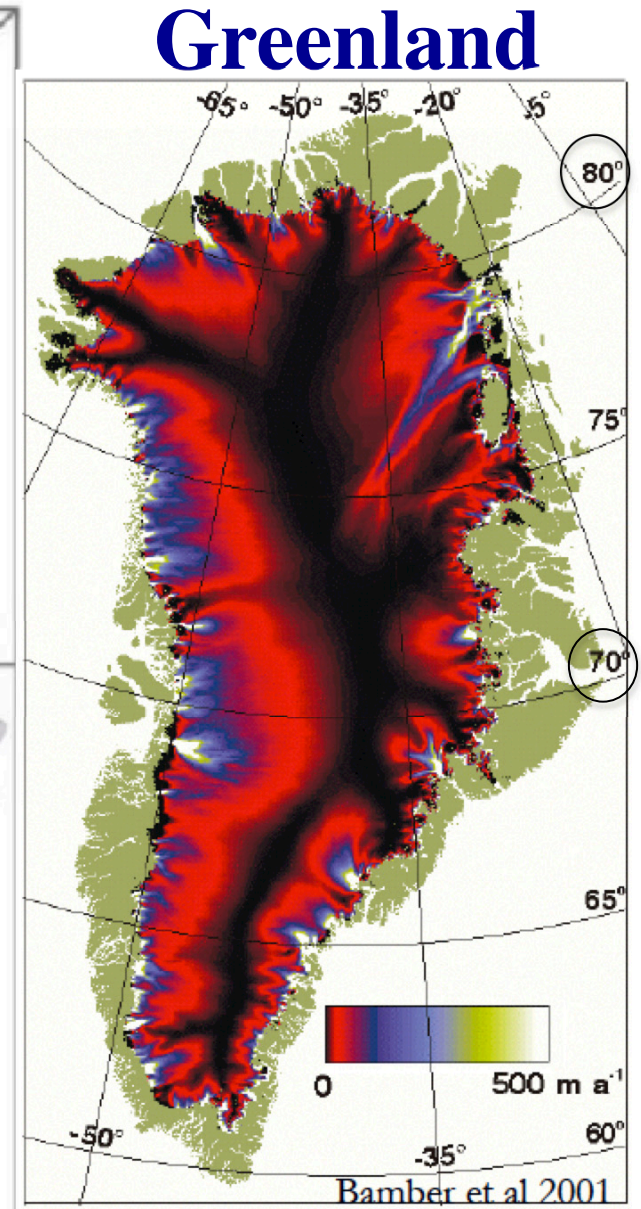
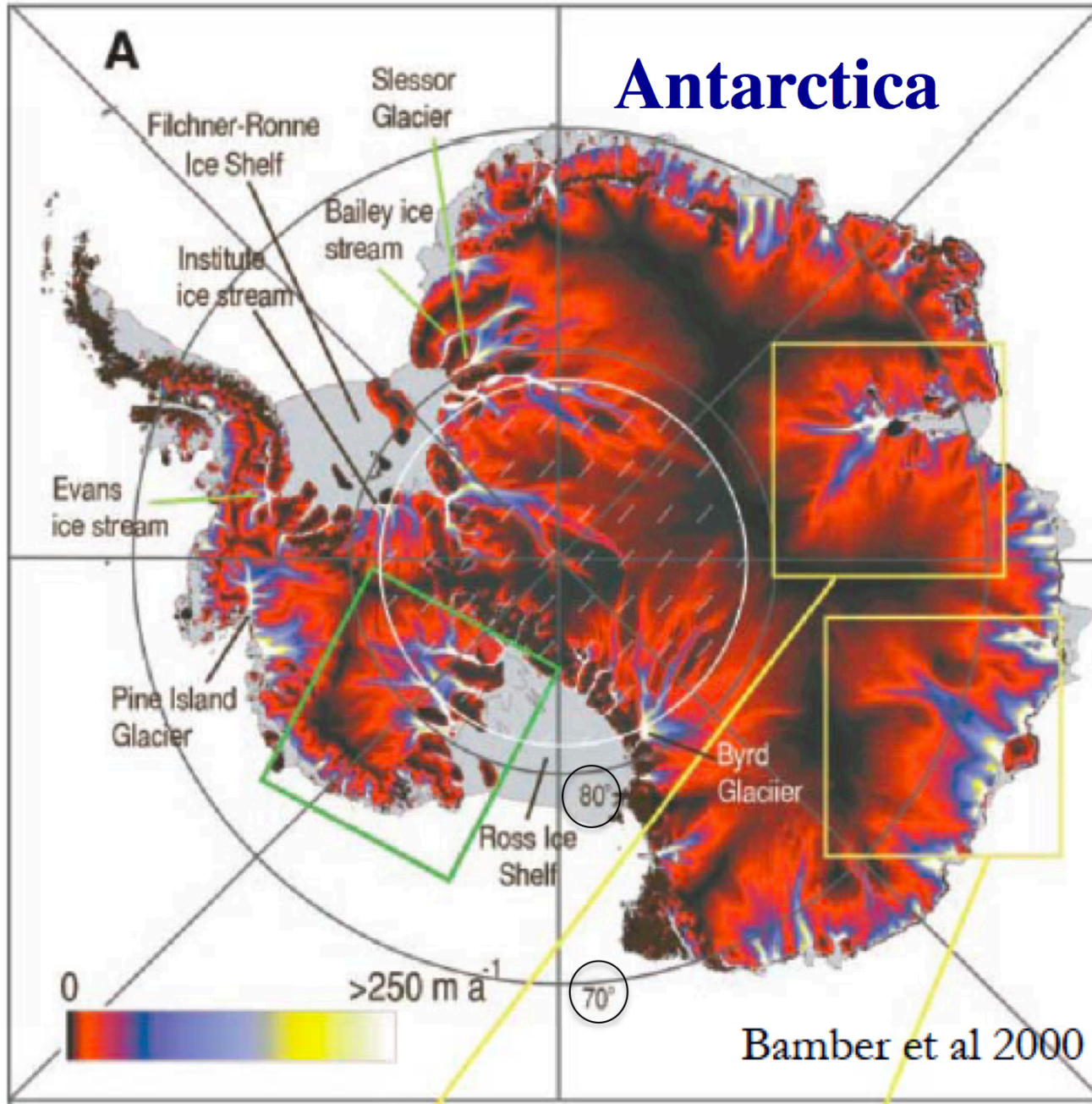
Mechanics on the Great Ice Sheets

James R. Rice (Harvard)

Collaborators:

***Victor C. Tsai (Caltech), Thibaut Perol (Harvard),
John D. Platt (Carnegie Inst.), Jenny Suckale (Stanford),
Matheus C. Fernandes (Harvard), Colin R. Meyer (Harvard)***

The major ice sheets - *not to scale (reduce Greenland)*



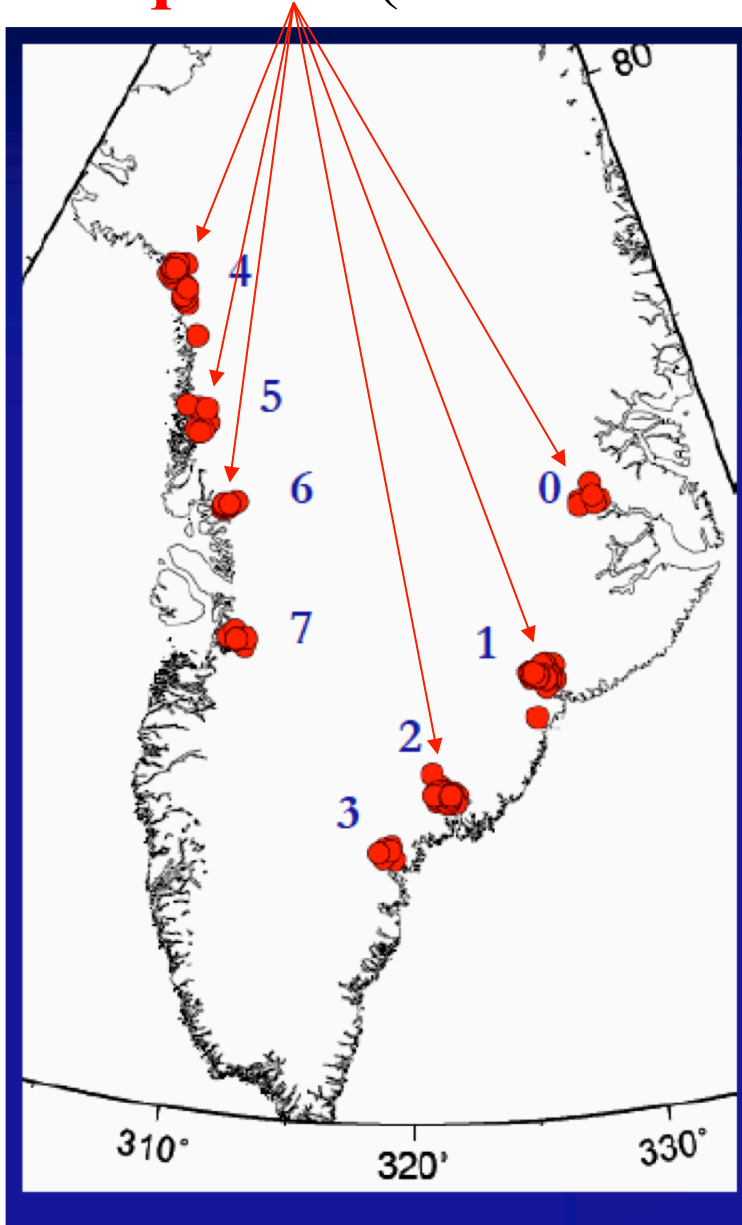
Greenland Ice Sheet:

*Glacial Earthquakes (discovered and
located by Göran Ekström), and
their unexpected mechanism*

with

Victor C. Tsai (Caltech)

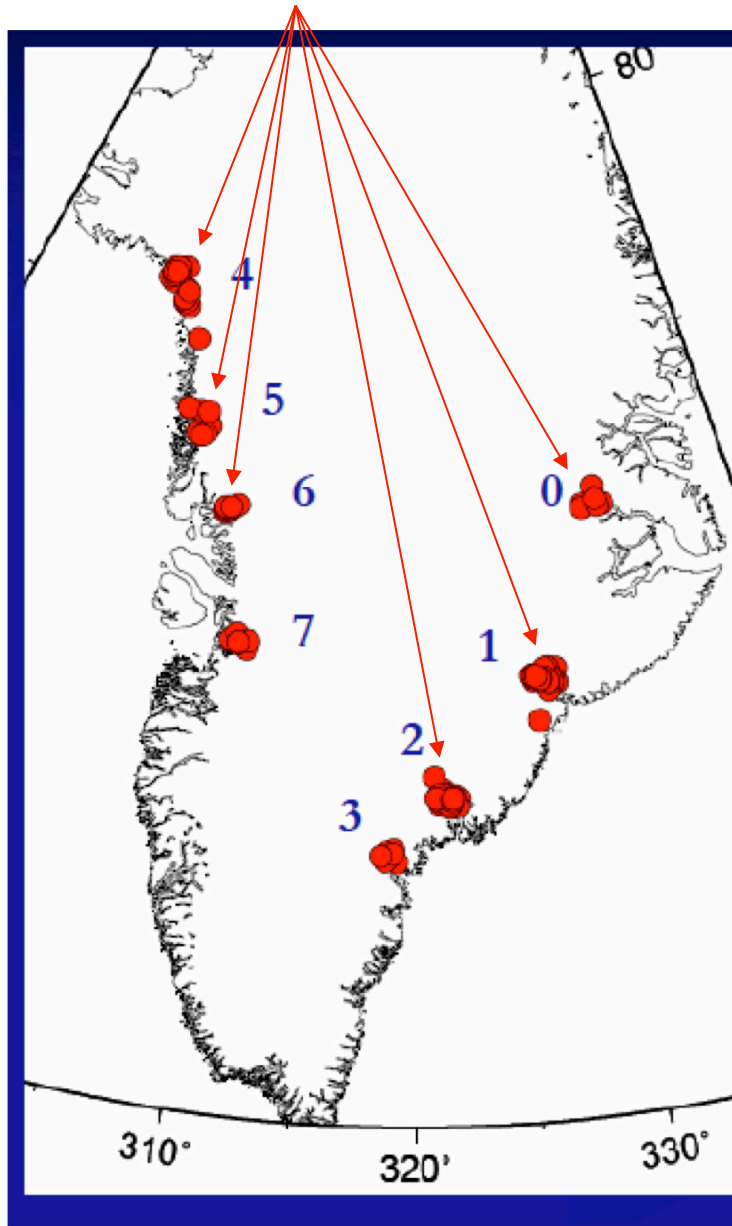
Source locations of **glacial earthquakes** (G. Ekström)



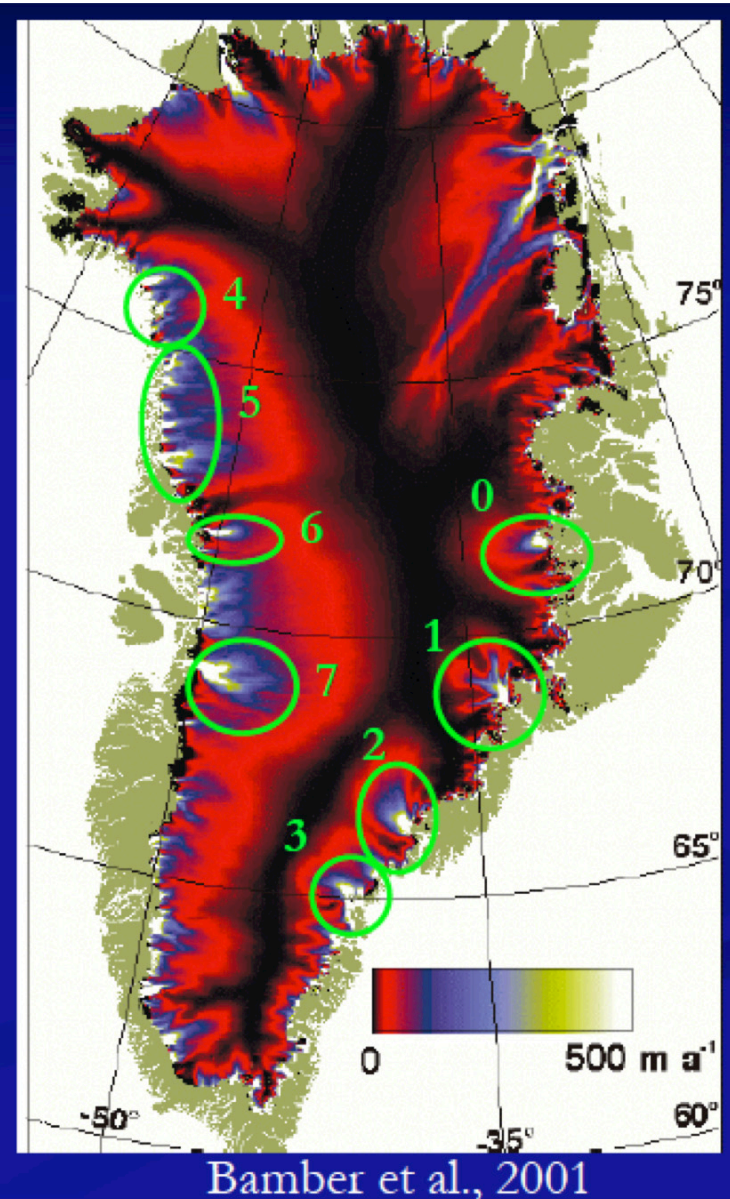
Unusual earthquakes:

- Magnitude $M_{SW} \sim 4.6$ to 5.1, measured at 35-150 sec periods; significant energy in periods between 20 and 100 sec (much longer than for standard earthquakes of similar M_S).
- Distant seismic wave patterns consistent with applying a horizontal point impulse + I followed, after \sim tens of seconds to minute, by $-I$ at shallow source location.

Source locations of **glacial earthquakes** (G. Ekstrom)

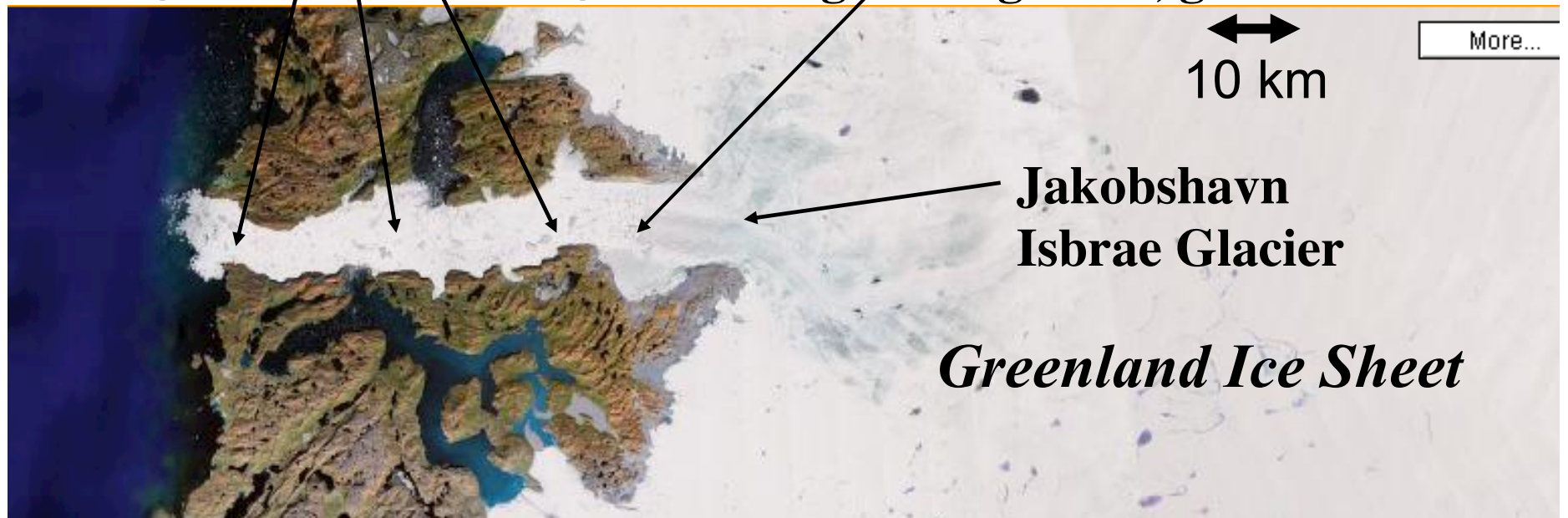


Correlation with areas of high ice flow rates -- at major fjords



Melange of calved icebergs

Iceberg calving front, glacier terminus



**Jakobshavn
Isbrae Glacier**

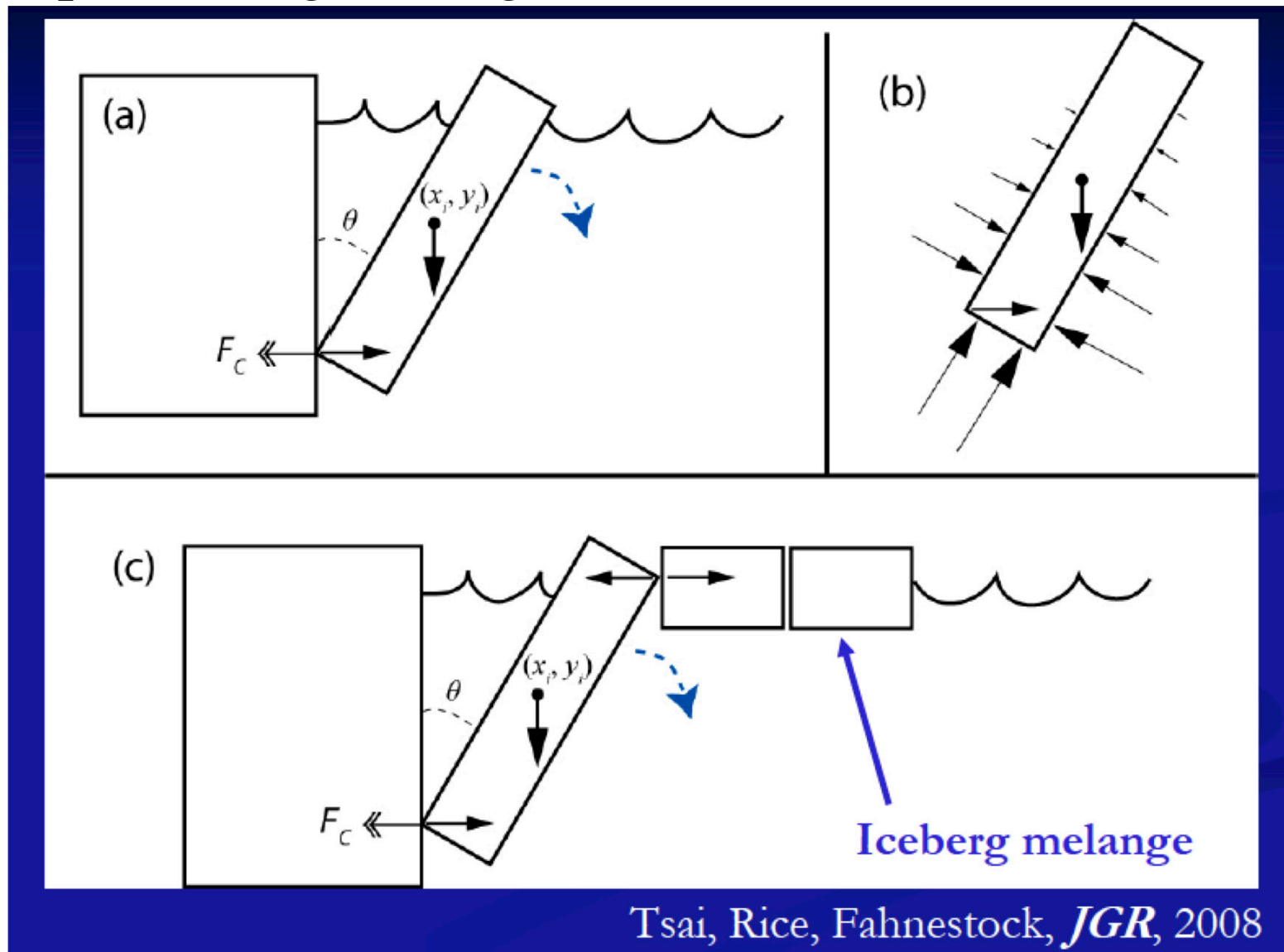
Greenland Ice Sheet



~10 km

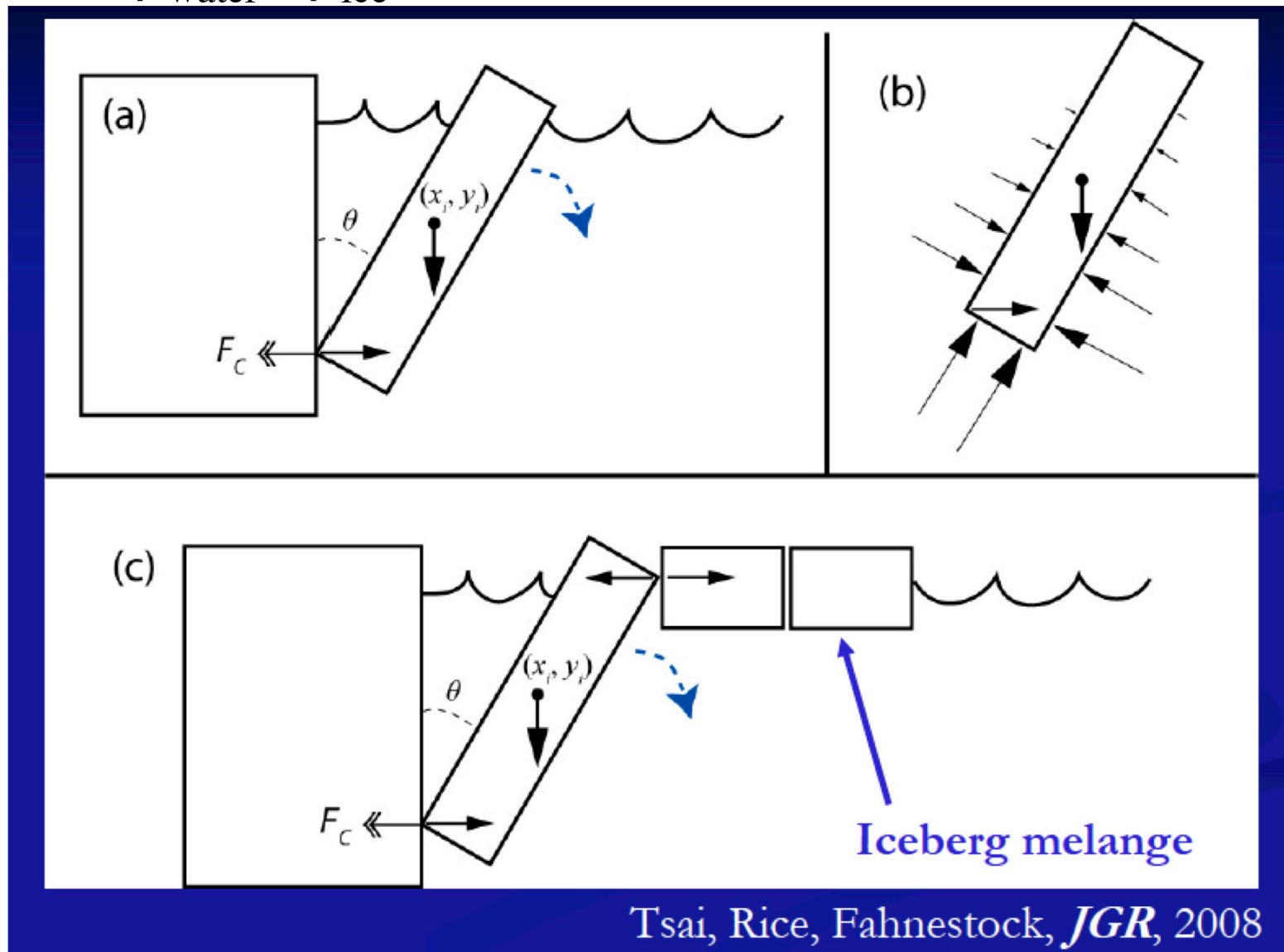
What causes glacial EQs?

- Fast sliding at bed of ice sheet? -- analogous to normal EQs.
- Simple iceberg calving models work best! -- timescale.

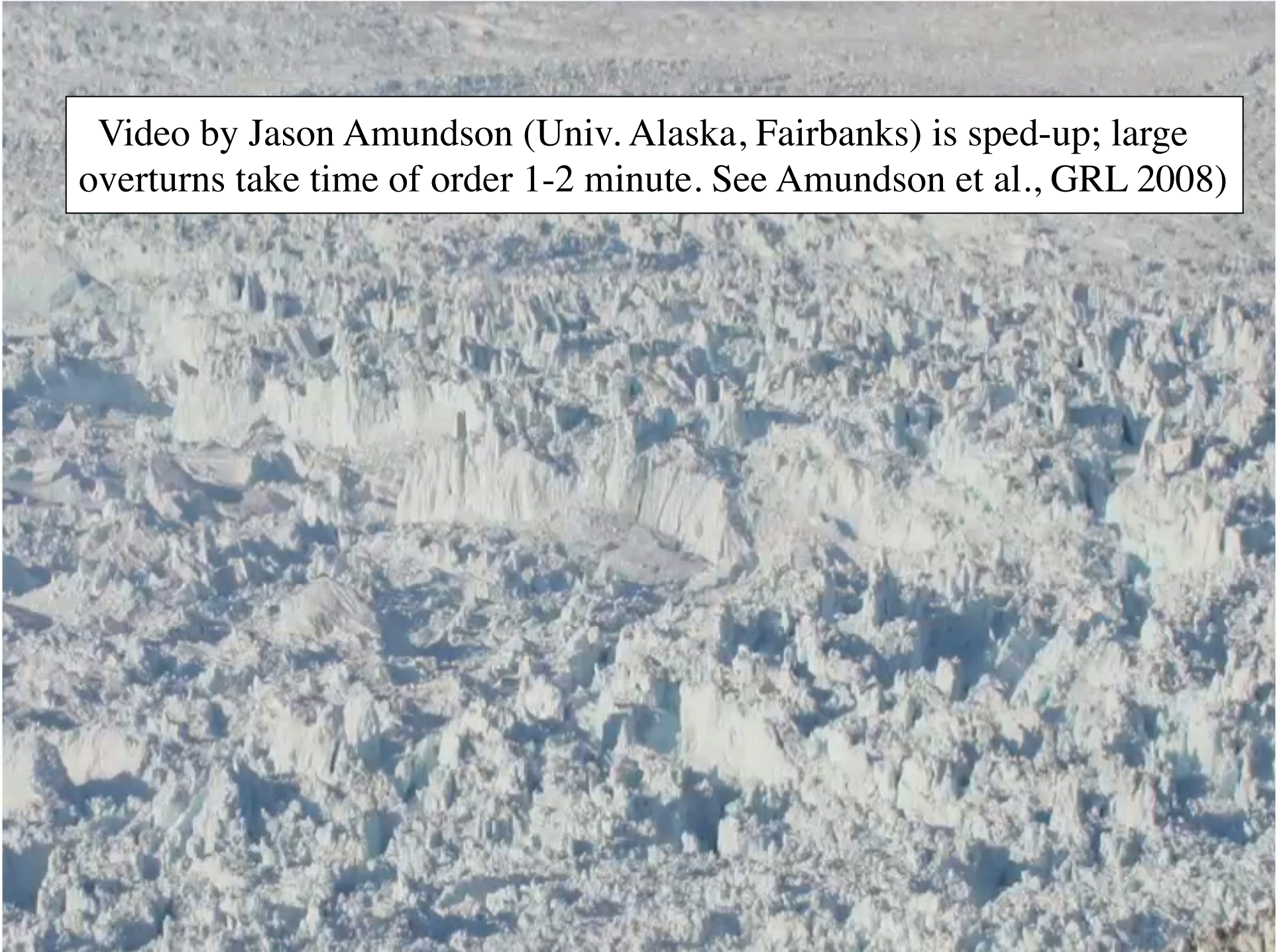


Long period of calved block turnover, because:

1. Long pendulum period (size scale large);
2. Small gravity drive, $\rho_{\text{water}} \sim \rho_{\text{ice}}$;
3. Mélange adds to effective mass.



Video by Jason Amundson (Univ. Alaska, Fairbanks) is sped-up; large overturns take time of order 1-2 minute. See Amundson et al., GRL 2008)



Greenland Ice Sheet:

*Rapidly draining surficial lakes
and natural hydraulic fractures*

Principally with

Victor C. Tsai (Caltech),

with further contributions by

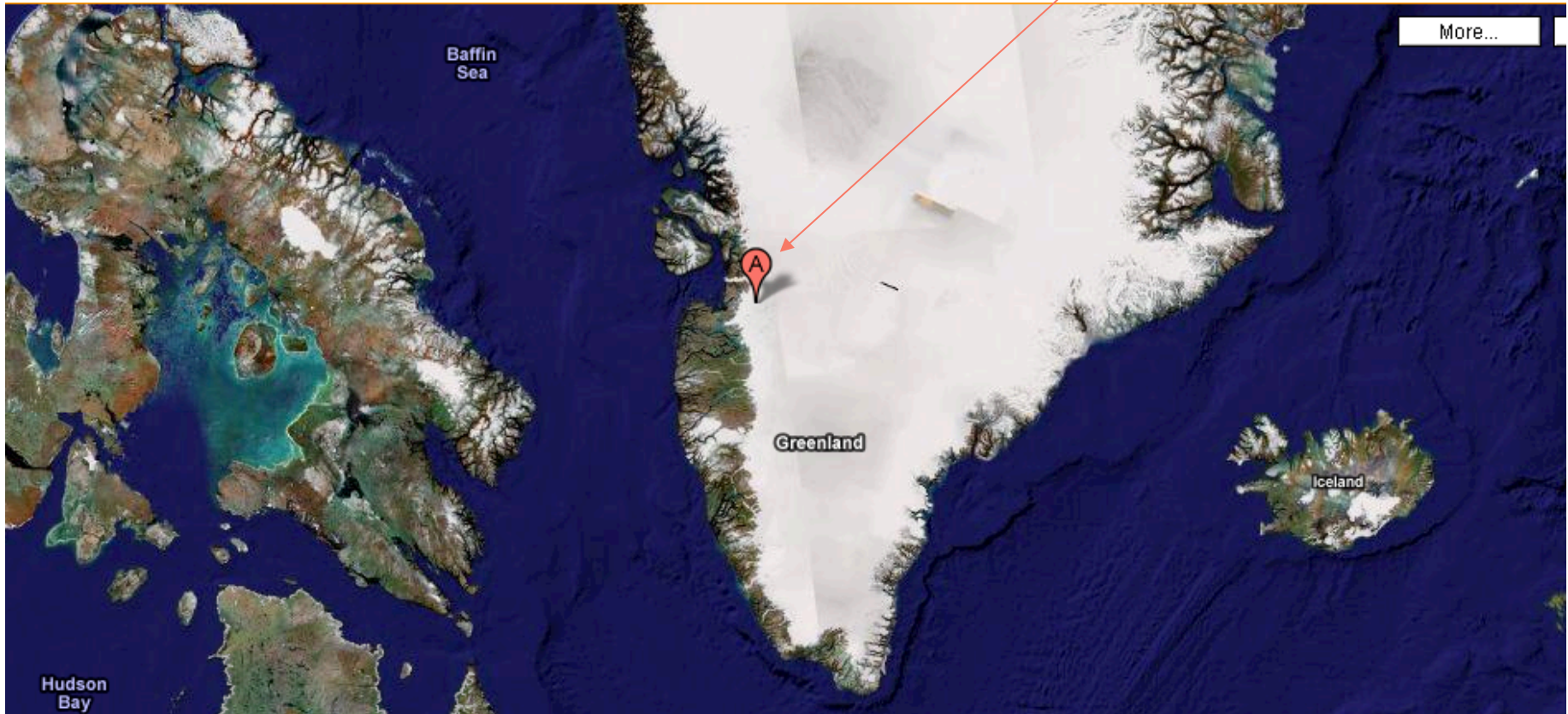
Matheus C. Fernandes (Harvard)

and

John D. Platt (Carnegie Inst.)

A natural hydraulic fracture of interest for evaluating scenarios of accelerated deglaciation

**Where are we?
A below**



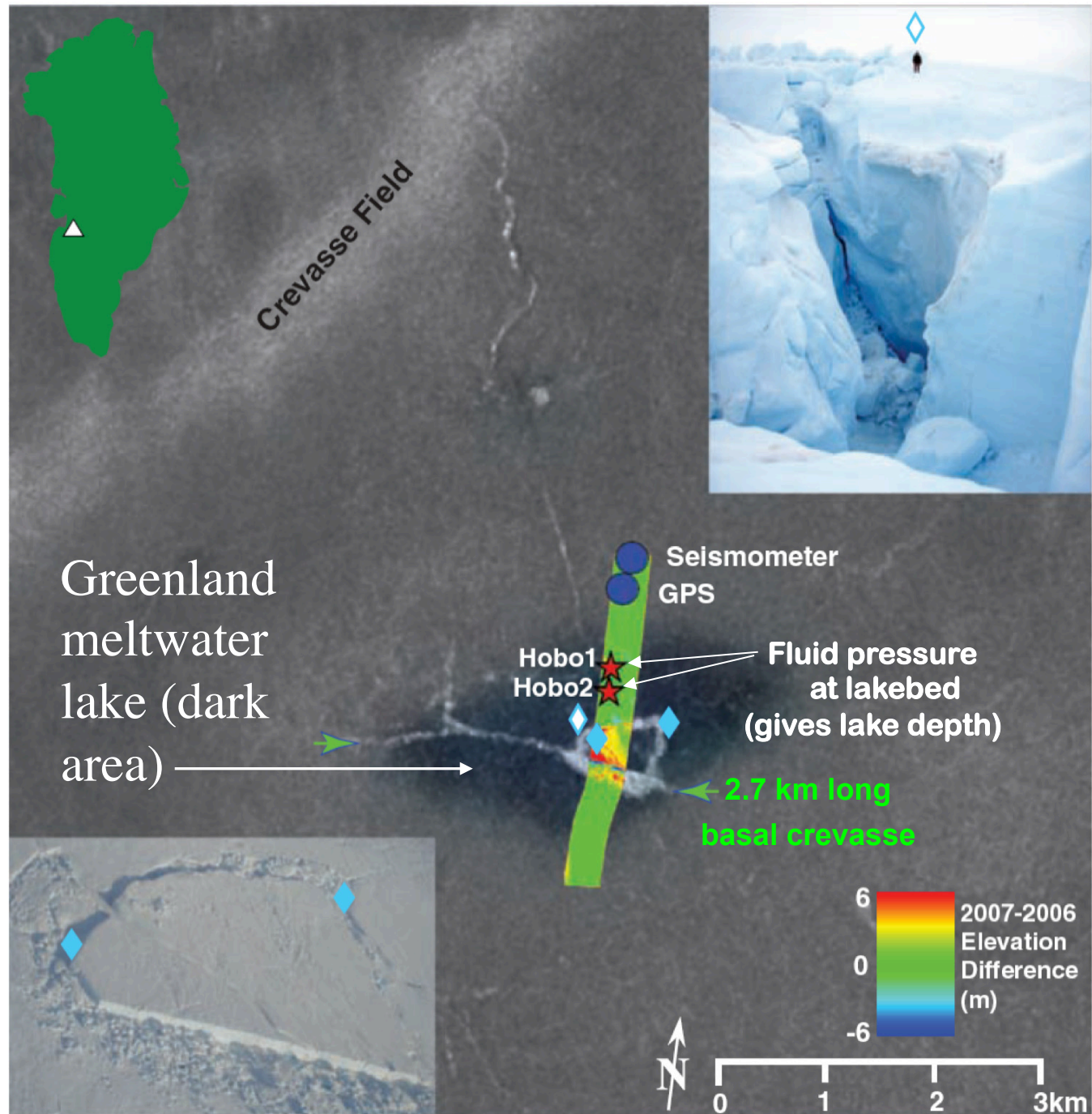
Study motivated by the paper *Fracture Propagation to the Base of the Greenland Ice Sheet During Supraglacial Lake Drainage*, by Das, Joughin, Behn, Howat, King, Lizarralde & Bhatia, *Science*, May 2008.



Study motivated by the paper *Fracture Propagation to the Base of the Greenland Ice Sheet During Supraglacial Lake Drainage*, by Das, Joughin, Behn, Howat, King, Lizarralde & Bhatia, *Science*, May 2008.

(Das et al.,
Sci., 2008)

Early October 2006
SAR image (gray-
scale background)
overlaid with a
semi-transparent
image recorded by
NASA's Moderate
Resolution Imaging
Spectroradiometer
(MODIS) showing
the lake extent
(blue) on 29 July
2006.

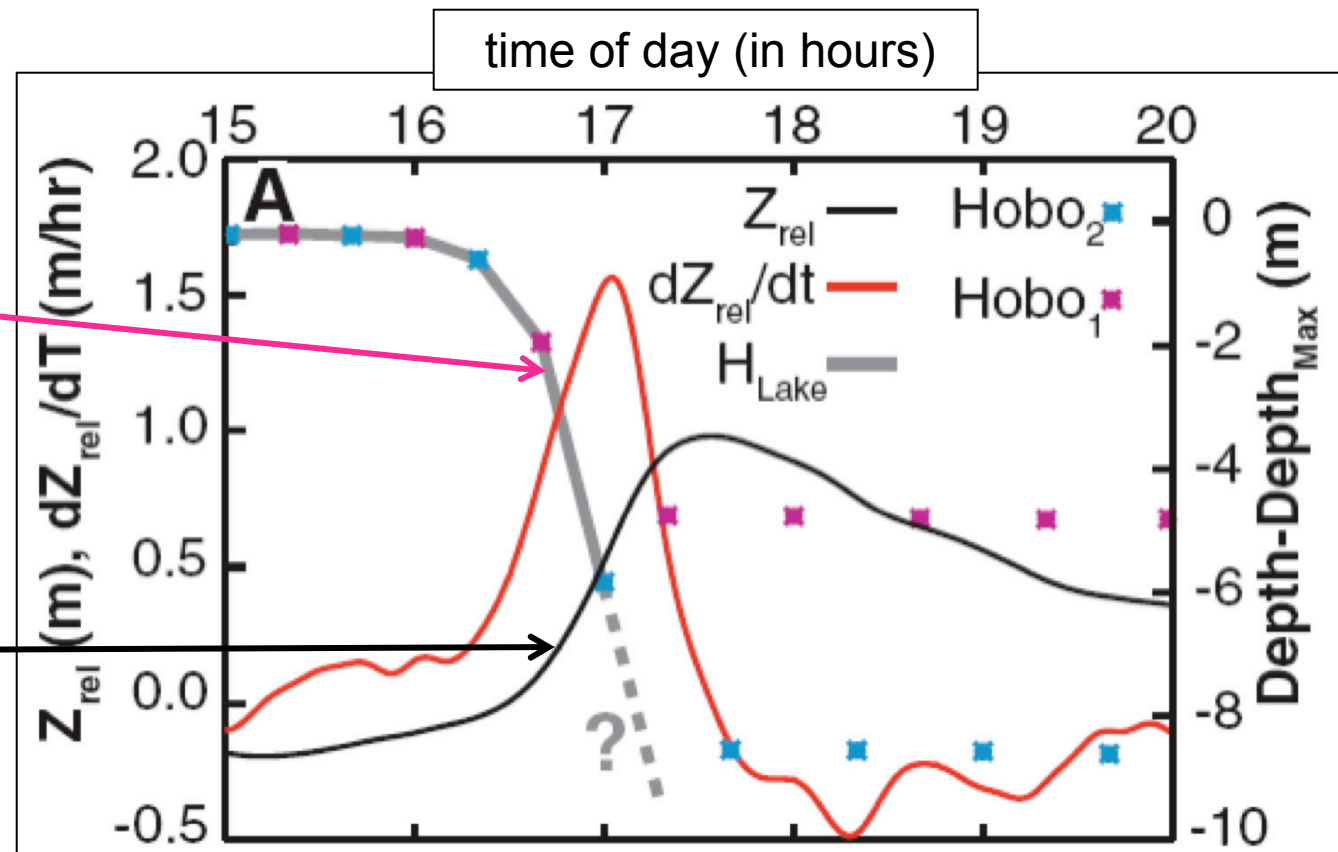


- *Supraglacial meltwater lake* began filling July 2006
- Maximum ~0:00 29 July 2006, Vol. = $44 \times 10^6 \text{ m}^3$, Surf. = 5.6 km^2
- Level slowly/steadily falls, 15 mm/hr
- Rapid from 16:00-17:30, max 12 m/hr ($Q > 10,000 \text{ m}^3/\text{s}$),
avg $Q \sim 8,700 \text{ m}^3/\text{s}$ [Compare, Niagra Falls $Q \sim 6,000 \text{ m}^3/\text{s}$]

(Das et al.,
Sci., 2008)

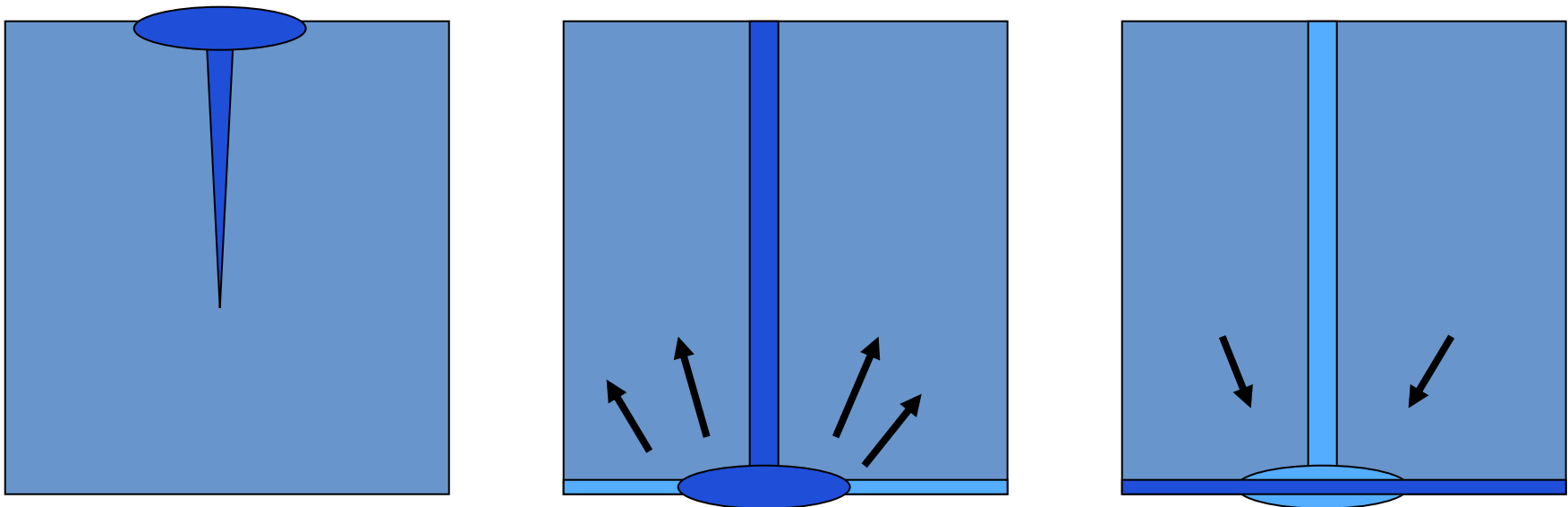
Falling
lake level
[m]
(right scale)

Ice surface
uplift [m]
(left scale)



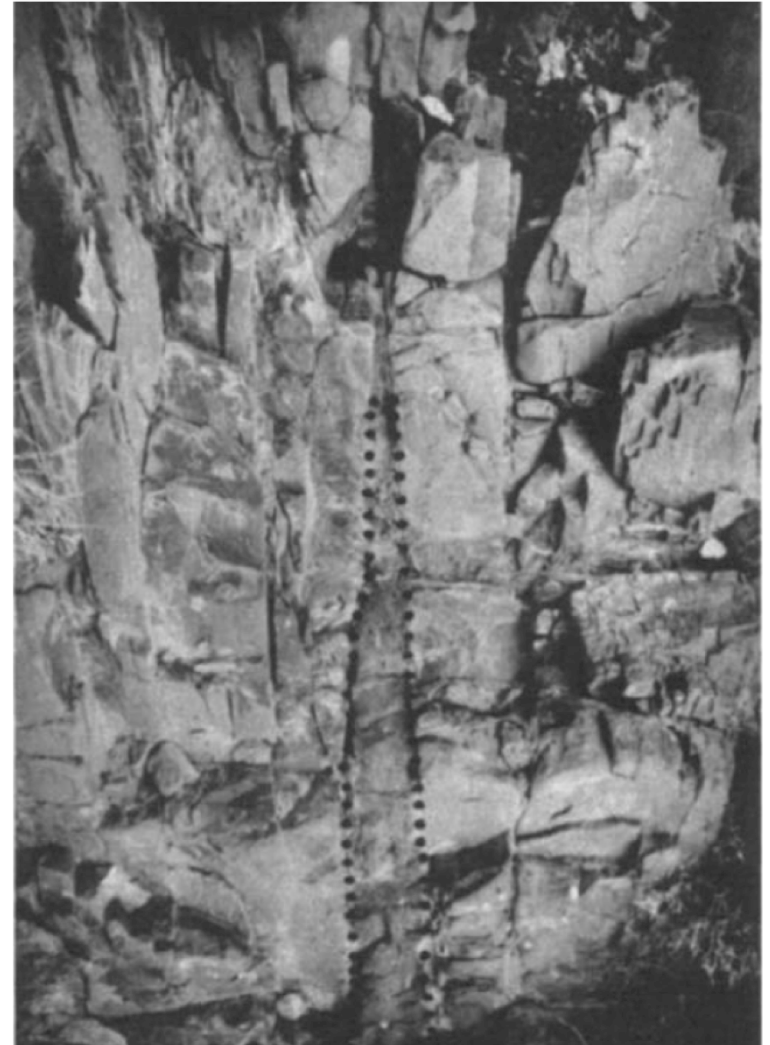
Interpretation

- Initially: Crevasse/moulin system gradually propagates to bed by *Weertman* gravitational instability, $\rho_{water} > \rho_{ice}$.
- Middle Stage: Hydraulic cracking and flooding along bed by over-pressure, $p > \sigma_o$ (σ_o = ice overburden pressure).
- End: Fracture closes, subglacial water layer drains.



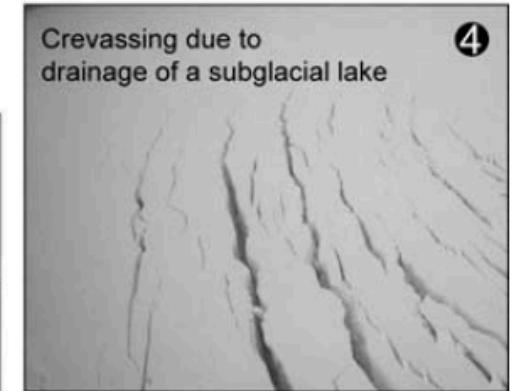
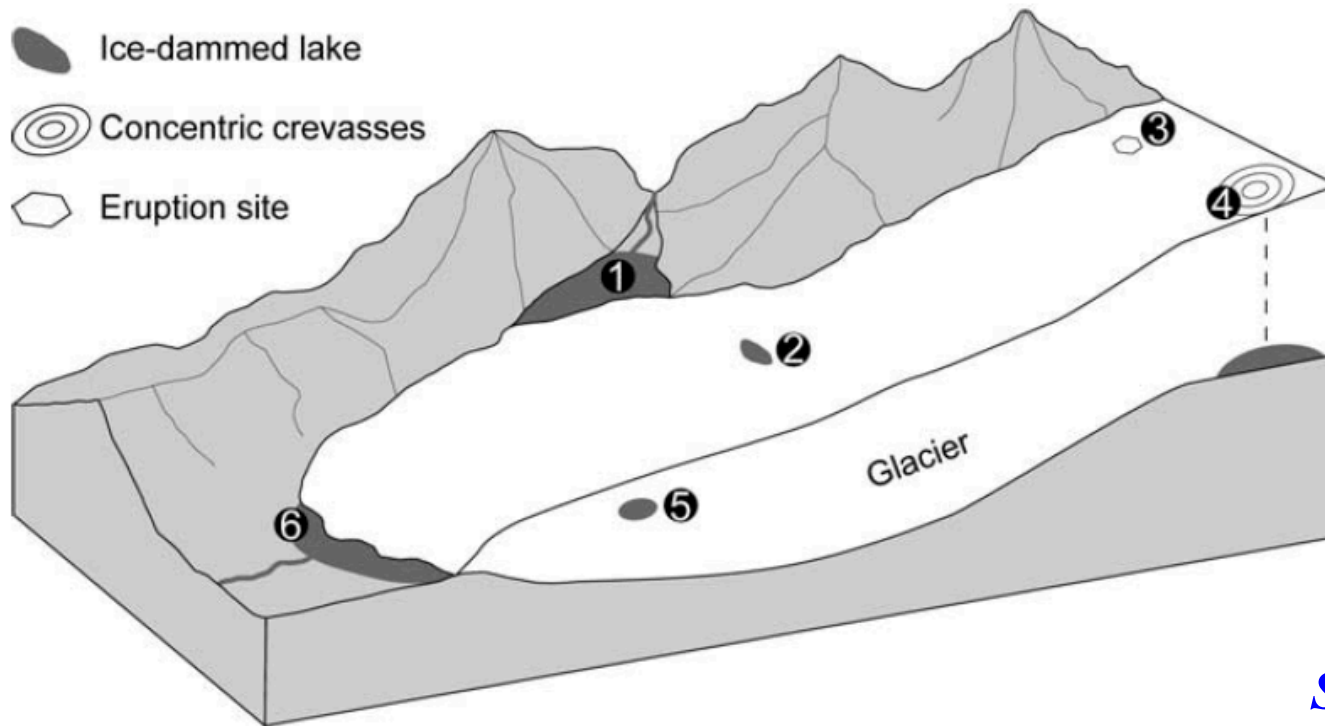
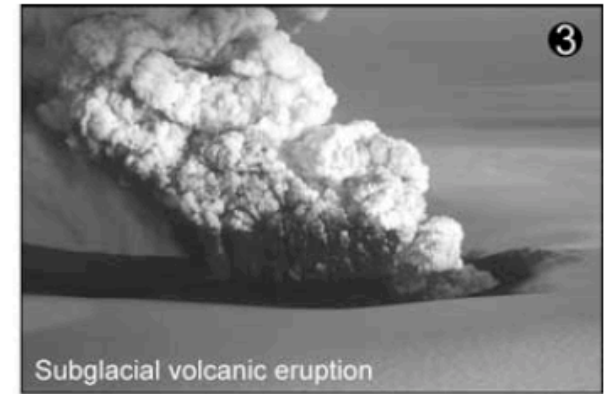
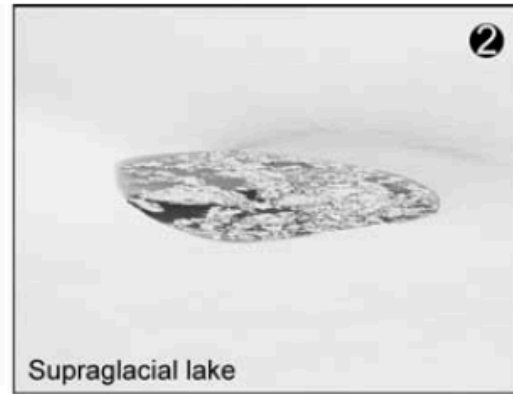
Rubin, ***Propagation of magma-filled cracks*** [Annu. Rev. Earth Planet. Sci., 1995]

$$\rho_{\text{magma}} < \rho_{\text{rock}}$$



Basaltic dike at tip of Reykjanes Peninsula, southwest Iceland, exposed by glacial erosion (did not make it to surface). Thickness = 40 cm.

Dike (boundaries dotted) terminating in shear zone on Colorado Plateau.



**Other scenarios:
Sub-Glacial Flooding
(Jökulhlaup)**

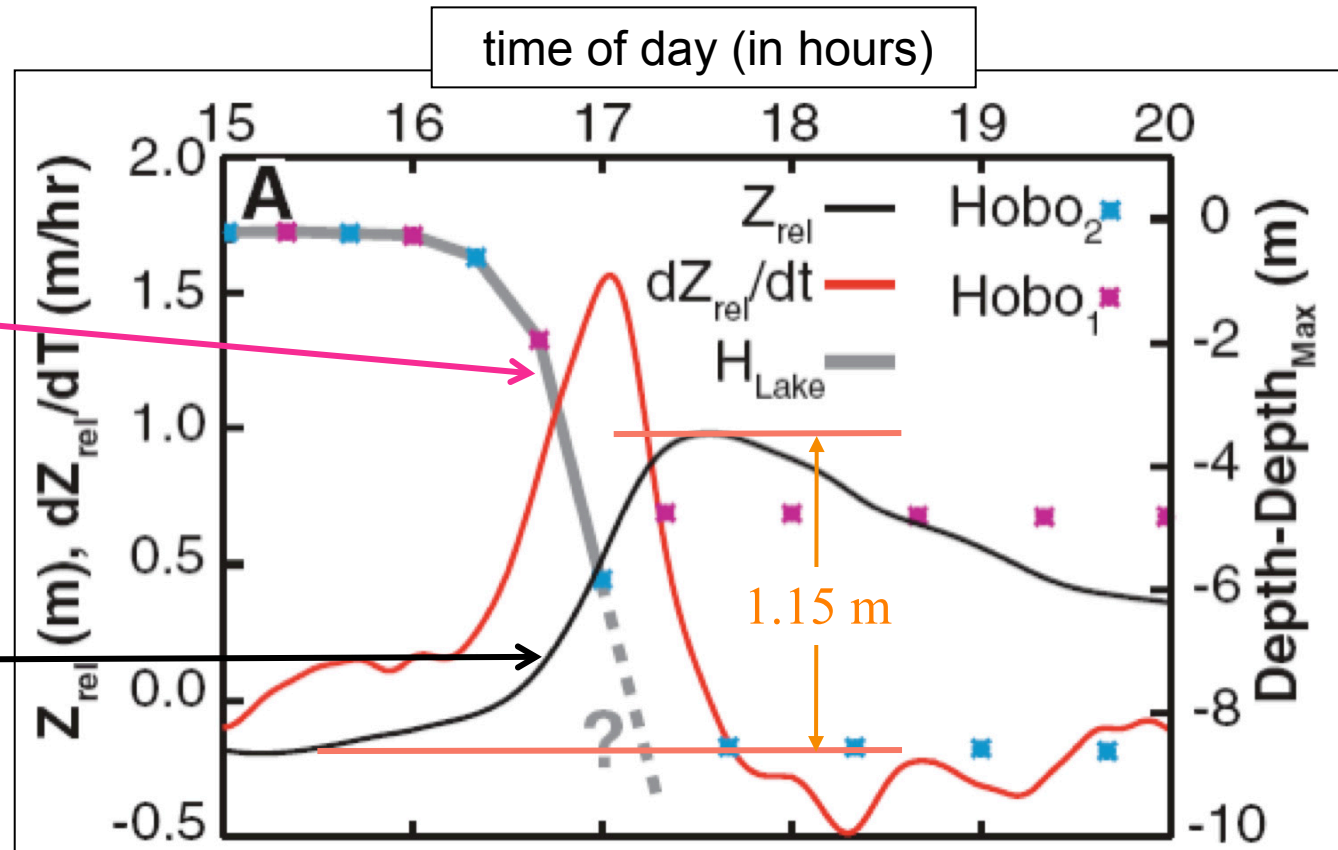
Figure 1. Reservoir sites and meltwater sources for jökulhlaups.

from: Roberts, M. J. (2005), Jökulhlaups: A reassessment of floodwater flow through glaciers, *Rev. Geophys.*, 43, RG1002.

(Das et al.,
Sci., 2008)

Falling
lake level
[m]
(right scale)

Ice surface
uplift [m]
(left scale)



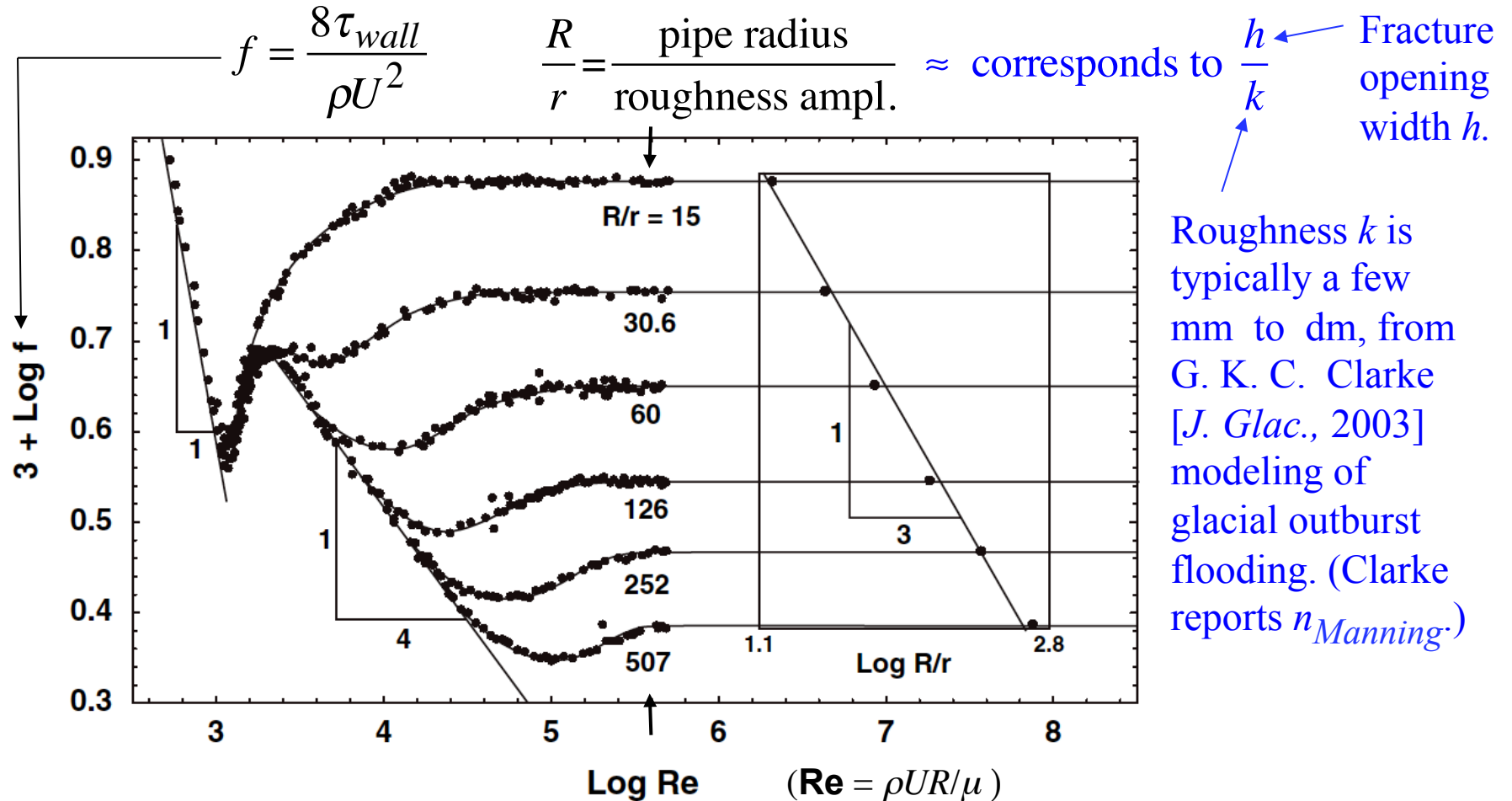
Approximate radius R of sub - glacial fracture at full lake discharge :

$$\pi R^2 \times \text{Uplift of } 1.15 \text{ m} = \text{Lake volume of } 44 \times 10^6 \text{ m}^3 \Rightarrow R \approx 3.5 \text{ km}$$

$$\Rightarrow \text{Average growth speed} \approx R / 1.2 \text{ hr} \approx 3 \text{ km / hr}$$

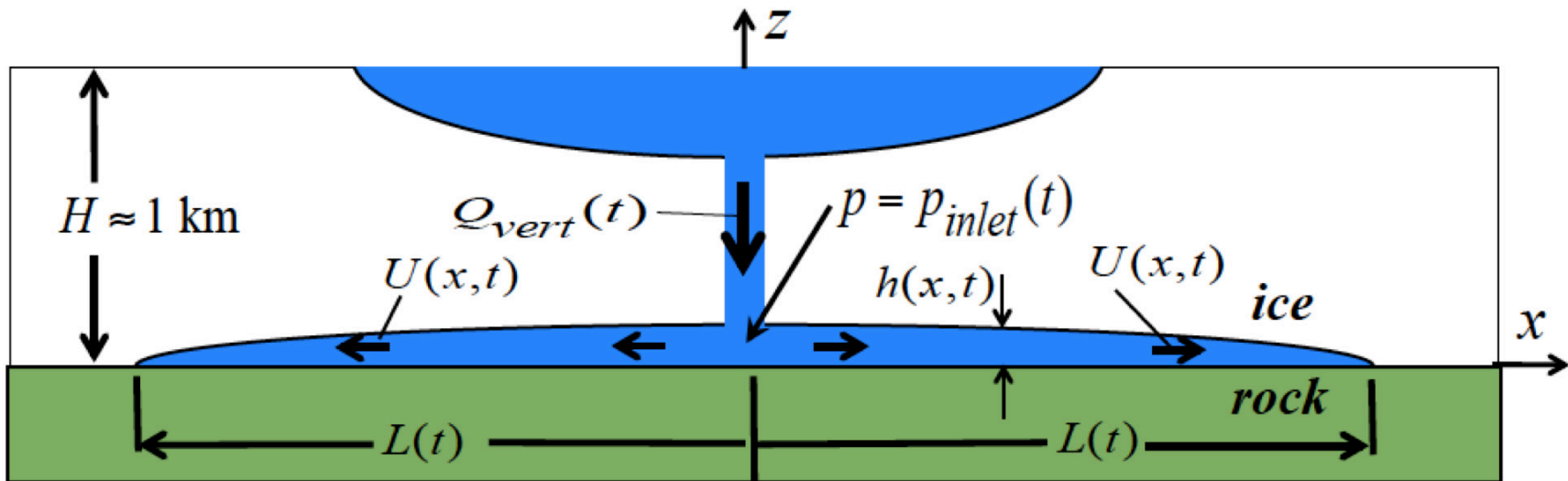
$$\Rightarrow \text{Reynolds number } Re \text{ for flow in fracture} \approx \frac{3 \text{ km / hr} \times 0.5 \text{ m}}{10^{-6} \text{ m}^2/\text{s}} \approx 4 \times 10^5$$

Gioia & Chakraborty [*PRL*, 2006] replot, Nikuradse [1933] rough-wall pipe-flow data

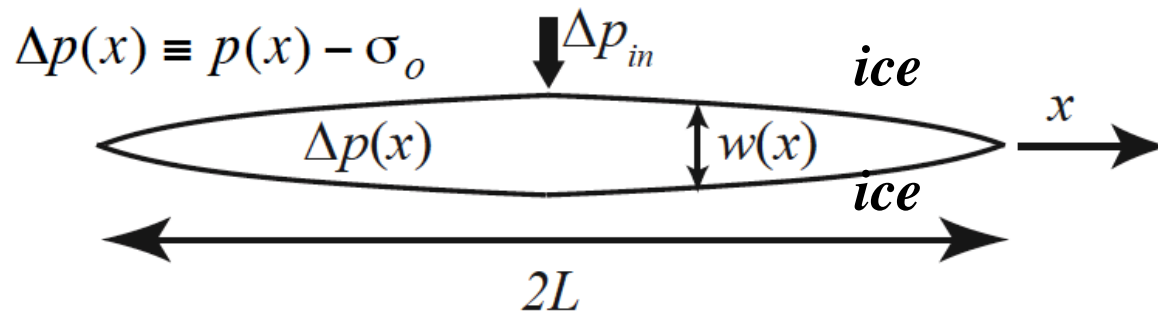


Nikuradse's data, Darcy-Weisbach f versus Reynolds number Re , pipe flow with rough walls. At large Re , f becomes independent of Re .

Inset: Manning-Strickler scaling, $f \approx 0.143(r/R)^{1/3}$. Means $f \approx 0.143(k/h)^{1/3}$.



(Analysis simplified by treating ice and bed as a *homogeneous* medium.)



$$h(x,t) \approx \xi w(x,t), \quad \xi \approx 0.55$$

Governing Equations, valid for range $L \ll H = \text{ice thickness} \approx 1 \text{ km}$

[Tsai & Rice, *JGR*, 2010]

$p(x,t) - \sigma_0$, $h(x,t) = \xi w(x,t)$, and $U(x,t)$ related by

- Linear elasticity for cracks:** $p(x,t) - \sigma_0 = \frac{E'}{2\pi\xi} \int_{-L}^L \frac{\partial h(x',t)}{\partial x'} \frac{dx'}{x-x'}$
 ($w = \text{opening in homog. ice};$
 $h = \text{opening in ice/rock}$)

- Fracture mechanics, ice-rock interface:**

(toughness $K_{Ic} \approx 0.1 \text{ MPa m}^{1/2}$
 is negligible, for $L > \sim 10 \text{ m};$
 “fracture” becomes “lift-off”)

$$K_{Ic} = 0 \implies r^{1/2} \sigma_{ij} \rightarrow 0 \text{ as } r \rightarrow 0$$

- Conserv. of fluid mass (fluid volume):**

$$\frac{\partial(hU)}{\partial x} + \frac{\partial h}{\partial t} = 0$$

- Manning-Strickler turbulent flow:**

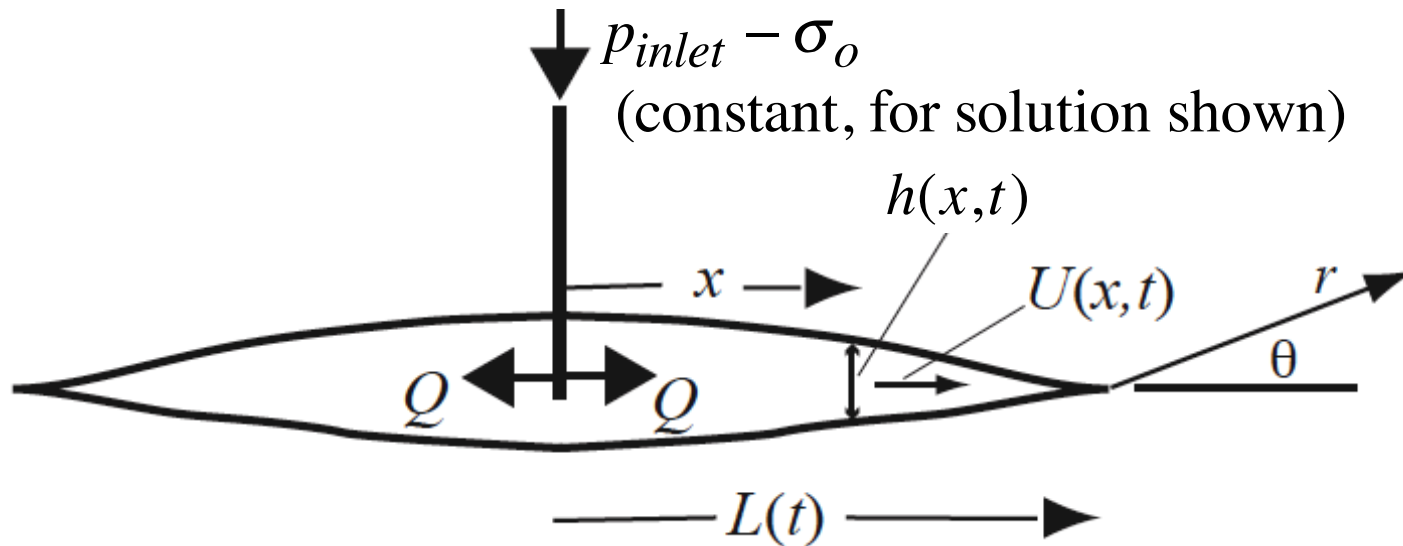
($k = \text{Nikuradse}$
 roughness scale)

$$-h \frac{\partial p}{\partial x} = 0.0357 \rho U^2 \frac{k^{1/3}}{h^{1/3}}$$

$\nwarrow \quad \nearrow$
 $2\tau_{\text{wall}}$

Self-Similar Solution (2D plane-strain, $L \ll H$ [Tsai & Rice, *JGR*, 2010])

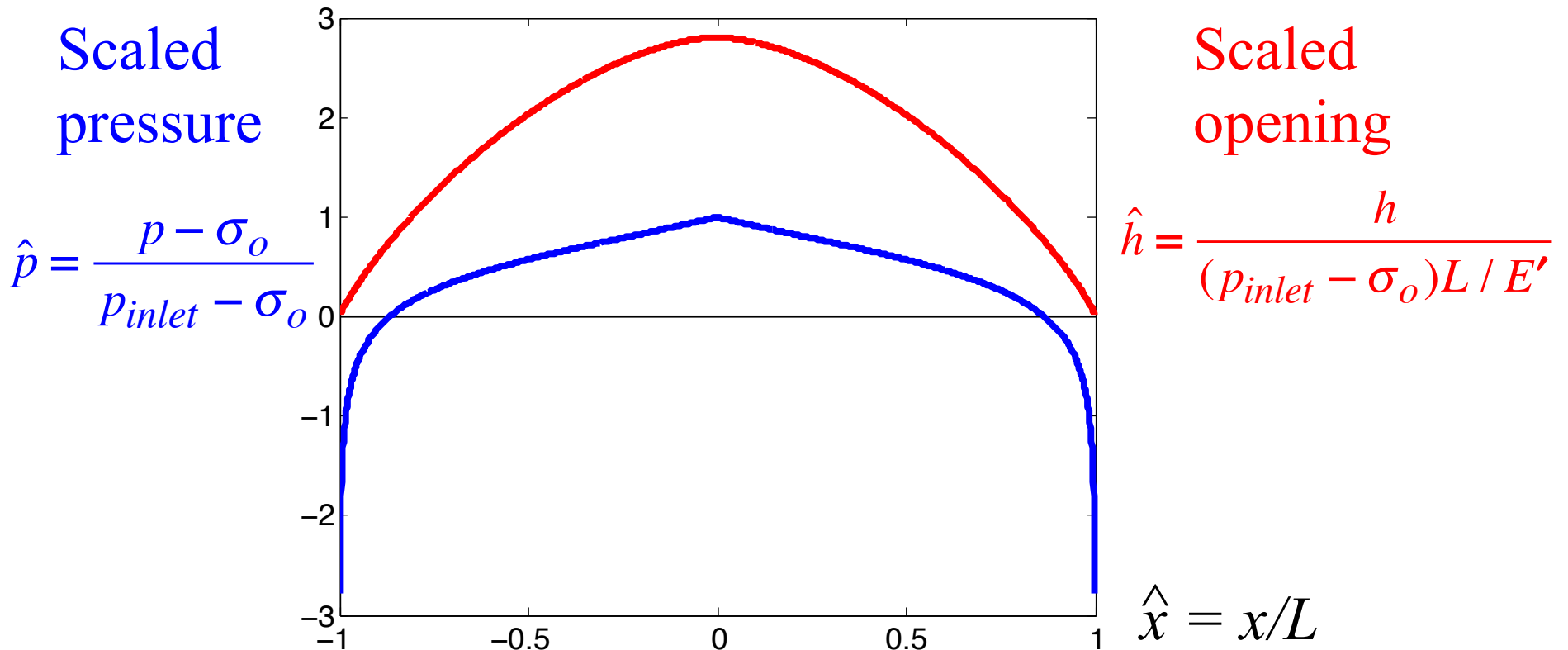
(Approach similar to Adachi and Detournay [*Int. J. Numer. Anal. Meth. Geomech.*, 2002], who solved the same problem for a power-law viscous fluid in locally laminar flow.)



Our case (turbulent, high **Re**): $\tau_{wall} = \frac{f}{8} \rho U^2 = -\frac{1}{2} h \frac{\partial p}{\partial x}$, $f = 0.143 \left(\frac{k}{h} \right)^{1/3}$

$$L(t) = C t^{6/5}, \quad h(x,t) \sim C t^{6/5} F(x/L(t)),$$

$$p(x,t) - p_o = G(x/L(t)), \quad U(x,t) = C t^{1/5} H(x/L(t)).$$



- Crack growth rate:

$$\frac{dL(t)}{dt} = 5.17 \sqrt{\frac{p_{inlet} - \sigma_o}{\rho}} \left(\frac{p_{inlet} - \sigma_o}{E'} \right)^{2/3} \left(\frac{L(t)}{k} \right)^{1/6}$$

Making contact with the observations [Das et al., '08] of surface-lake drainage driving hydraulic fracture near a margin of the Greenland Ice Sheet, and using analytical results for self-similar plane strain fracture:

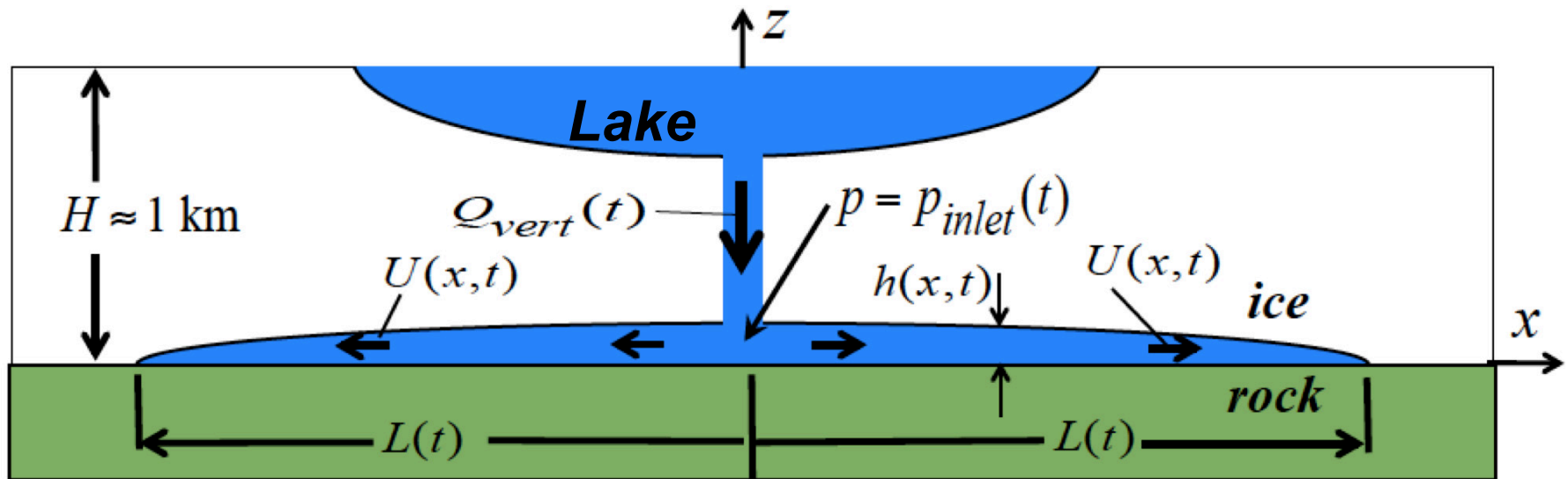
For $p_{hydrostatic} - \sigma_o = 0.87 \text{ MPa}$, $k = 1 \text{ cm}$, $L = 1 \text{ km}$:

- If $p_{inlet} - \sigma_o = p_{hydrostatic} - \sigma_o$, $U_{tip} = 9.4 \text{ km/hr}$, $h_{avg} = 0.13 \text{ m}$.
 - If $p_{inlet} - \sigma_o = 0.5 (p_{hydrostatic} - \sigma_o)$, $U_{tip} = 4.3 \text{ km/hr}$, $h_{avg} = 0.07 \text{ m}$.
 - If also k decreased by factor of 5, to $k = 2 \text{ mm}$, $U_{tip} = 5.6 \text{ km/hr}$, $h_{avg} = 0.07 \text{ m}$.
-

- Young's modulus $E = 6.2 \text{ GPa}$ at -5°C [Jellinek et al., '55] and Poisson's ratio $\nu = 0.3$ [Vaughan, '95], gives $E' = 6.8 \text{ GPa}$.
- Liquid density $\rho = 1000 \text{ kg/m}^3$, ice density $\rho_{ice} = 910 \text{ kg/m}^3$.
- Ice thickness $H = 980 \text{ m}$ [Das et al., '08], so $p_{hydrostatic} - \sigma_o = 0.87 \text{ MPa}$.
- Dependence of U on channel wall roughness k is weak (power law exponent = 1/6); estimate $k = 1 \text{ cm}$, which is consistent with $n_{\text{Manning}} \sim 0.018 \text{ s m}^{-1/3}$.

[Tsai & Rice, *J. Appl. Mech.*, 2012]

Finite L/H -- but still a 2D plane strain model
starting as our *JGR* [2010] solution for $L/H \ll 1$.



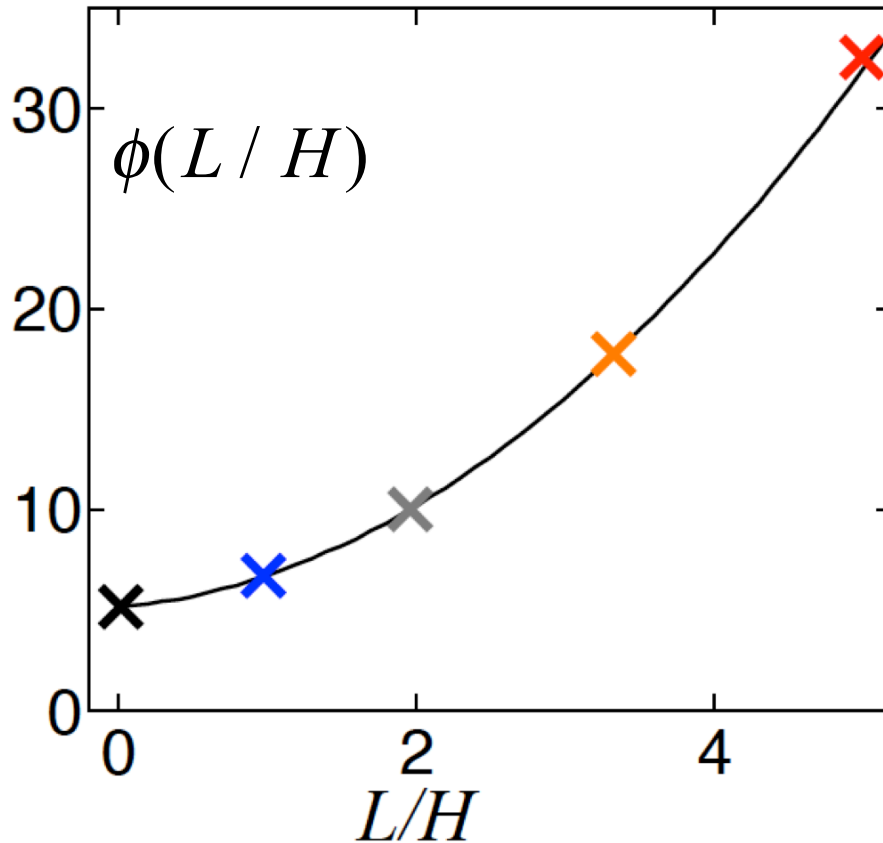
$$p_{hydrostatic} \equiv \rho_{water} g H \geq p_{inlet} \geq \rho_{ice} g H \equiv \sigma_o$$

Schematic for turbulent hydraulic fracture
(Analysis again simplified by treating ice
and bed as a *homogeneous* medium.)

Crack growth rate =

[Tsai & Rice, *J. Appl. Mech.*, 2012]

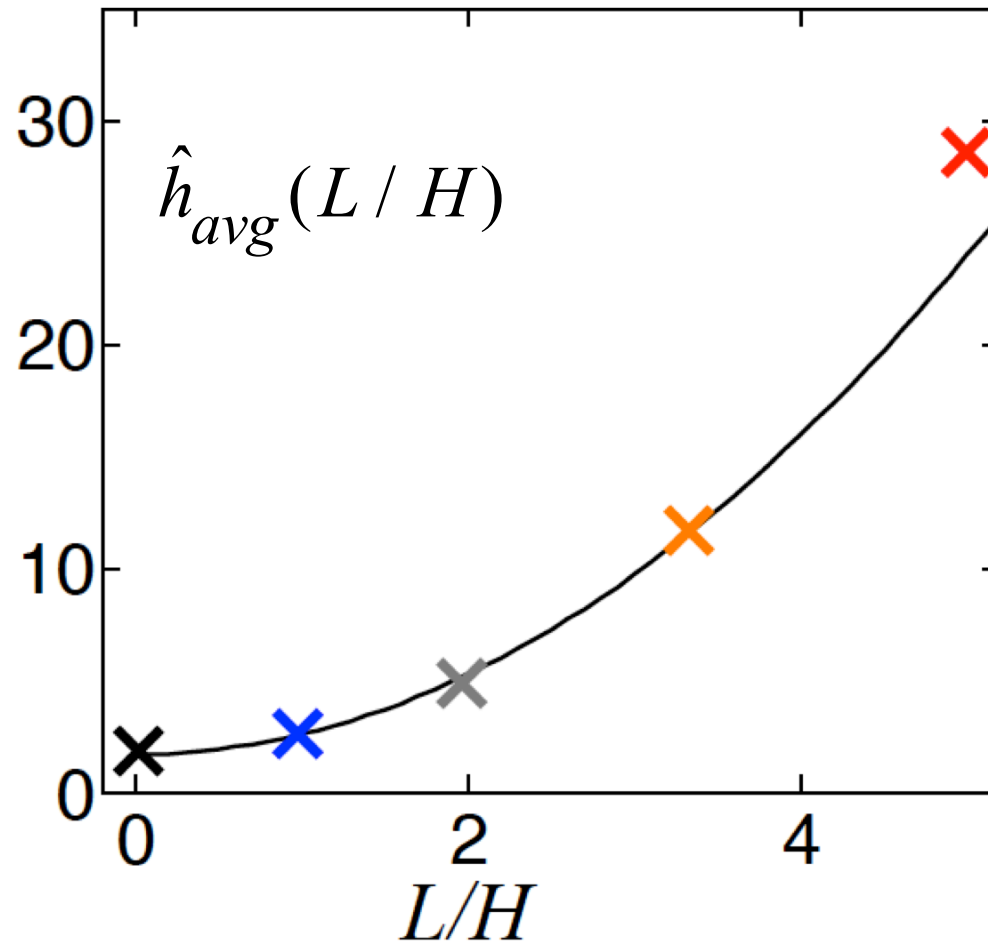
$$\frac{dL}{dt} \equiv U_{tip} = \left(\frac{p_{inlet} - \sigma_o}{\rho} \right)^{1/2} \left(\frac{p_{inlet} - \sigma_o}{E'} \right)^{2/3} \left(\frac{L}{k} \right)^{1/6} \phi(L/H)$$



For a given L/H ,
 $dL/dt \propto (p_{inlet} - \sigma_o)^{7/6}$

— $\phi(L/H) \approx 5.13[1 + 0.125(L/H) + 0.183(L/H)^2]$

Average opening of fracture $\equiv h_{avg} = \frac{(p_{inlet} - \sigma_o)L}{E'} \hat{h}_{avg}(L/H)$



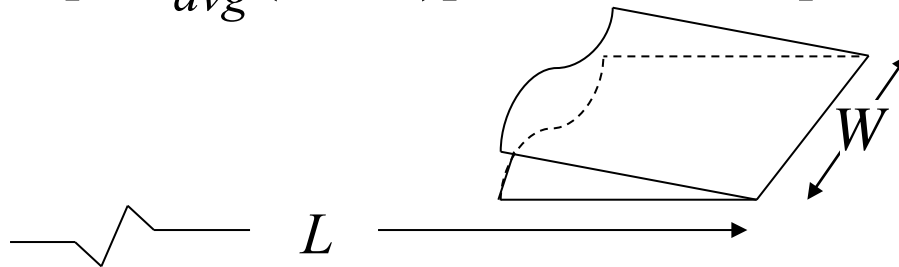
— $\hat{h}_{avg}(L/H) \approx 1.72 [1 + 0.517 (L/H)^2]$

Volumetric inflow rate to glacier bed

($W \approx 3$ km taken as effective length perpendicular to plane for use of our 2D plane - strain solution; e.g., major crevasse extends 2.7 km along the lake bed - - ultimately, 3D is needed!):

$$Q_{basal} = \frac{d(2LWh_{avg})}{dt} = \frac{2(p_{inlet} - \sigma_o)W}{E'} \frac{\partial[L^2 \hat{h}_{avg}(L/H)]}{\partial L} \frac{dL}{dt}$$

$$\left(\text{here, } \partial[L^2 \hat{h}_{avg}(L/H)] / \partial L \approx 3.44L [1 + 1.035(L/H)^2] \right)$$



Note : For a given L/H , $dL/dt \propto (p_{inlet} - \sigma_o)^{7/6}$,
 so $Q_{basal} \propto (p_{inlet} - \sigma_o)^{13/6}$

$$P_{hydrostat} \equiv \rho_{water} g H \geq P_{inlet} \geq \rho_{ice} g H \equiv \sigma_o$$

Average vertical conduit opening:

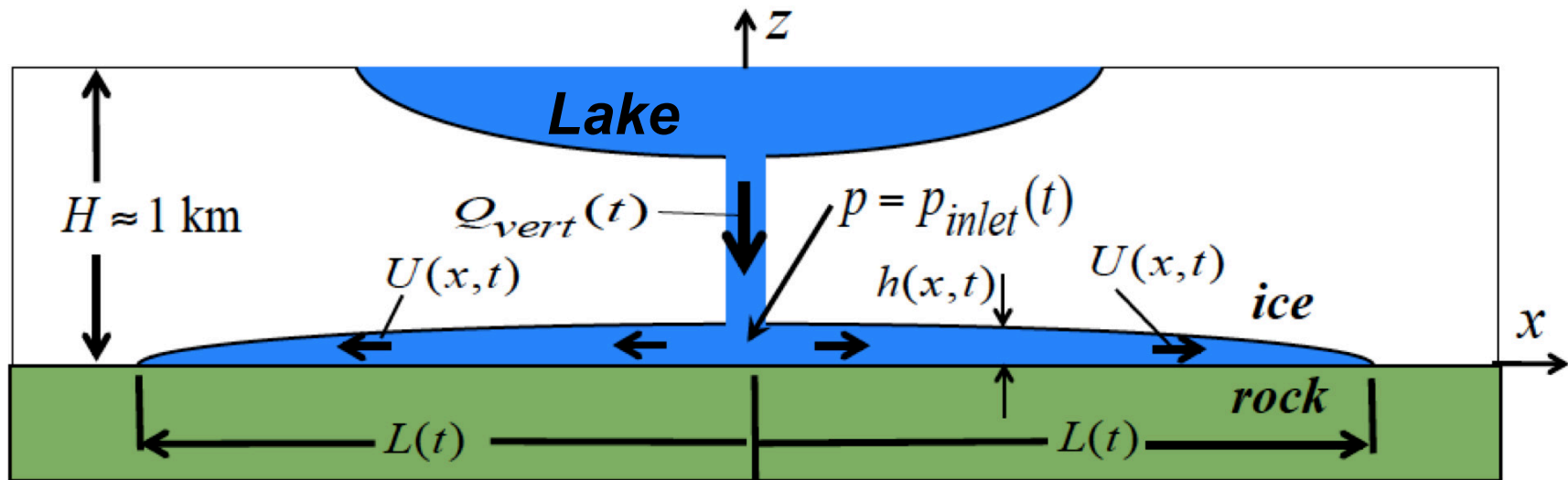
$$\Delta \bar{u} = \Delta \bar{u}^{el} + \Delta \bar{u}^{cr} \text{ (elastic + prior creep)}$$

$$\Delta \bar{u}^{el} \propto P_{inlet} - \sigma_o$$

Important term!

For a given conduit opening $\Delta \bar{u}$,
vertical flow rate

$$Q_{vert} \propto (P_{hydrostat} - P_{inlet})^{1/2}$$



$P_{inlet} - \sigma_o \sim$ controls flow rate
 Q_{basal} into basal fracture

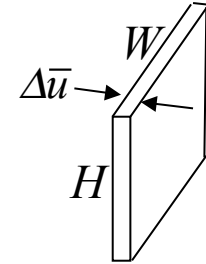
P_{inlet} ultimately
determined by setting
 $Q_{basal} = Q_{vert}$

To evaluate the vertical crack - crevasse system as a feeder channel :

For evaluating **flow resistance**: Vertical crack-crevasse system treated as a vertical slit of depth H , uniform width W , and uniform (but time-dependent) opening gap $\Delta\bar{u}$:

$$\Rightarrow Q_{vert} \approx 1.97 \left(\frac{\rho g H - p_{inlet}}{\rho g H - \sigma_o} \right)^{1/2} g^{1/2} W \Delta\bar{u}^{3/2} \left(\frac{\Delta\bar{u}}{k} \right)^{1/6}$$

$$\Delta\bar{u} = \text{short-time } \mathbf{elastic} (\Delta\bar{u}^{el}) + \text{longer term } \mathbf{creep} (\Delta\bar{u}^{cr})$$



Elastic opening gap Δu^{el} : • Calculated by 2D plane strain elasticity, $\Delta\bar{u}^{el} = \frac{\pi(p_{inlet} - \sigma_o)}{2E'} W$

Creep opening gap $\Delta\bar{u}^{cr}$: • Will be \approx constant during the short timescale of rapid drainage.
 • Will depend on how long the vertical crack-crevasses system has been hydrostatically pressurized before nucleation of basal fracture.

Power - law creep, $\dot{\gamma} / 2 = A(T)\tau^n$, where $n = 3$ (Glen's law) is typical for glacial flow.

$$\frac{d\Delta\bar{u}^{cr}}{dt} \approx \kappa(n) \frac{\pi}{2} A(T) \left(\frac{(\rho - \rho_{ice})gH}{2n} \right)^n W \text{ during hydrostatic pressure loading of walls.}$$

$\kappa(n)$ (≈ 0.8 for $n = 3$) is a numerical correction for the average crack opening [**M. C. Fernandes**]

Define $C \equiv \frac{\Delta\bar{u}^{cr}}{(\Delta\bar{u}^{el})_{p_{inlet}=p_{hydrostat}}}$, so that $\Delta\bar{u} \approx C \frac{\pi(\rho g H - \sigma_o)}{2E'} W + \frac{\pi(p_{inlet} - \sigma_o)}{2E'} W$

At -5° to -2° C, hydrostatic p over 16 hr of slow leakage $\Rightarrow C \approx 1.0$ to 2.1

(based on $H = 1$ km, $E' \approx 6.8$ GPa, $n = 3$, and $A_{-5^\circ\text{C}} \approx 9 \times 10^{-25} \text{ s}^{-1} \text{ Pa}^{-3}$, $A_{-2^\circ\text{C}} \approx 2 A_{-5^\circ\text{C}}$)

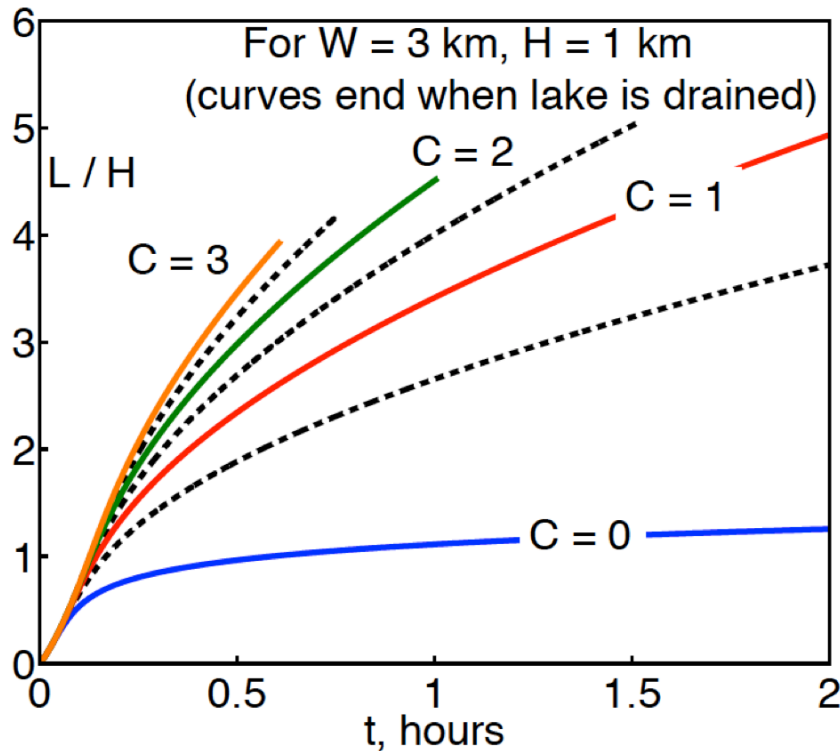
$$C = \frac{\text{prior creep opening of vertical crevasse channel}}{\text{elastic opening under hydrostatic pressurization}} = \frac{\Delta \bar{u}^{cr}}{(\Delta \bar{u}^{el})_{p=\text{hydrostatic}}}$$

$C \approx 1.0$ to 2.1 is achieved in ~ 16 hours of hydrostatic pressurization

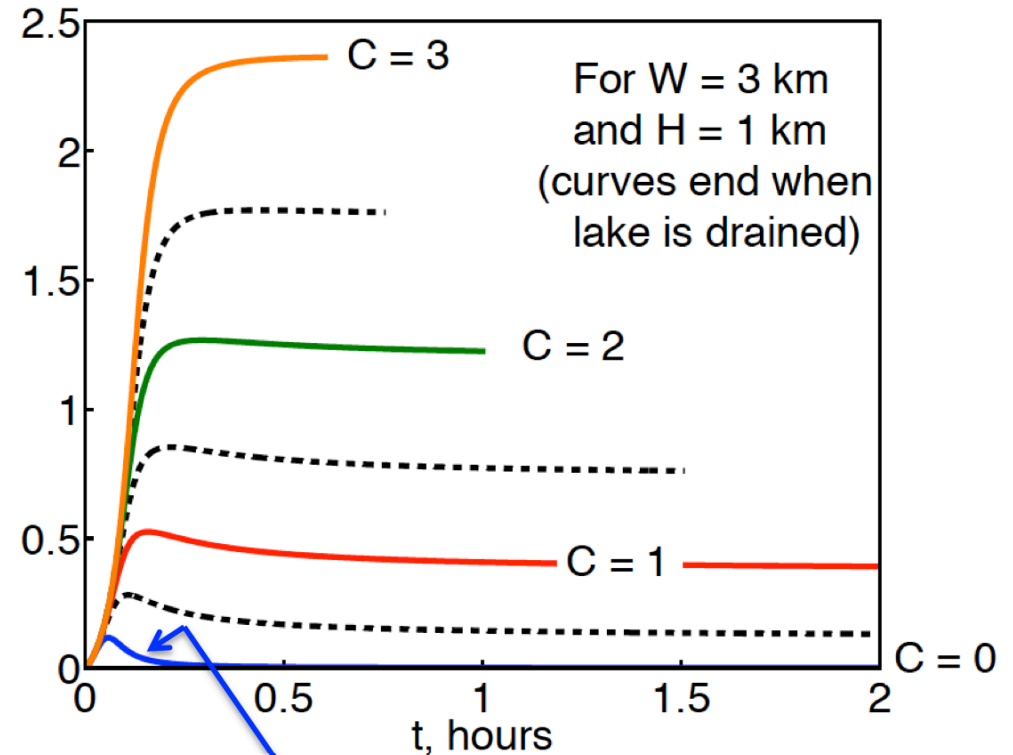
(Slow prior drainage suggests ~ 16 hours of high pressurization)

Plots by **J. D. Platt**, based on paraboloid lake shape with constrained volume and surface area:

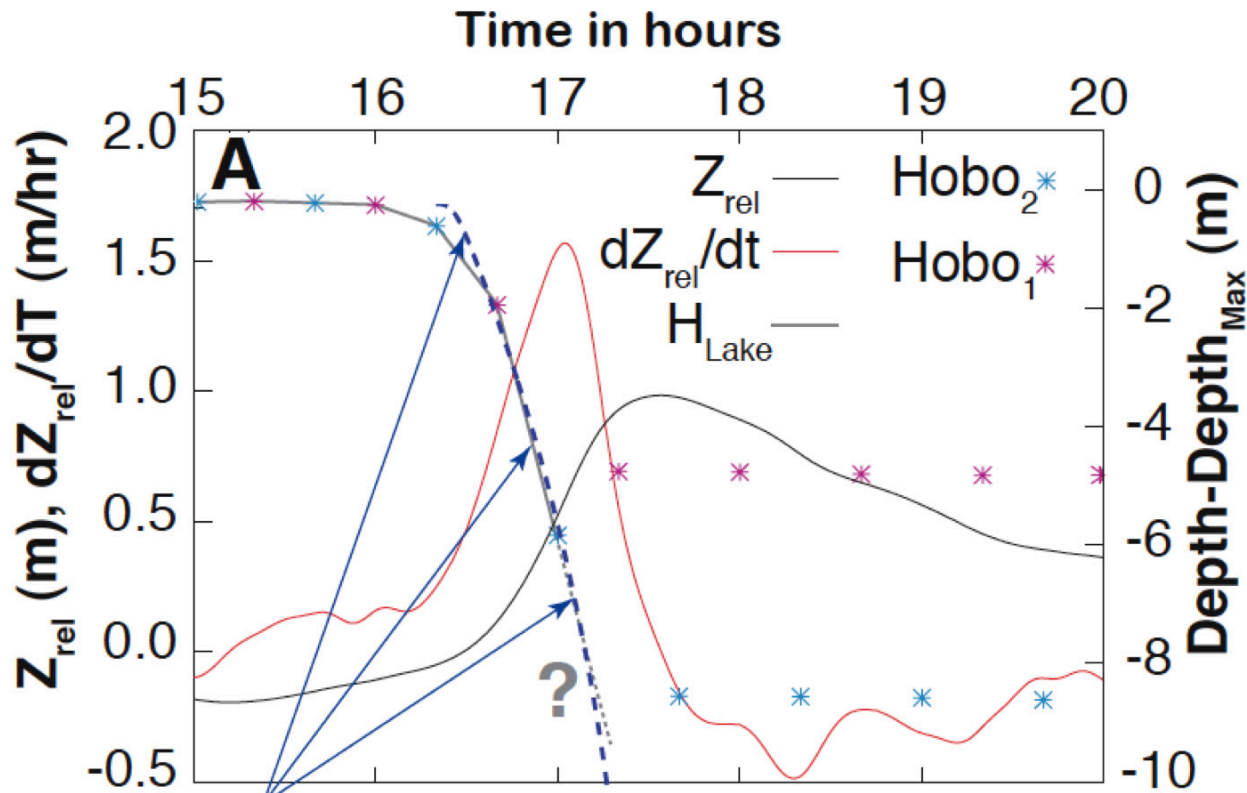
Crack Length L , km



Discharge Rate, $\text{m}^3 \text{s}^{-1} \times 10^4$



The vertical crack - crevasse system shuts down, well before full discharge, when creep - opening is neglected, i.e., when C = 0.



Results of model including creep opening of vertical crack-crevasse system, with $C = 1.75$ (creep opening = 1.75 X initial elastic opening), $H = 1$ km, and $W = 3$ km.

$C = 1.75 \Rightarrow$ Time for Drainage = 1.21 hr;
 (This C is within roughly estimated range $C \approx 1.0$ to 2.1)

$\frac{\text{Lake Volume}}{\text{Crack Area } 2WL \text{ at Drainage}} = 1.54 \text{ m; compare, } 1.15 \text{ m GPS uplift } (Z_{rel}).$

West Antarctic Ice Sheet:

*Rapidly flowing ice streams: What
processes control their width?*

Principally with

Thibaut Perol (Harvard),

with further contributions by

John D. Platt (Carnegie Inst.)

and

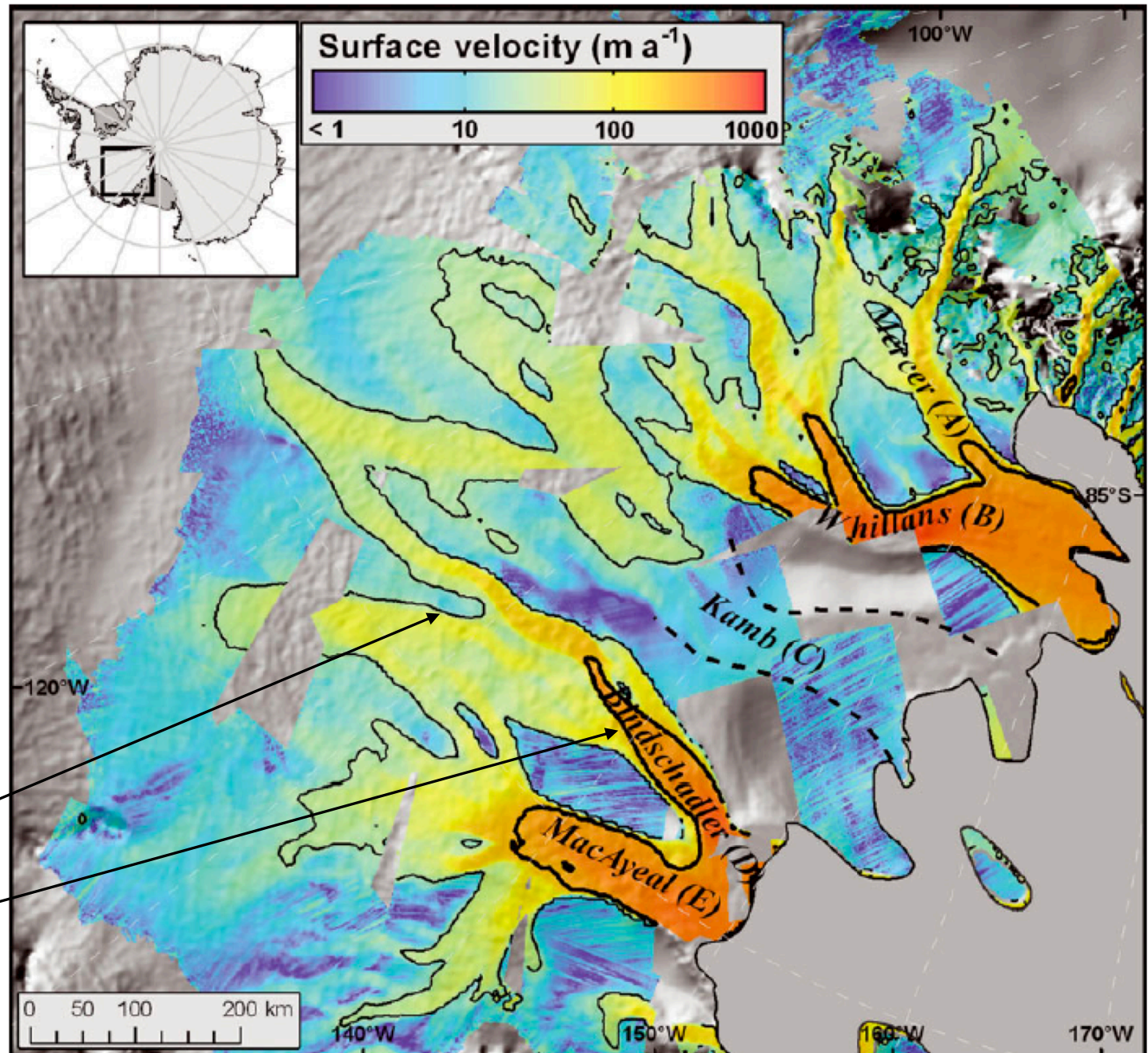
Jenny Suckale (Stanford)

[from Le Brocq, Payne, Siegert & Alley, *J. Glac.*, 2009]

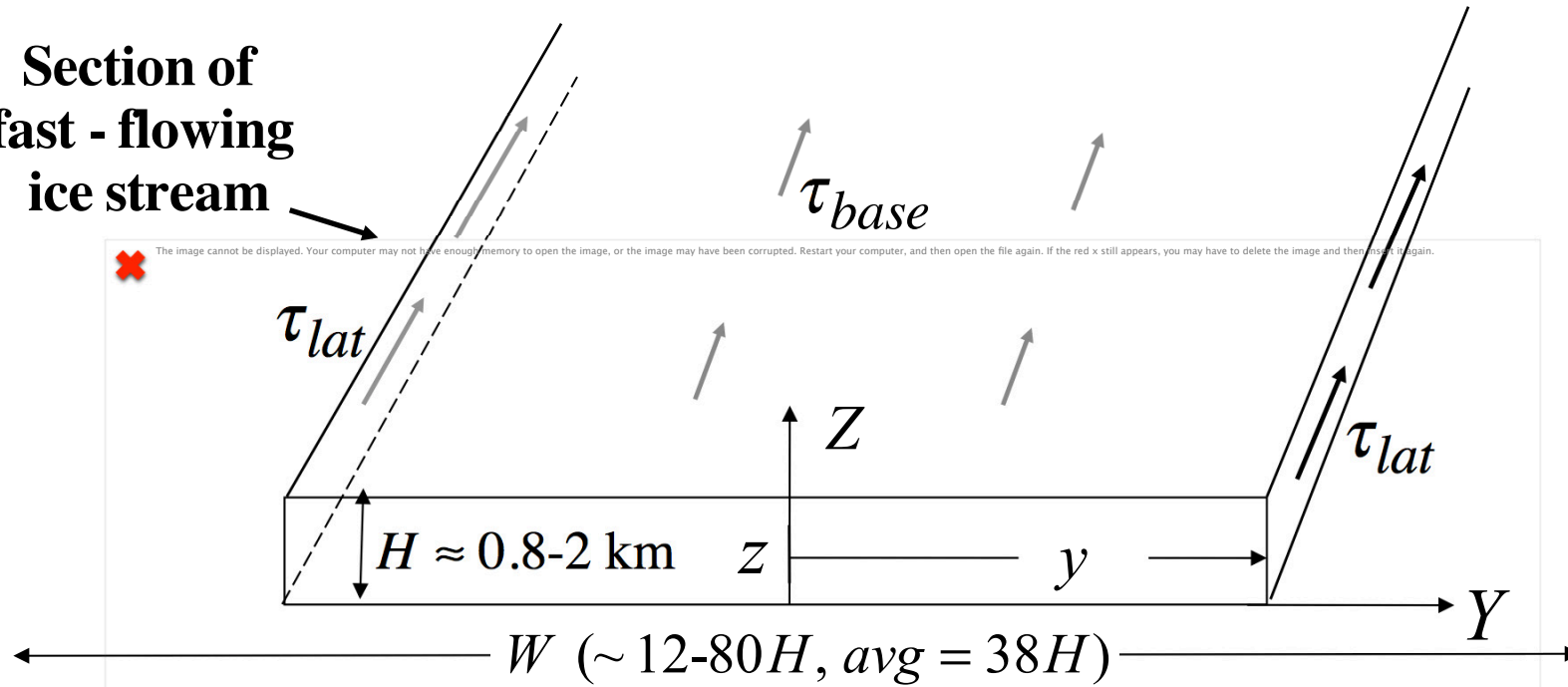
- **Western Antarctica, Siple Coast, Ice Streams**, flowing to the Ross Sea ice shelf.

- InSAR velocity (from Joughin et al., *J. Geophys. Res.*, 2002) overlaid on a digital elevation model (Bamber et al., 2009).

- Velocity contours shown are 25 m/yr (thin line) and 250 m/yr (thick line).



Section of fast-flowing ice stream



$$\tau_{grav} = \rho g H S \quad (S = \text{slope})$$

= downslope gravity force per unit base area

Equilibrium*: $\bar{\tau}_{lat} H = (\tau_{grav} - (\tau_{base})_{avg}) y$

$$\bar{\tau}_{lat} \rightarrow (\tau_{grav} - (\tau_{base})_{avg}) \quad W / 2H \text{ at margins}$$

*neglecting any variation in net axial force in sheet, roughly justified [Whillans and van der Veen, *J. Glac.*, 1993]

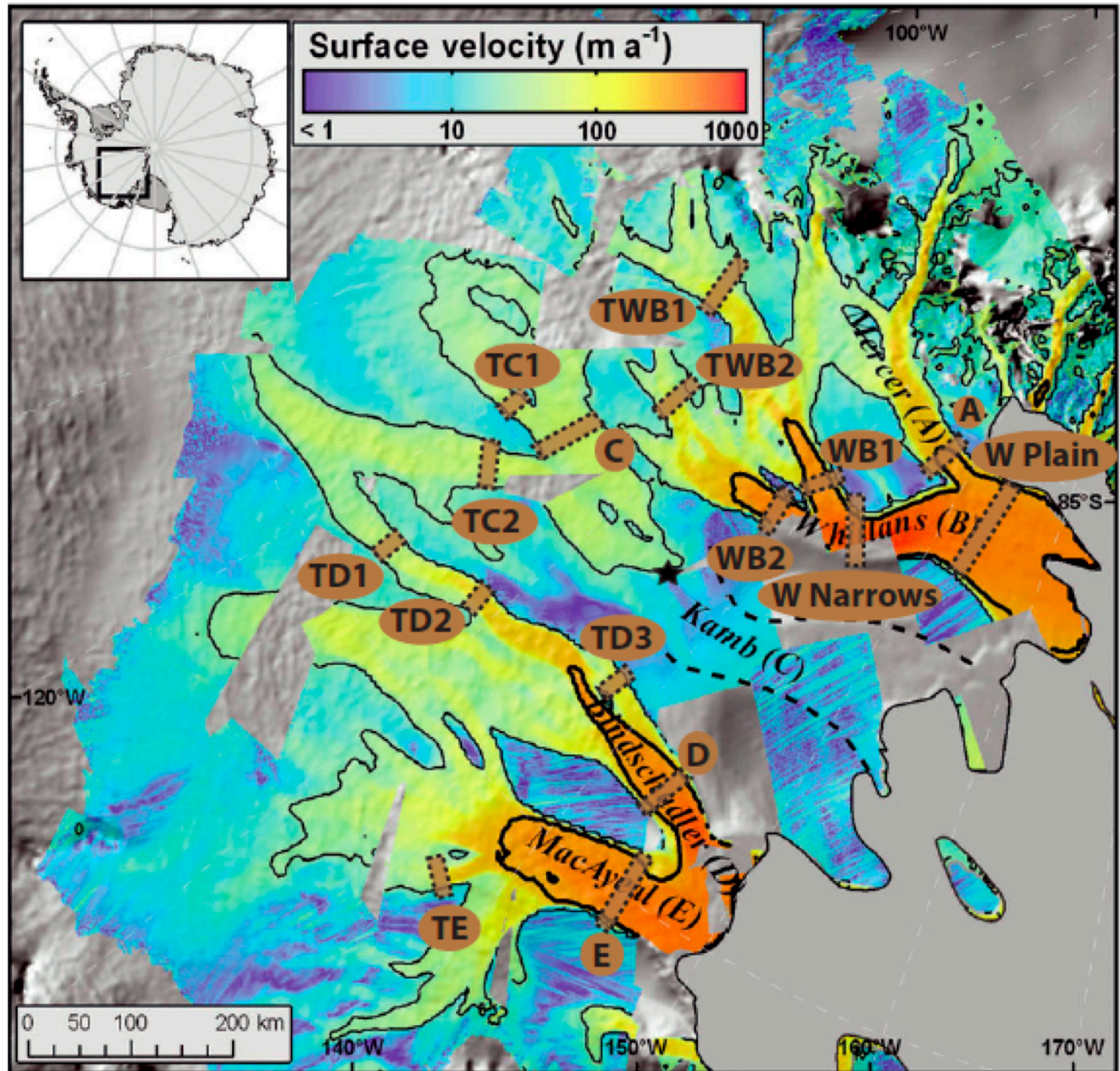
Increases with stream width W / H ($\sim 6-40$ at current margins)

\Rightarrow increasing strain rate,
 $\dot{\gamma}_{lat} \sim \bar{\tau}_{lat}^3 \sim (W / H)^3$,
 \Rightarrow increasing shear heating, $\sim (W / H)^4$,
 \Rightarrow onset of melting ?

Our data set,
to test
concepts:

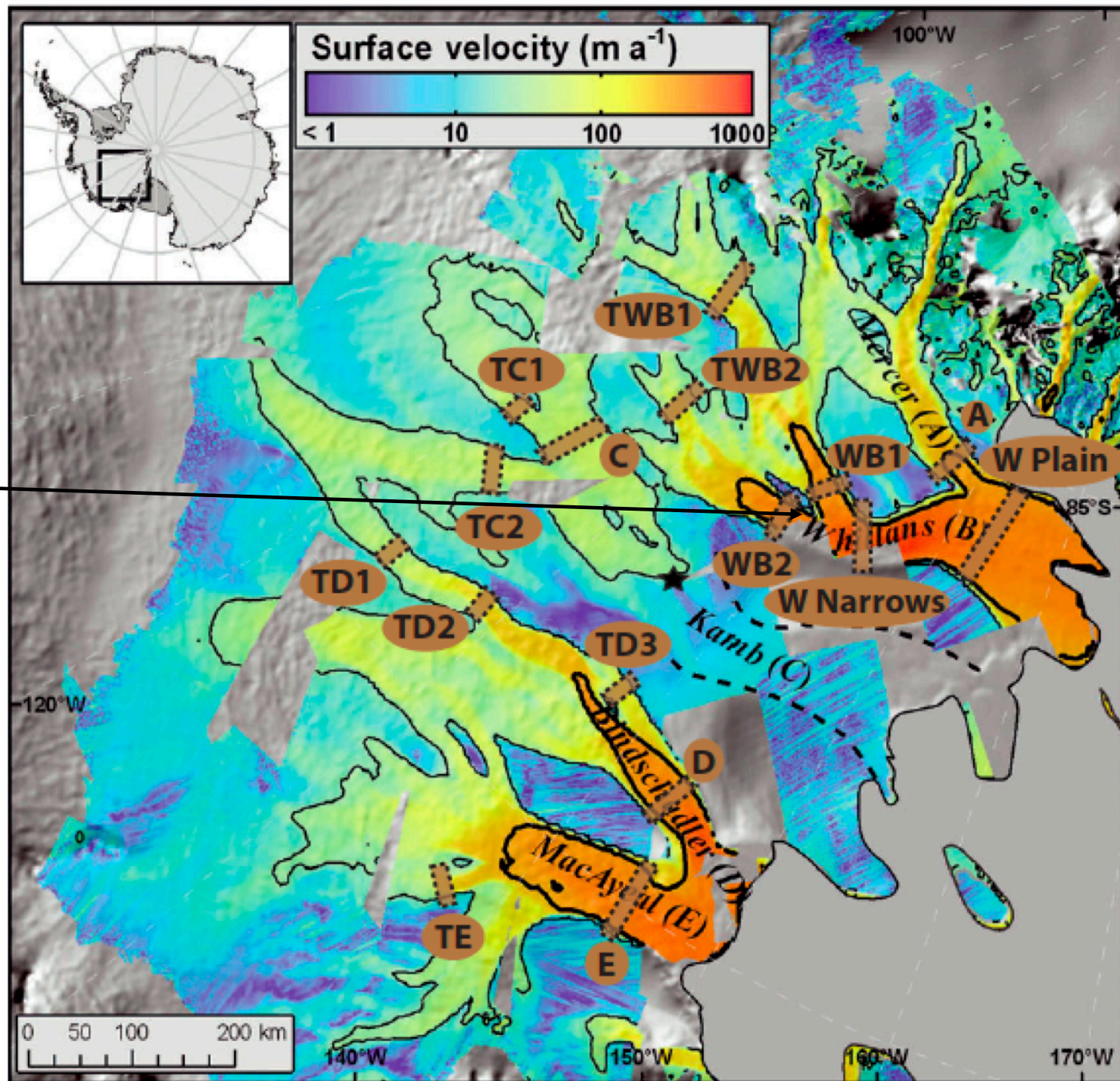
Sixteen
ice stream
traverses
(dotted-lines)
for velocity
profiles.

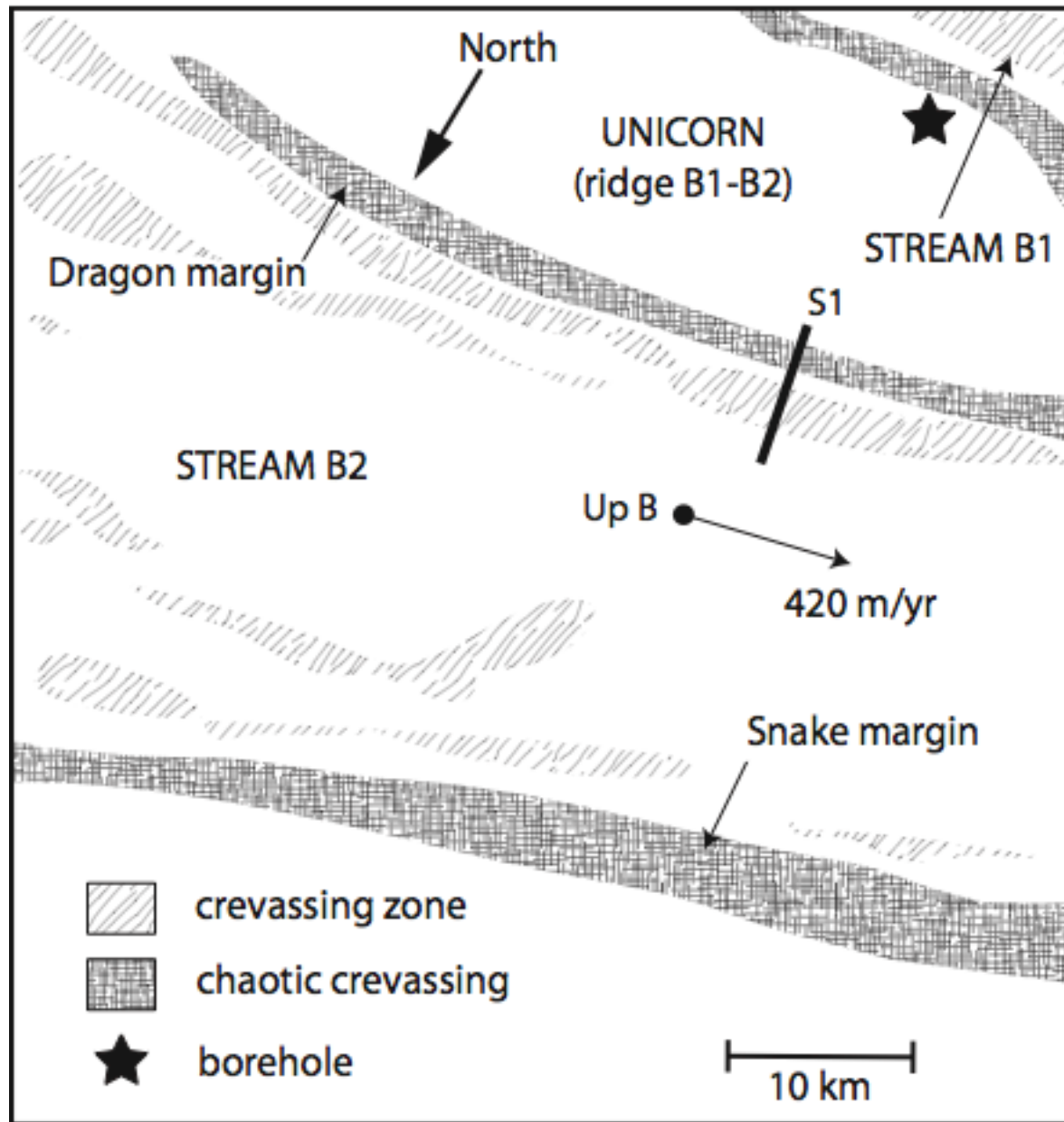
Characterized
by Joughin et
al. (*J. Geoph.
Res.*, 2002)



Focus for most detailed study:

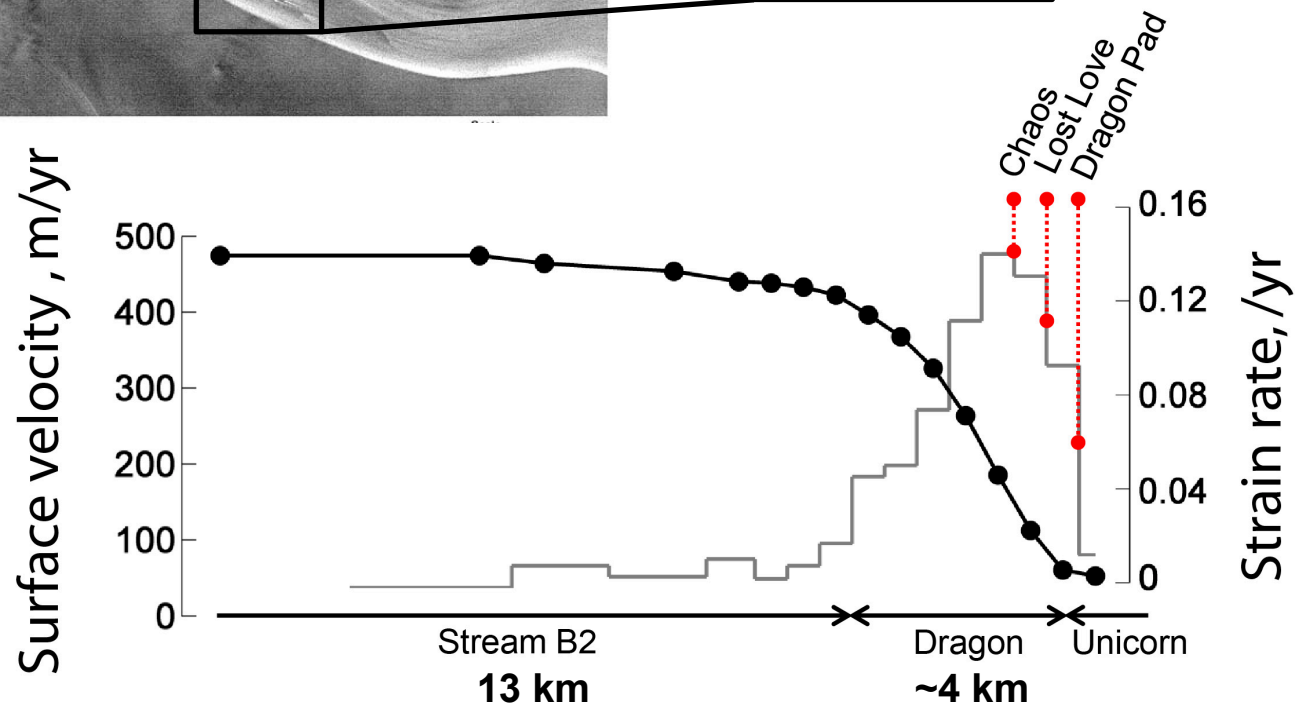
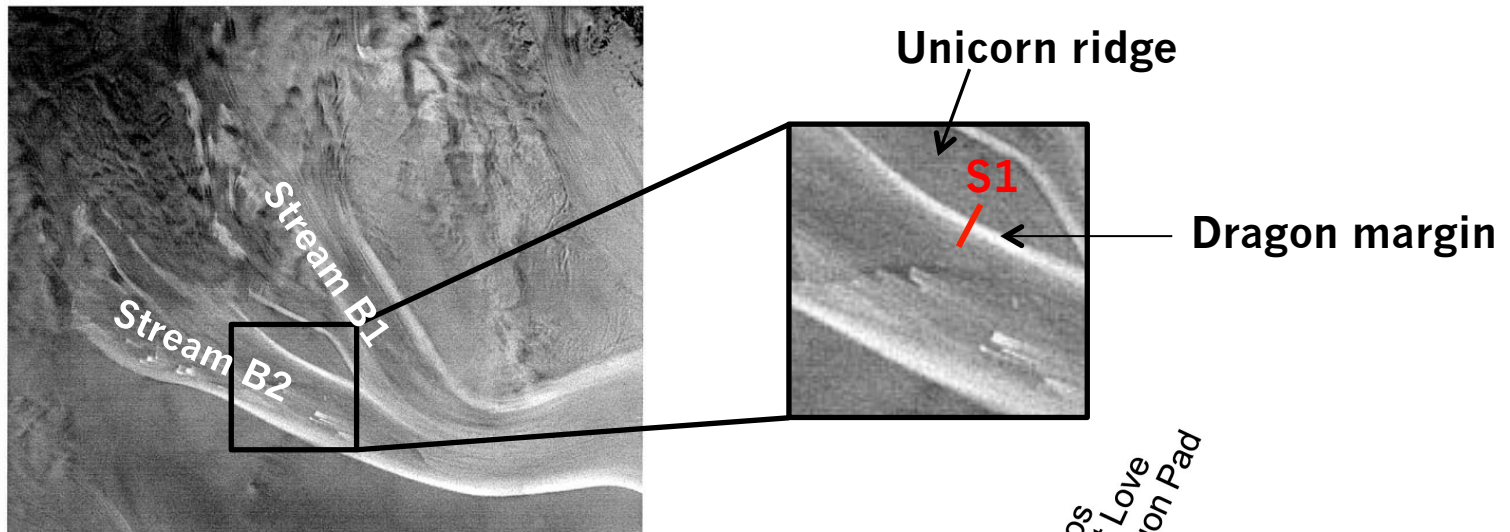
Dragon Margin
(very near to, but not the same as, the WB2 profile)





Echelmeyer and Harrison (1999)

Dragon margin



Suckale et al. (2014); data from Harrison et al. (1998), Echelmeyer and Harrison (1999)

Table 1. Parameters taken from *Joughin et al.* [2002] and used for margins of the profiles located in Figure 2. Profiles beginning with the letter T are made at the tributaries of the ice streams.

Ice Stream	Profile	H (m)	W (km)	$\dot{\gamma}_{lat}$ ($10^{-2} \cdot \text{yr}^{-1}$)
Mercer	A	1242	39	4.2
Whillans	WB1	1205	35	7.0
	WB2	985	34	9.5
	W Narrows	846	48	13.5
	W Plain	735	121	5.1
	TWB1	2188	25	3.8
	TWB2	1538	25	4.0
Kamb	C	1805	69	1.0
	TC1	1802	17	1.4
	TC2	2196	43	0.9
Bindschadler	D	888	55	5.8
	TD1	1952	24	2.5
	TD2	1412	35	5.4
	TD3	1126	21	2.2
MacAyeal	E	916	78	8.1
	TE	1177	19	5.5

Lateral strain rate

$\dot{\gamma}_{lat}$
**here is an average
over ~ 2 km width
at Ice Stream margin**

Temperature distribution implied at West Antarctic Ice Stream margins.

1-D Model: Neglecting horizontal (but not vertical) advective ice motions, and horizontal T gradients at the margins, and considering only the strain rate $\dot{\gamma}_{lat}$, the temperature distribution through the column of ice at *steady state* ($\partial T(z,t) / \partial t = 0$; $T = T(z)$) satisfies:

$$\frac{d}{dz} \left(K(T) \frac{dT}{dz} \right) + \tau_{lat}(\dot{\gamma}_{lat}, T) \dot{\gamma}_{lat} = \rho C_i(T) w \frac{dT}{dz}$$

- We take $\dot{\gamma}_{lat}$ to be **uniform** in depth, with **Glen's law** giving

$\tau_{lat}(\dot{\gamma}_{lat}, T) = (1 / A(T))^{1/3} (\dot{\gamma}_{lat} / 2)^{1/3}$, and write *vertical velocity* w as $w = -az / H$ (Zotikov form, where $a \approx$ surface accumulation rate).

- Thus, **with solutions constrained by** $T \leq T_{melt}$, $T(z)$ is given by

$$\frac{d}{dz} \left(K(T) \frac{dT}{dz} \right) + 2 (1 / A(T))^{1/3} (\dot{\gamma}_{lat} / 2)^{4/3} = -\rho C_i(T) \left(\frac{az}{H} \right) \frac{dT}{dz}$$

Thermo - mechanical properties of ice

Glen's flow law for ice (dislocation creep):

$$\dot{\gamma} / 2 = A(T)\tau^3,$$

$$\tau = B(T)(\dot{\gamma} / 2)^{1/3}$$

$$\left(B(T) = [1 / A(T)]^{1/3} \right)$$

With diffusion creep too,

$$\dot{\gamma} / 2 = \tau / 2\eta(T, d_g) + A(T)\tau^3$$

Ice is still strong at T_{melt} :

For a given $\dot{\gamma}$:

$$\tau_{T=0^\circ\text{C}} \approx 0.5 \times \tau_{T=-13^\circ\text{C}}$$

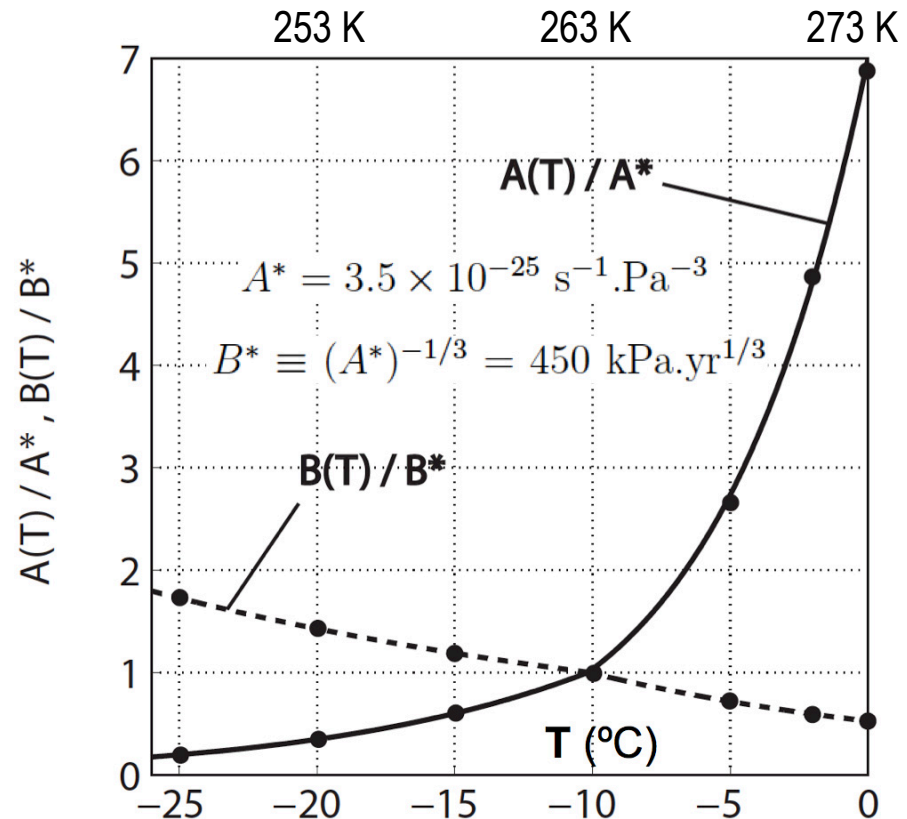
Thermal conductivity :

$$K(T) = 9.828 \frac{\text{J}}{\text{m s K}} \exp\left(-5.7 \times 10^{-3} \frac{T}{\text{K}}\right)$$

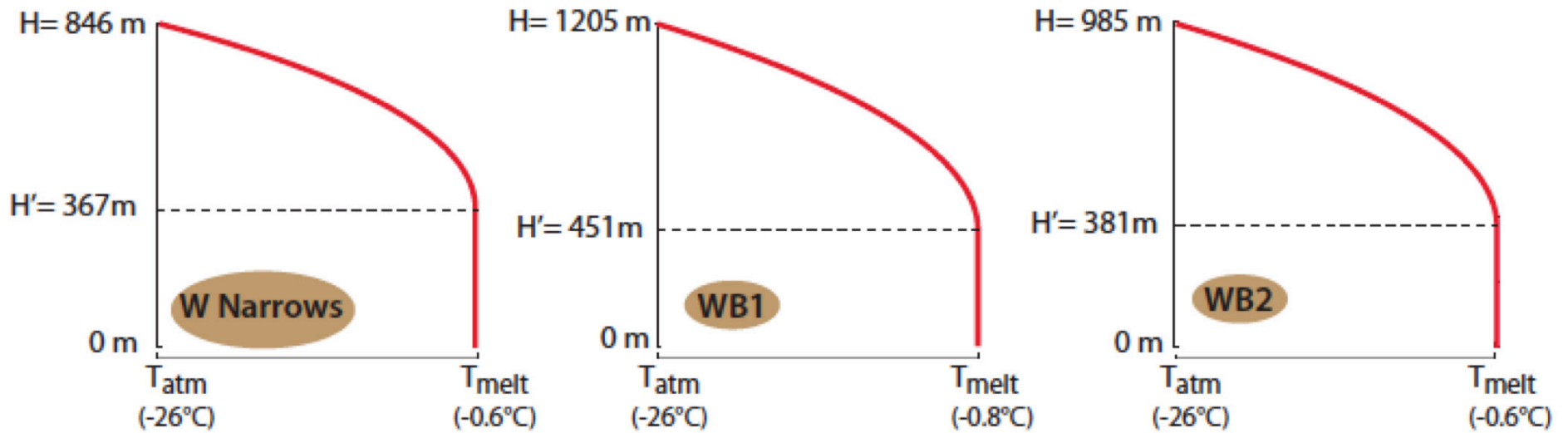
Specific heat :

$$C_i(T) = \left(152.5 + 7.122 \frac{T}{\text{K}} \right) \frac{\text{J}}{\text{kg K}}$$

Data fits as suggested by Cuffy & Paterson [2010]



$$\frac{d}{dz} \left(K(T) \frac{dT}{dz} \right) + \left(\frac{1}{2A(T)} \right)^{1/3} (\dot{\gamma}_{lat})^{4/3} + \rho C_i(T) (a_z / H) \frac{dT}{dz} = 0 \quad \& \quad T \leq T_{melt} \Rightarrow$$



(For all cases,
 $a = 0.1$ m/yr)

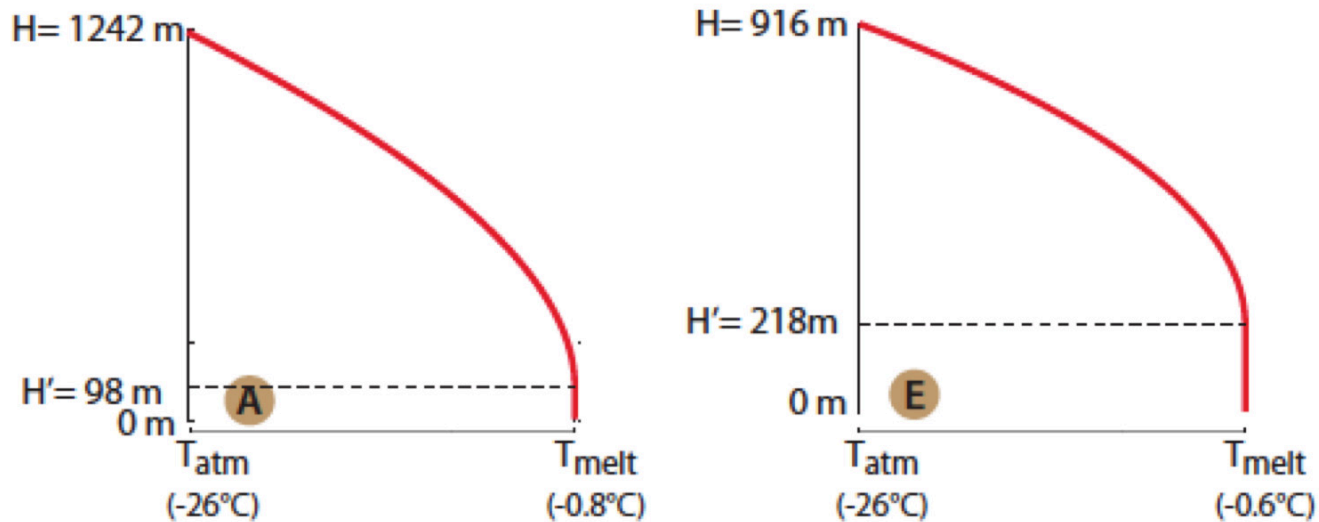
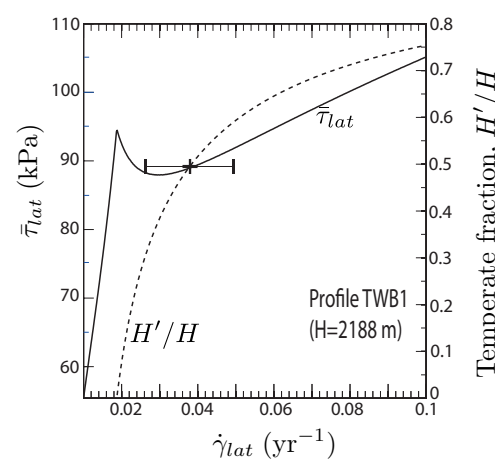
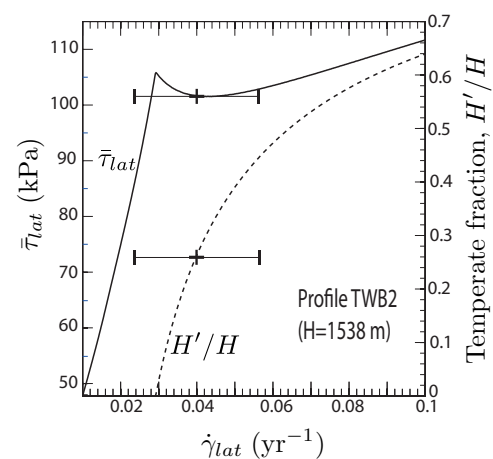
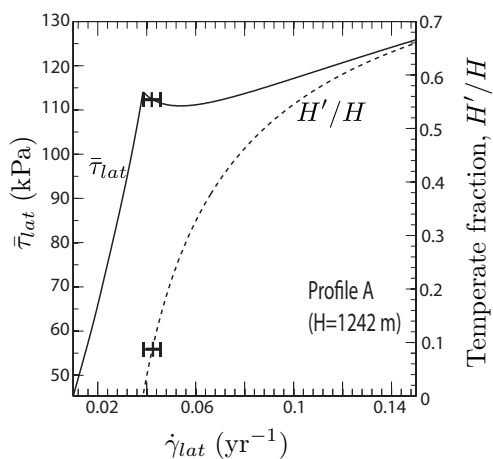
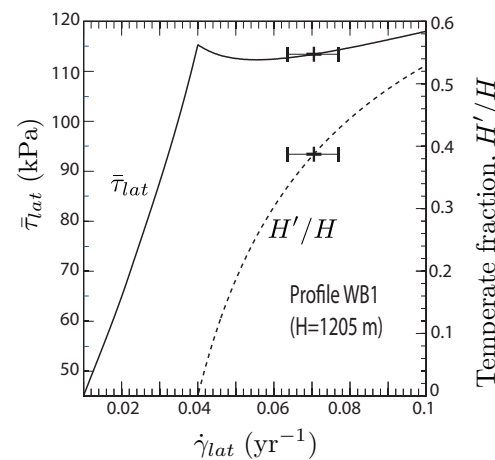
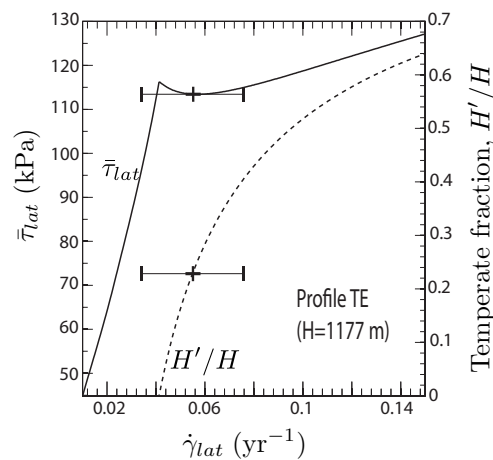
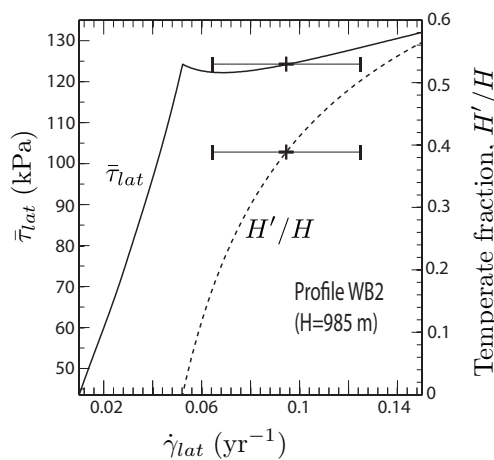
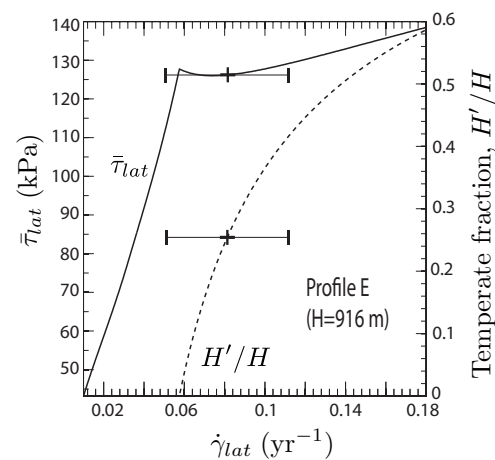
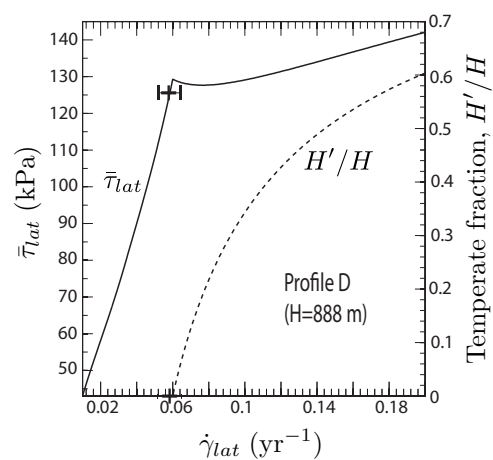
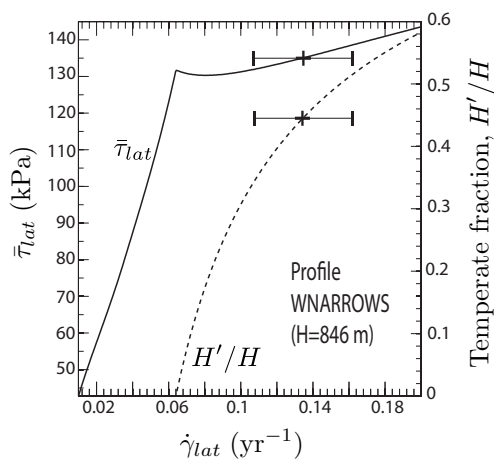


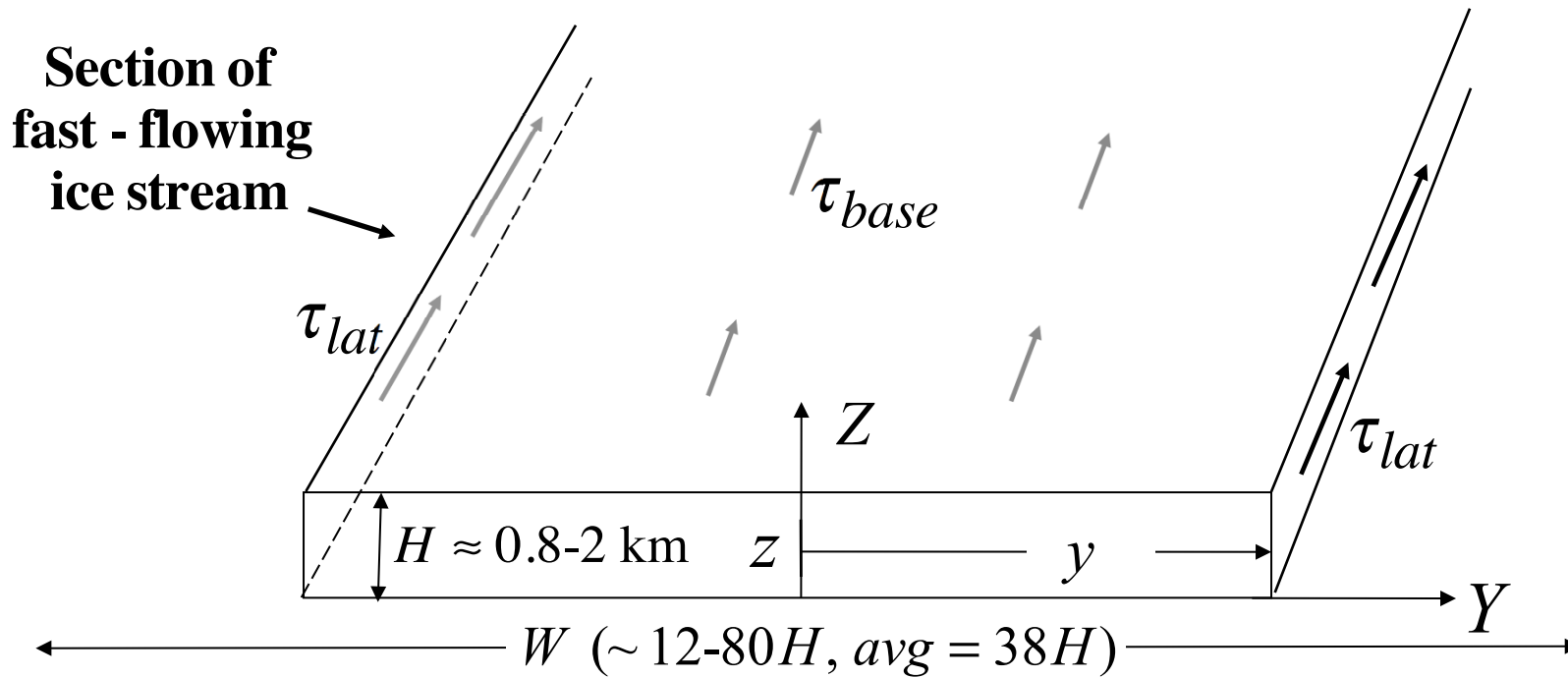
Table A.1: Ice sheet thickness H and shear strain rates $\dot{\gamma}_{lat}$ at the margins of the profiles located in Figure A.1 (Joughin et al., 2002). Temperate ice height fraction H'/H and lateral shear stress $\bar{\tau}_{lat}$ are predicted by our one-dimensional thermal model. Profiles beginning with the letter T are made at the tributaries of the ice streams.

(Perol & Rice, in prep., 2015)

Ice Stream	Profile	H (m)	$\dot{\gamma}_{lat}$ ($10^{-2} \cdot \text{yr}^{-1}$)	H'/H	$\bar{\tau}_{lat}$ (kPa)
Mercer	A	1242	4.2	9	112.3
Whillans	WB1	1205	7.0	39	113.4
	WB2	985	9.5	39	124.2
	W Narrows	846	13.5	45	135.0
	W Plain	735	5.1	0	97.0
	TWB1	2188	3.8	50	89.0
	TWB2	1538	4.0	26	101.6
Kamb	C	1805	1.0	0	50.6
	TC1	1802	1.4	0	64.5
	TC2	2196	0.9	0	51.5
Bindschadler	D	888	5.8	0	125.1
	TD1	1952	2.5	16	94.1
	TD2	1412	5.4	37	105.5
	TD3	1126	2.2	0	67.4
MacAyeal	E	916	8.1	26	126.1
	TE	1177	5.5	23	113.7

(Perol
& Rice,
in prep.,
2015)





$$\tau_{grav} = \rho g H S \quad (S = \text{slope})$$

✗ = downslope gravity force per unit base area

$$\text{Equilibrium*}: H \frac{d\bar{\tau}_{lat}}{dy} = \tau_{grav} - \tau_{base}$$

$$\frac{d\bar{\tau}_{lat}}{dy} = \left(\frac{d\bar{\tau}_{lat}}{d\dot{\gamma}} \right) / \left(\frac{d\dot{\gamma}}{dy} \right)$$

$$\frac{d\bar{\tau}_{lat}}{d\dot{\gamma}} < 0 \text{ when } \frac{d\dot{\gamma}}{dy} > 0 \Rightarrow \tau_{base} > \tau_{grav}$$

(normally, $\tau_{base} < \tau_{grav}$)

Suggests enhanced basal resistance near the margin.

Could that be related to why the margin forms?

*neglecting any variation in net axial force in sheet, roughly justified [Whillans and van derVeen, *J. Glac.*, 1993]

2D, antiplane strain analysis : velocity = $u(y,z)\vec{e}_x$, $\dot{\gamma} = \sqrt{\vec{\nabla}u \cdot \vec{\nabla}u}$

Coupled non - linear Poisson equation system

(for velocity u and temperature T) :

$$\frac{\partial}{\partial y} \left(\frac{\tau(\dot{\gamma}, T)}{\dot{\gamma}} \frac{\partial u}{\partial y} \right) + \frac{\partial}{\partial z} \left(\frac{\tau(\dot{\gamma}, T)}{\dot{\gamma}} \frac{\partial u}{\partial z} \right) = -\rho g S \quad \dot{\gamma} = \max \left(2A(T)\tau^3, \tau / \eta(T) \right)$$

$$\frac{\partial}{\partial y} \left(K(T) \frac{\partial T}{\partial y} \right) + \frac{\partial}{\partial z} \left(K(T) \frac{\partial T}{\partial z} \right) = -[1 - \hat{H}(T - T_{melt})] \tau(\dot{\gamma}, T) \dot{\gamma} + \rho C(T) \left(v \frac{\partial T}{\partial y} + w \frac{\partial T}{\partial z} \right)$$

(here, v & w are regarded as given, e.g., Zotikov's $w = -az / H$, $v = \text{const.}, v_0$)

Computational Approach (Suckale, Platt, Perol, Rice [JGR, 2014]) :

- **Multigrid methodology** for iterative solution of coupled nonlinear Poisson systems, embedding constraint $T \leq T_{melt}$.

(Suckale, Platt, Perol, and Rice, JGR 2014)

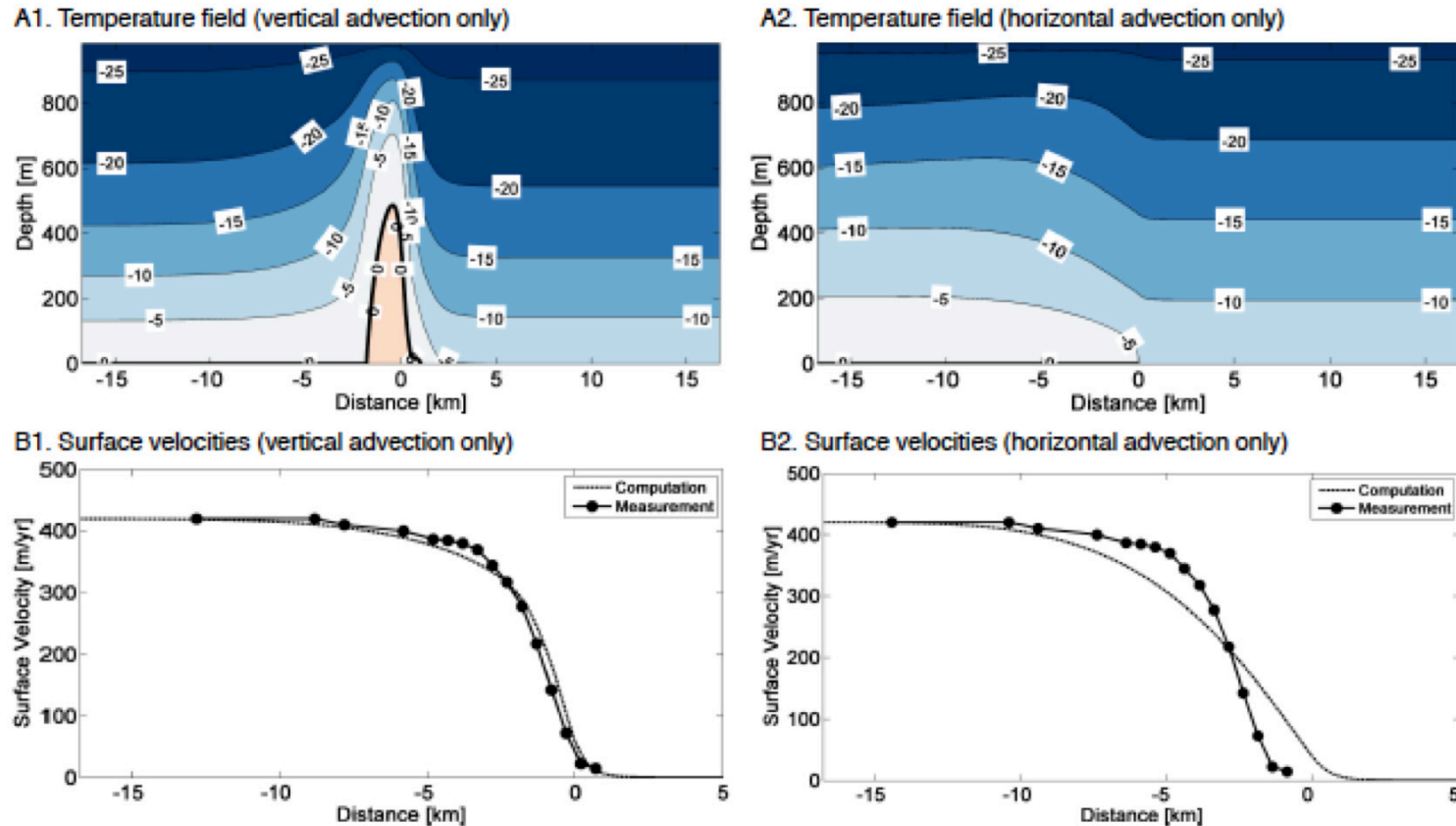
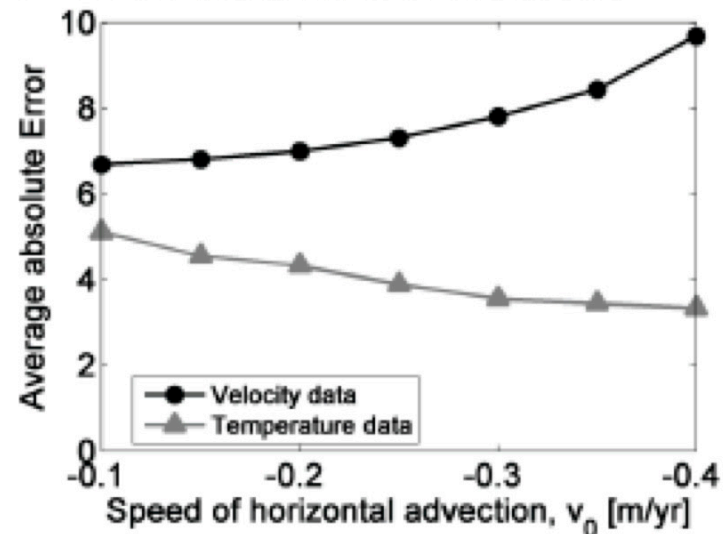


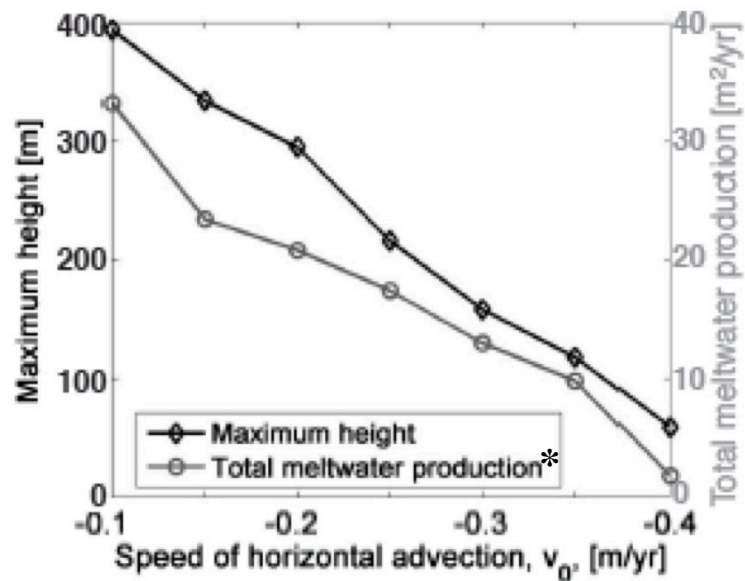
Figure 8. Temperature fields and surface velocities for Dragon margin when including only vertical advection (A1 and B1) with $a = 0.1$ m/yr and only horizontal advection (A2 and B2) with $v = -7.3$ m/yr, respectively. The best fitting basal stresses are $\tau_{base} = 5.31$ kPa (A1 and B1) and $\tau_{base} = 0.94$ kPa (A2 and B2), respectively. Both computations neglect surface crevassing.

(Suckale, Platt, Perol, and Rice, JGR 2014)

A. Error in reproducing observational data

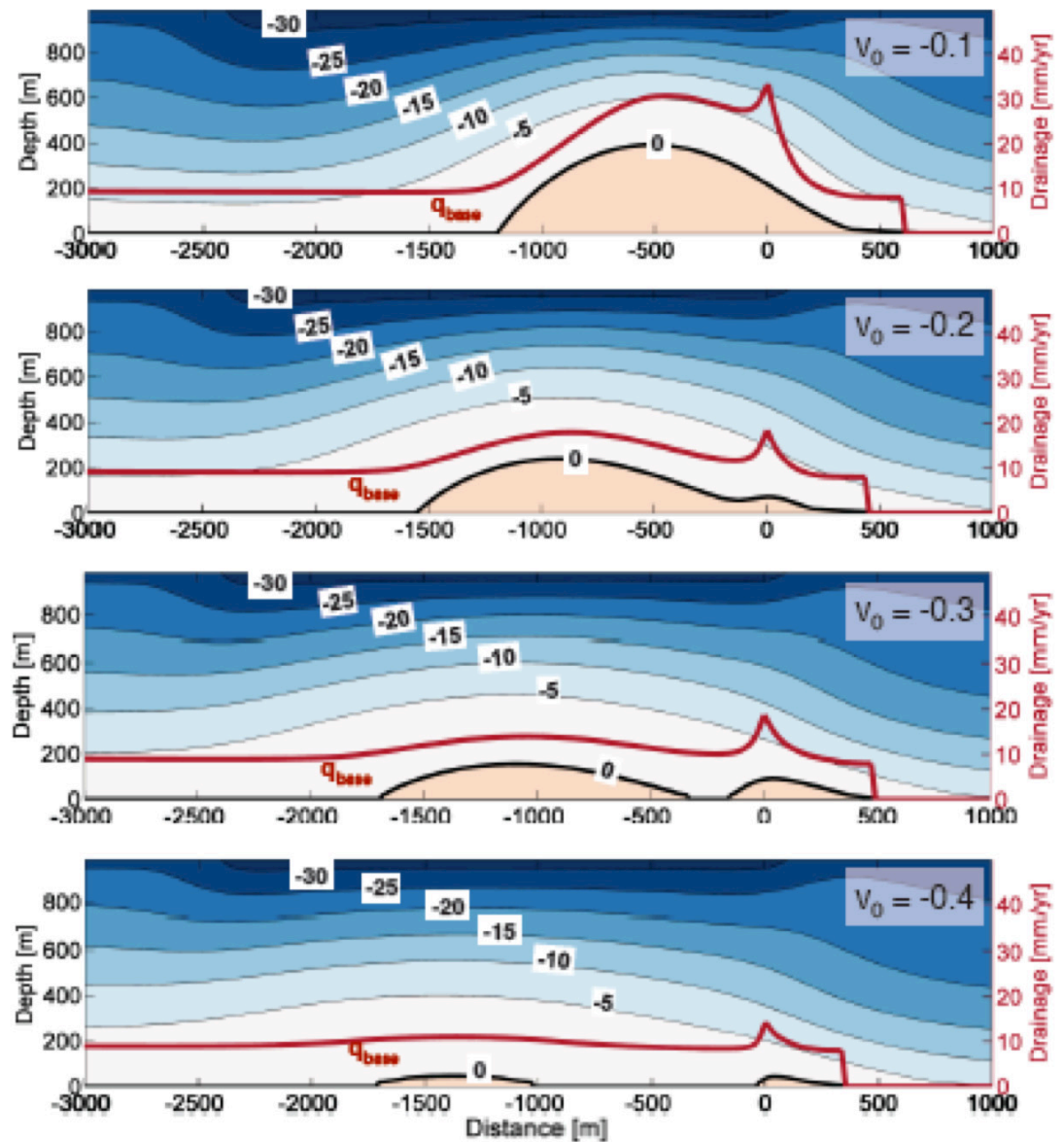


B. Properties of the temperate zones



* In the temperate ice only; does not include q_{base} from melt generation at the slipping interface.

C. Temperature and drainage for specific speeds of horizontal advection



Mass rate of melt production per unit volume in temperate zone:

$$\dot{m} = \frac{\tau \dot{\gamma}}{L}, \quad \tau = \left(\frac{\dot{\gamma}}{2A_{melt}} \right)^{1/3} F(n) \quad (\text{where } F(n) \leq 1), \quad \dot{m} = \frac{\dot{\gamma}^{4/3} F(n)}{(2A_{melt})^{1/3} L}$$

↖ Latent heat per unit mass
 ↑ Porosity
 ↖ Strength reduction due to porosity (not yet quantified)

Seepage flux of melt water:

$$\vec{\nabla} \cdot (\rho_w \vec{q}) = \dot{m} \quad \Rightarrow \quad \frac{dq_z}{dz} = \frac{\dot{m}}{\rho_w} = \frac{\dot{\gamma}^{4/3} F(n)}{(2A_{melt})^{1/3} L \rho_w} \quad [\text{assumes } \vec{q} = (0, 0, q_z)]$$

Assuming $n \ll 1$, so that $F(n) \approx 1$, and that

$\dot{\gamma}$ is approximately uniform in z (like in the 1D model),

$$q_z \Big|_{z=0} \approx - \dot{\gamma}^{4/3} H' / [(2A_{melt})^{1/3} L \rho_w],$$

where H' is the height of the temperate interval at the location considered.

Water permeation through the partially melted ice:

J. F. Nye and F. C. Frank,
 [J. Glac., 1973], building on
 Frank's [Nat., 1968]
 analysis of melt convection
 in Earth's mantle:

Permeability

$$k = \alpha n^2 d_g^2$$

n = porosity,

d_g = grain size (1-10 mm),

$\alpha \approx 1/2000$ to $1/1500$

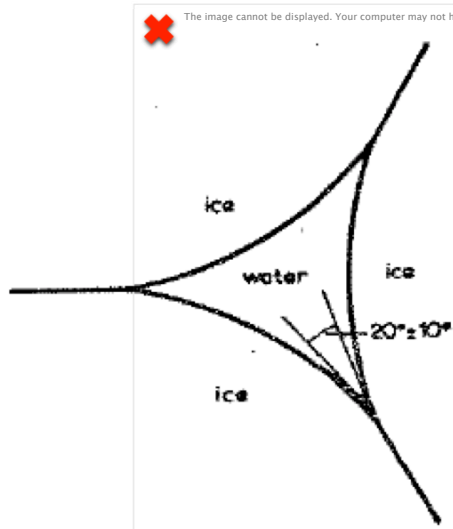


Fig. 2. Cross-section of a vein of liquid situated at a grain edge, where three grain boundaries meet. The figure is drawn for a dihedral angle φ equal to 20° , as measured for ice—water by Ketcham and Hobbs (1969).

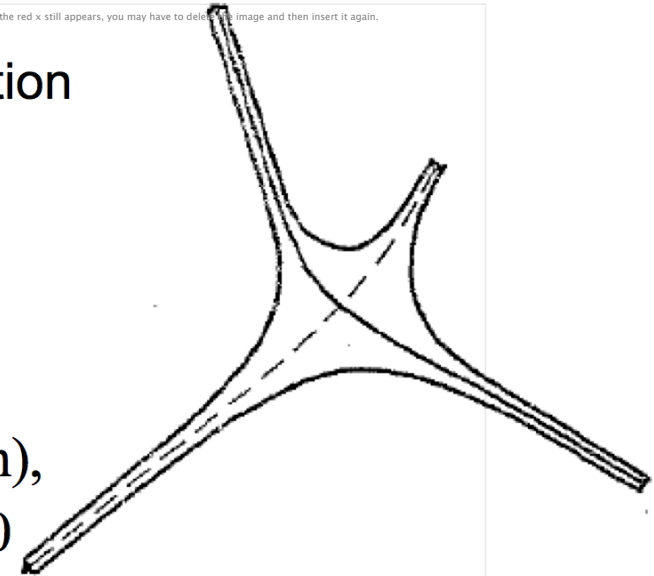


Fig. 3. A junction between four water veins in polycrystalline ice. The figure is a tetrahedron with non-spherical faces and with open corners.

For $Q_w = 100 \text{ km} \times 41 \text{ m}^3 / \text{m} \cdot \text{yr}$, and $S = 0.0012$:

Clarke sub-glacial flooding range

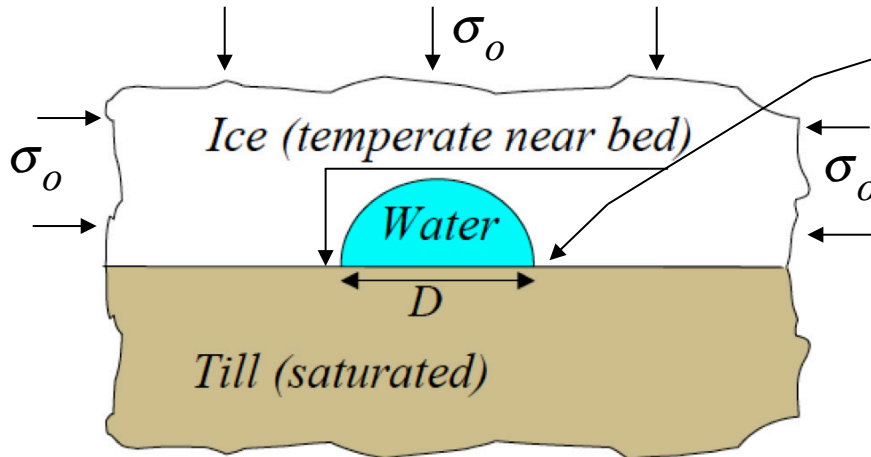
Rothlisberger-Shreve channel analysis

$$\sigma_{hoop} - p_{ch} = \frac{2}{3}(\sigma_o - p_{ch})$$

Manning Coefficient, n_M (s / m ^{1/3})	0.01	0.02	0.03	0.04
Equivalent Nikuradse Roughness, k (cm)	0.03	1.6	18.0	101.1
Channel Diameter, D (m)	0.9	1.1	1.3	1.5
Effective Normal Stress at Channel Margin, $\sigma_{hoop} - p_{ch}$ (kPa)	369	310	280	261

Assumed plausible here

Sensitivity : $Q_w \rightarrow 0.25Q_w \Rightarrow D \rightarrow 0.59D$, $(\sigma_{hoop} - p_{ch}) \rightarrow 0.89(\sigma_{hoop} - p_{ch})$



Strength $\tau_{ch} = f(\sigma_{hoop} - p_{ch})$

$\approx 0.5(\sigma_{hoop} - p_{ch}) \approx 150 \text{ kPa}$

$\therefore \tau_{ch} / \tau_{base} \approx 20 \text{ to } 45$

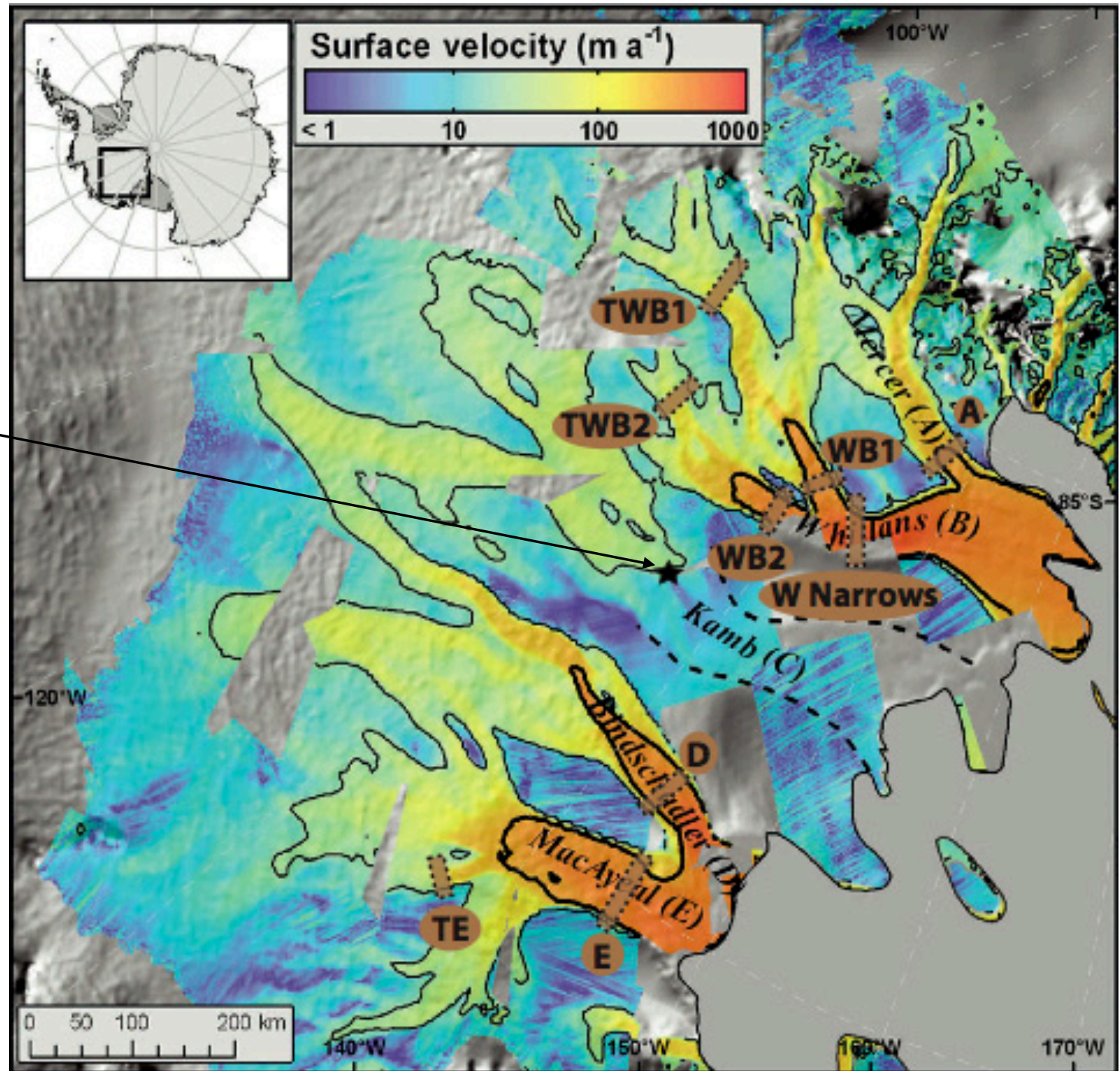
For the 6 major streams, τ_{ch} / τ_{base} average = 32, and range = 12 to 56.

So, a marginal drainage channel could be the source of enhanced basal resistance!

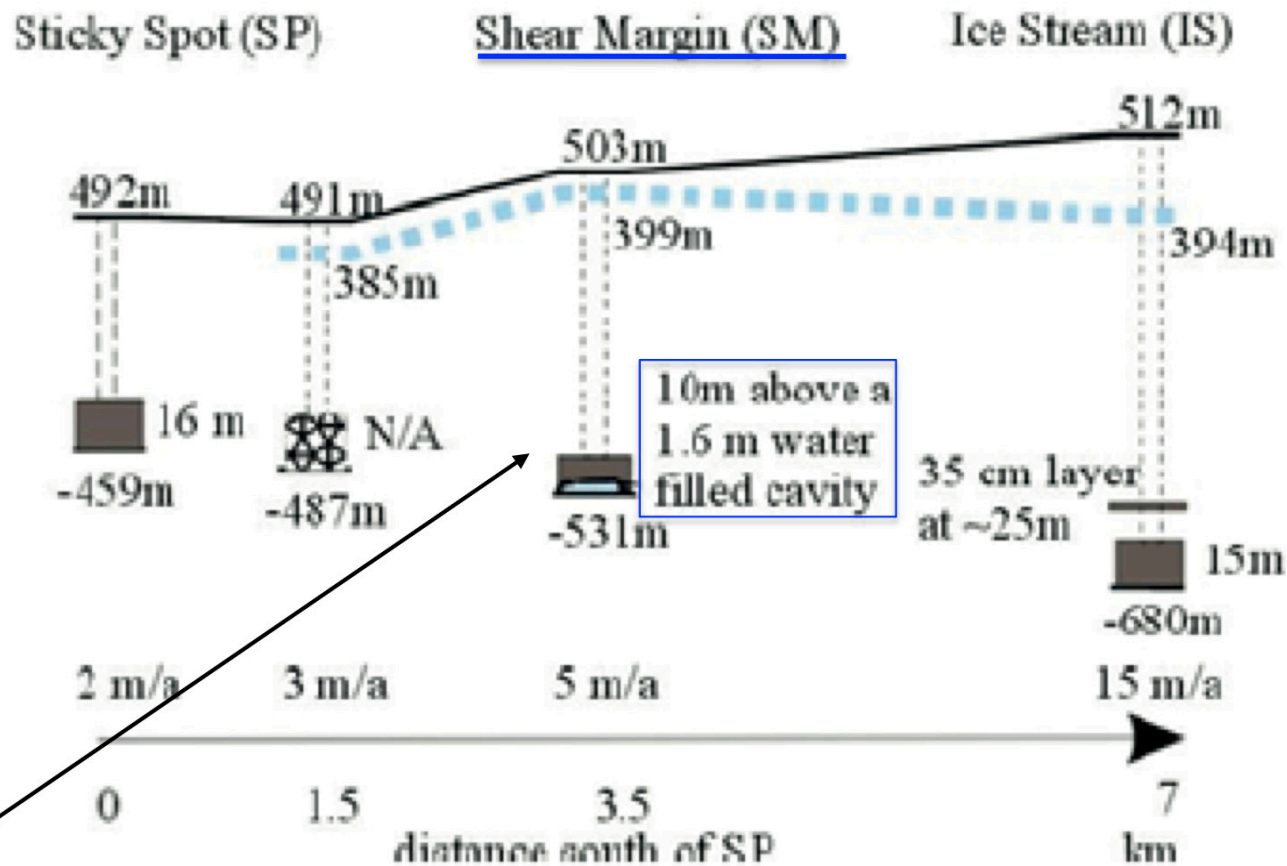
Field evidence, possible temperate ice and melt channels at margins

Borehole drilled into a dying shear margin of **Kamb (C)** ice stream

[Vogel (*PhD Thesis*, Caltech, 2004) and Vogel et al. (*Geophys Res Lett*, 2005)]



Evidence of channel at margins

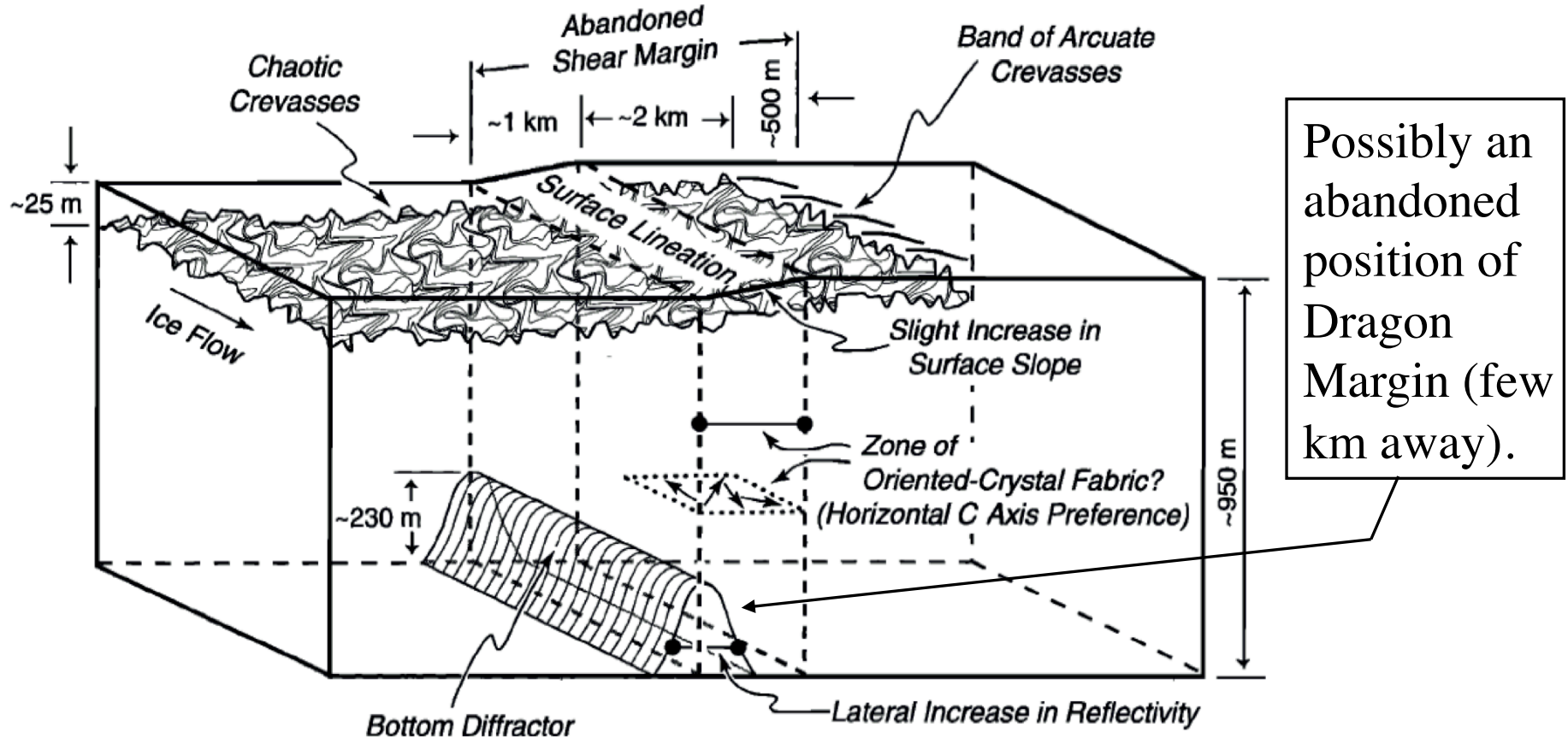


Borehole observation at the presently inactive shear margin of *Kamb* (C) ice stream:

- Found a 1.6 m tall water-filled cavity between 10 m of accreted ice and bed.
- Video of the borehole shows horizontal acceleration of particles sinking into the cavity, indicating flow of water within the cavity -- part of a channel?

[Modified from Vogel PhD (Thesis, 2004) and Vogel et al. (GRL, 2005).]

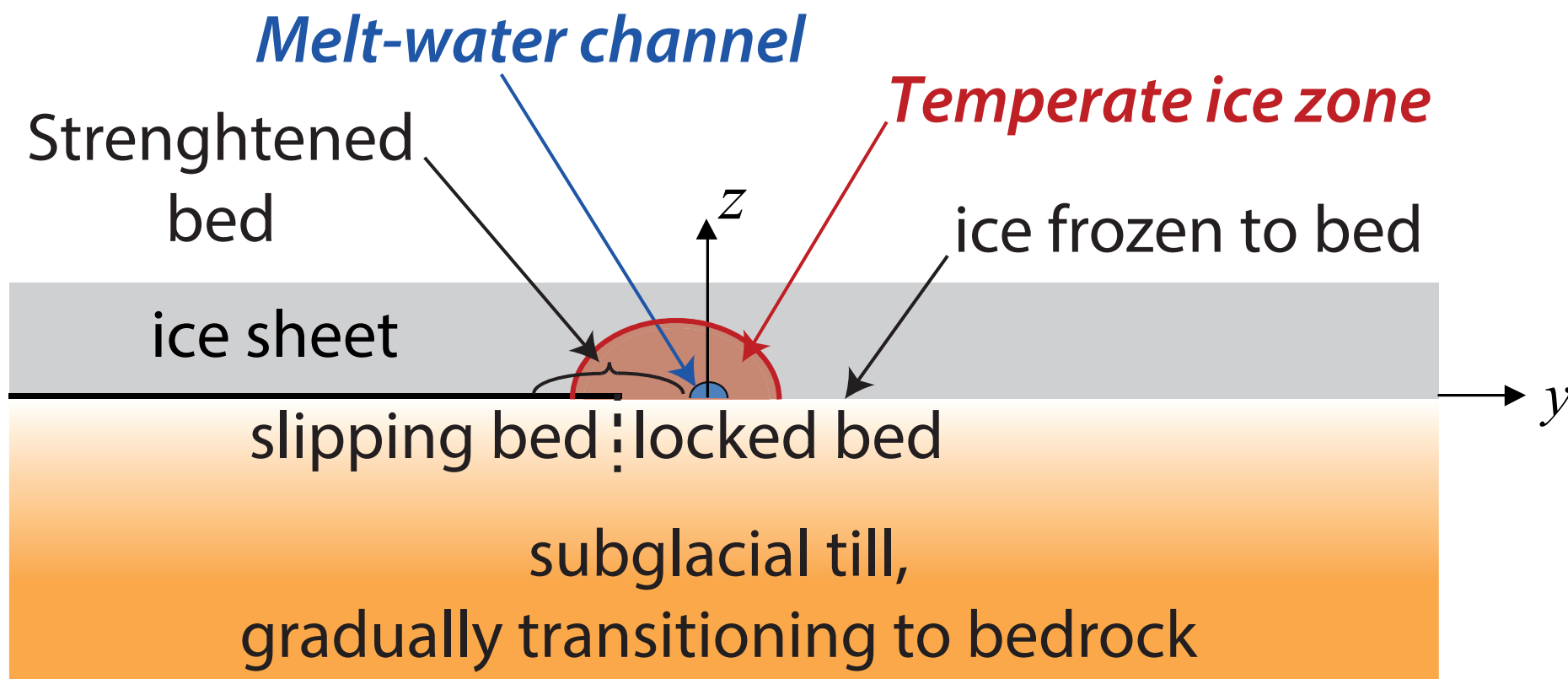
Possible field evidence of internal melting at margins



- Clarke et al. [2000], in order to explain the bottom diffractors, have invoked **partial melting in temperate ice to a height of 230 m**, due to strain heating, among other possibilities (**entrained sediments, bottom crevasses**).
- Also, Clarke et al. noted a personal communication from H. Engelhardt (Caltech): Abnormal drill resistance encountered from ≈ 56 m above bed. Fresh scratches found on drill tip (assumed to due to **entrained sediments**).

(Perol, Rice, Platt and Suckale, AGU Dec. 2014)

How subglacial hydrology can control the shear margin location of ice streams



Governing equations, mechanical-thermal-hydrologic model of ice stream

- **Mechanical model of an anti-plane shear flow driven by gravity**

$$\frac{\partial}{\partial y} \left(\frac{\tau(\dot{\gamma}, T)}{\dot{\gamma}} \frac{\partial u}{\partial y} \right) + \frac{\partial}{\partial z} \left(\frac{\tau(\dot{\gamma}, T)}{\dot{\gamma}} \frac{\partial u}{\partial z} \right) + \rho_{ice} g S = 0, \quad \tau(\dot{\gamma}, T) = \min \left[\left(\frac{\dot{\gamma}}{2A(T)} \right)^{1/3}, \eta(T) \dot{\gamma} \right]$$

- **Thermal model**

$$\frac{\partial}{\partial y} \left(K \frac{\partial T}{\partial y} \right) + \frac{\partial}{\partial z} \left(K \frac{\partial T}{\partial z} \right) - \rho_{ice} C_{ice} \left(v \frac{\partial T}{\partial y} + w \frac{\partial T}{\partial z} \right) + [1 - H(T - T_{melt})] \tau \dot{\gamma} = 0$$

(we take $v = 0$ (lateral advection neglected), and $w = -az / H$ (Zotikov))

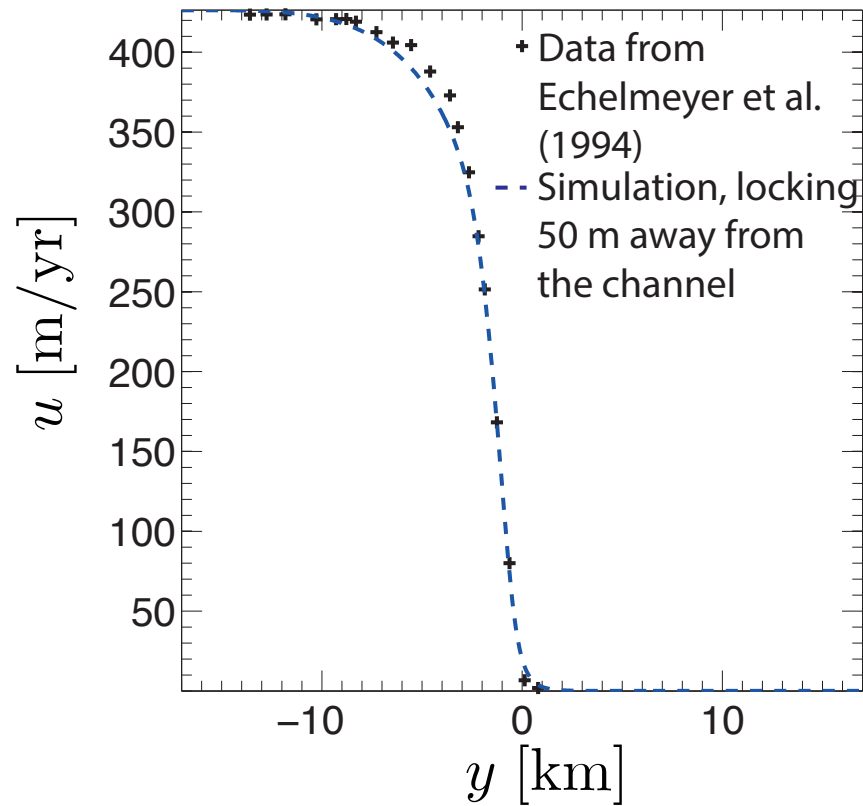
- **Subglacial hydrology model (Poiseuille flow in a thin water film)**

$$q_{melt} \equiv \frac{G_{geo} - G_{ice} + \tau_{base} u_b}{\rho_w L} = -\frac{\partial}{\partial y} \left(\frac{h^3}{12\mu_w} \frac{\partial p}{\partial y} \right) \quad (\text{we take thickness } h = \text{const.})$$

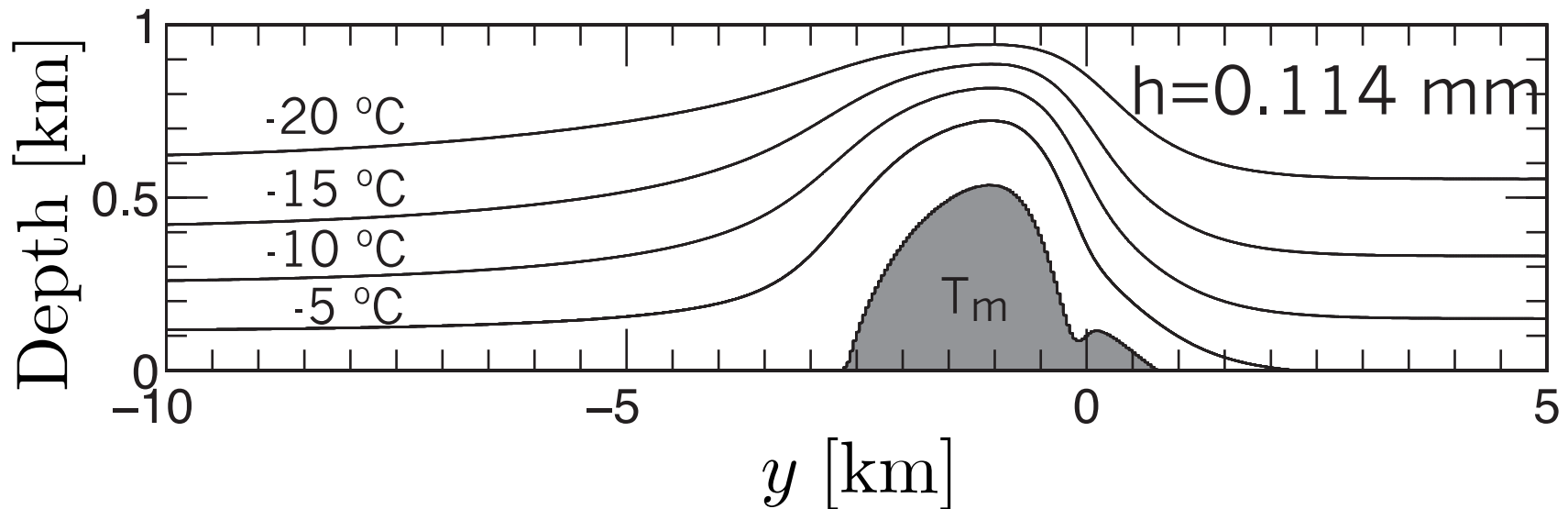
($\tau_{base} = (\tau_{zx})_{z=0} = f \times (\rho_{ice} g H - p) + c = \text{basal strength}$, $u_b = u_{z=0} = \text{basal sliding velocity}$)

System solved using Finite Element procedure in COMSOL

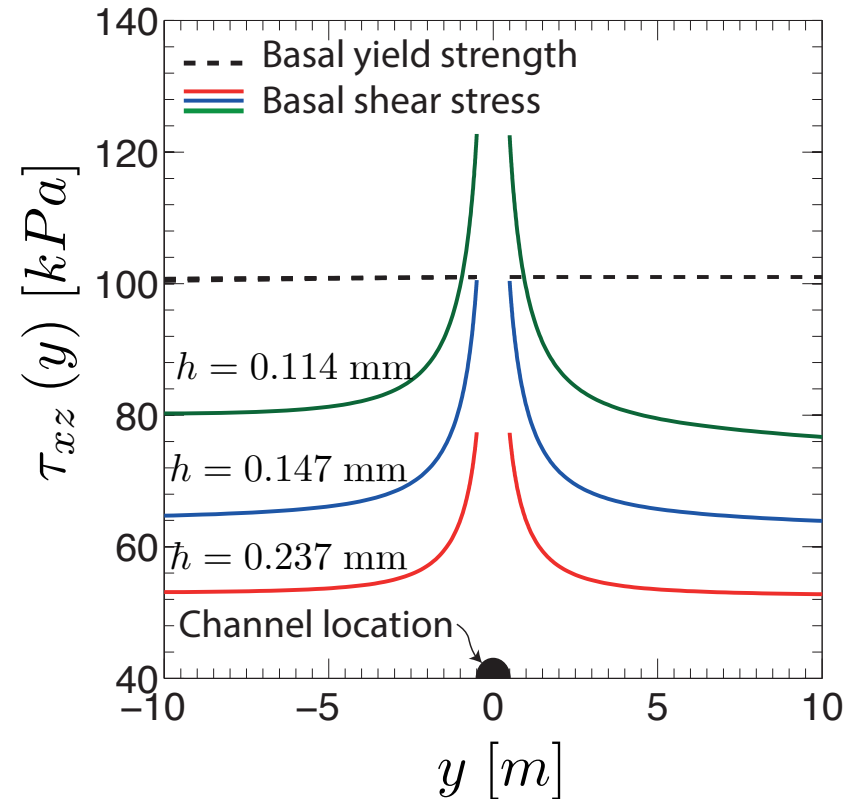
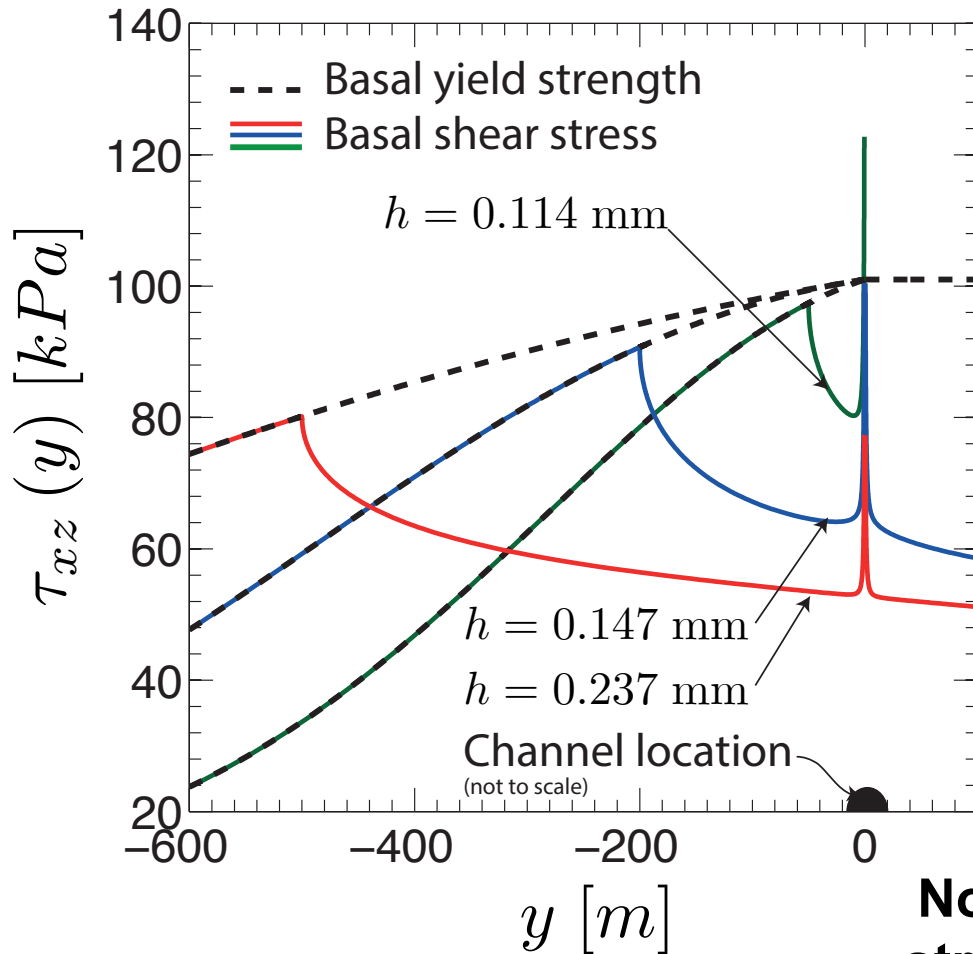
(Perol, Rice, Platt and Suckale, AGU Dec. 2014)



The COMSOL simulations so far done have neglected horizontal advection, expected to diminish the size of the temperate zone, and hence water supply to a subglacial channel, hence reducing the near-channel basal strength elevation.

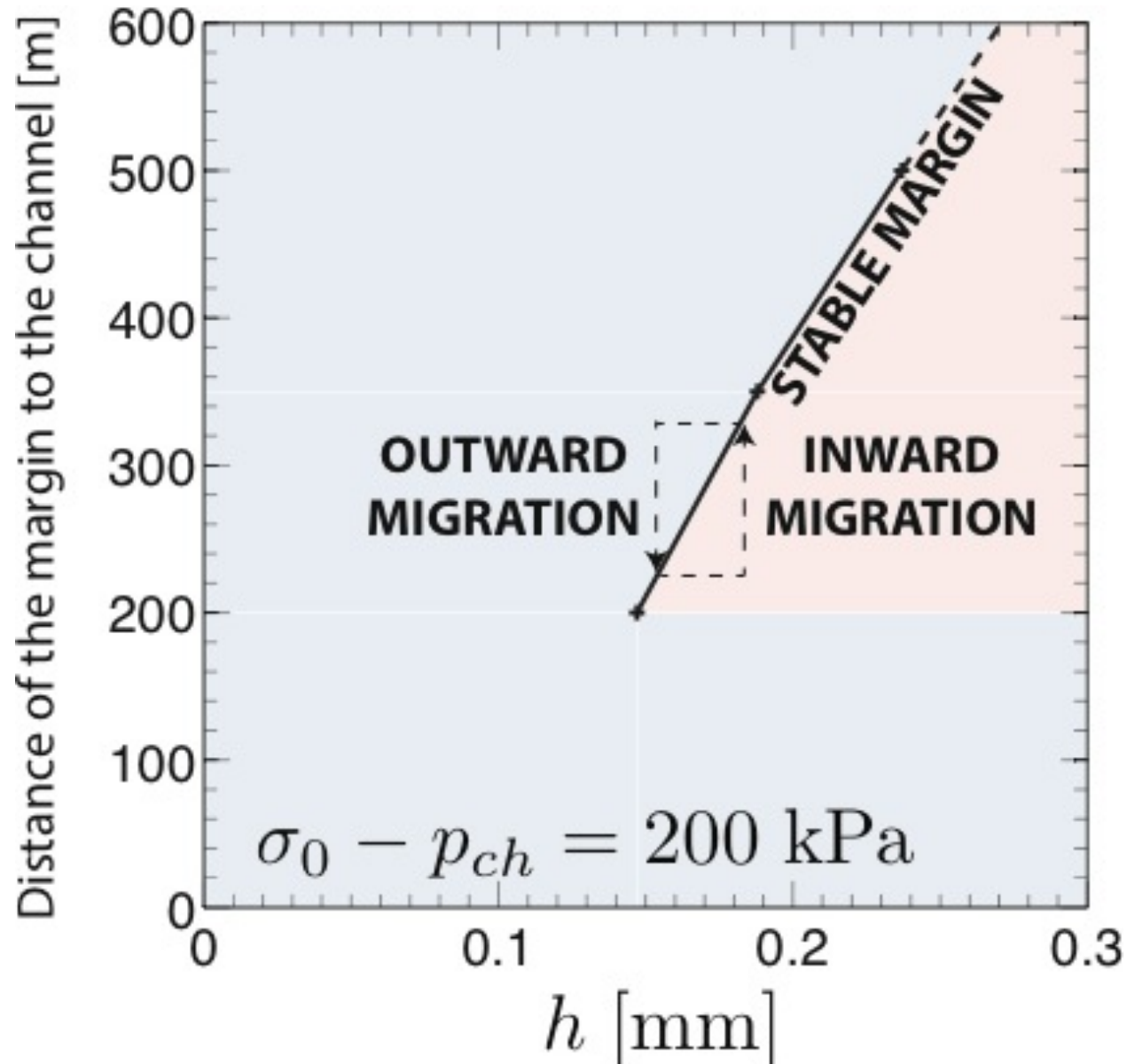


How subglacial hydrology can select the location of the margin



Note that the basal shear stress, and strength, near the channel is far larger than the inferred average $\tau_{base} \approx 4$ kPa.

Stability diagram, ice stream margin controlled by a channelized drainage



Conclusions, West Antarctic Ice Stream Margins

- The transition from a slipping to a locked bed concentrates stress beneath the ridge.
- Our model (**without lateral advection**) predicts that shear heating at the margin leads to temperate ice and melting for almost all ice streams. This melt may lead to channel formation beneath ice stream margins.
- Such a channel limits the maximum stress on the locked bed and increases the strength of the ice-bed interface, providing a mechanism that may facilitate locking.
- The maximum stress on the locked portion of the bed decreases with increasing channel radius.
- Glen's law leads to a substantially lower maximum stress than a Newtonian rheology.
- We have **not proven** that the mechanisms outlined could stabilize a shear margin, and we **have no simple way at present of more fully evaluating the important effects of lateral thermal advection.**

Concepts of fluid and solid mechanics, integrated with materials and thermal sciences, provide a valuable framework for addressing large-scale natural phenomena.

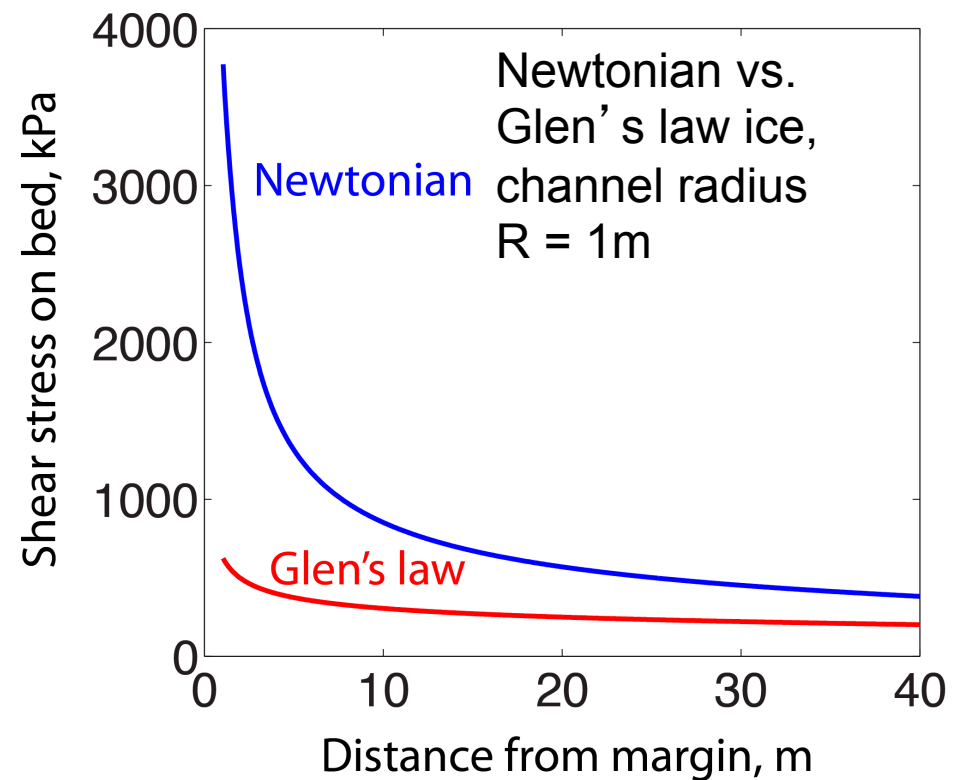
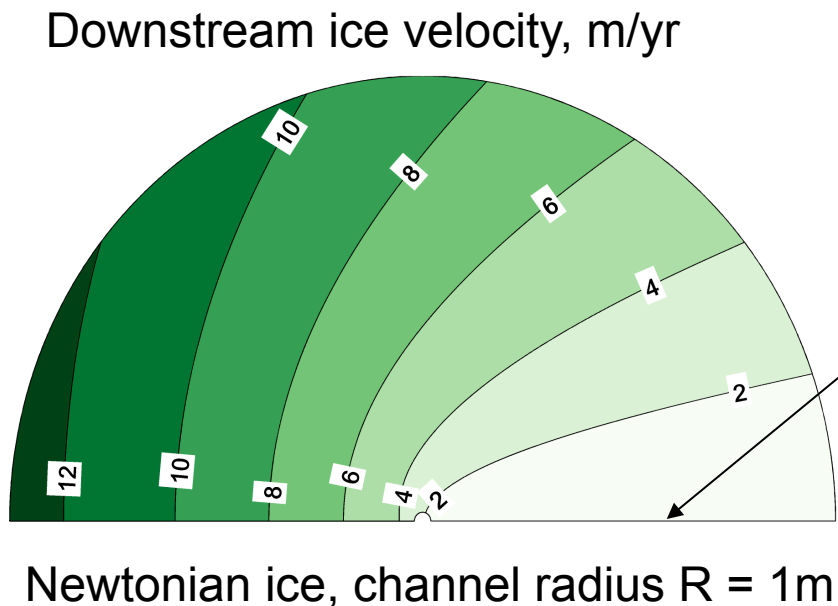
We considered their applications to

Ice sheet flow and subglacial hydrology:

- Large iceberg calving as the enigmatic source of glacial earthquakes.
- Rapid glacial underflooding events as natural hydraulic fractures, like in a well-characterized spontaneous lake drainage on the Greenland Ice Sheet.
- Partial internal melting from shear heating as a control on flow resistance at the margins of rapidly flowing ice streams as on the Western Antarctic Ice Sheet.

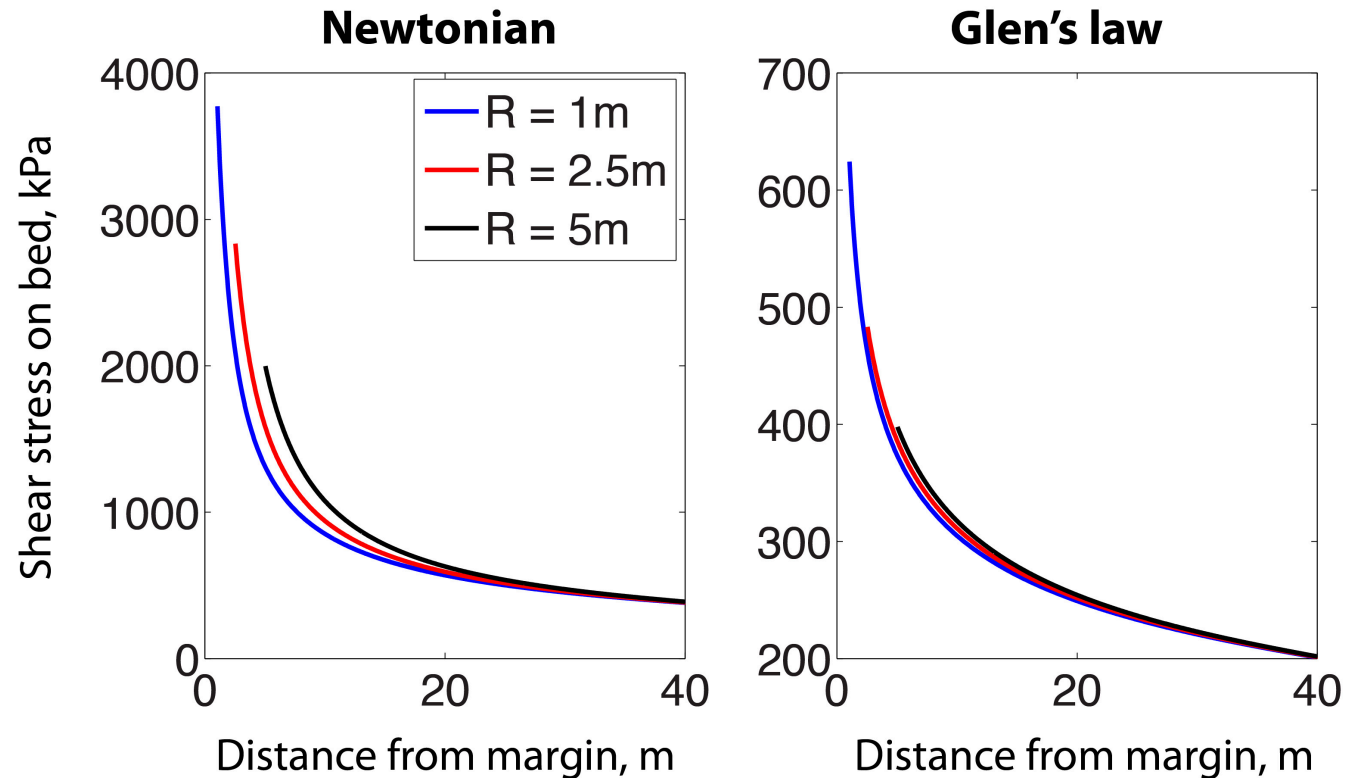
Flow of ice around a channel

- A finite radius of curvature at a crack tip blunts the stress concentration.
- Motivated by this we consider a slipping to locked transition that occurs across a channel.



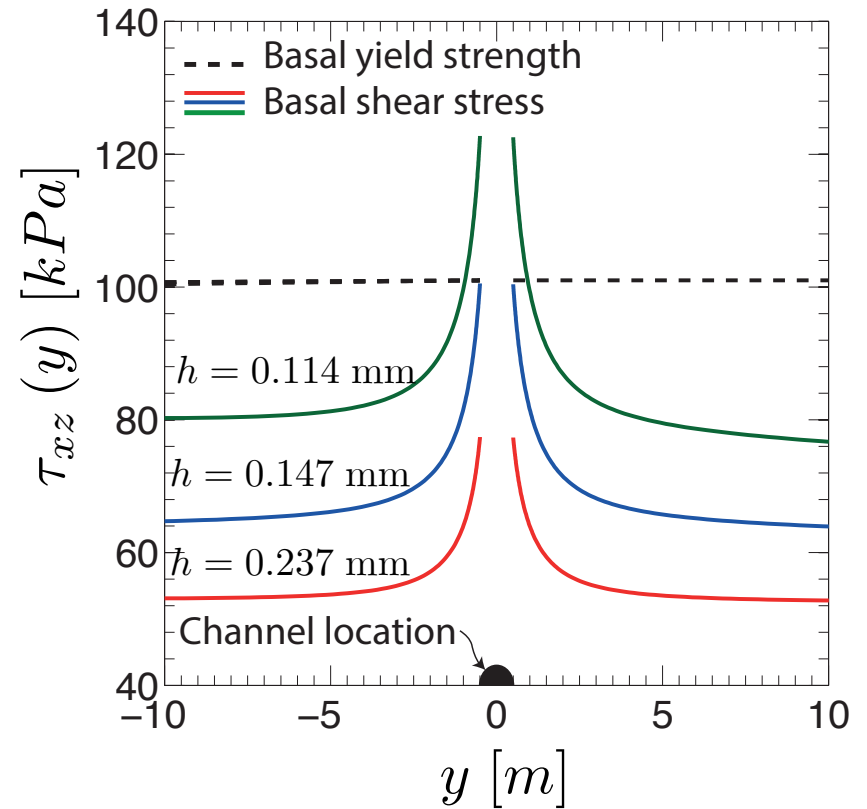
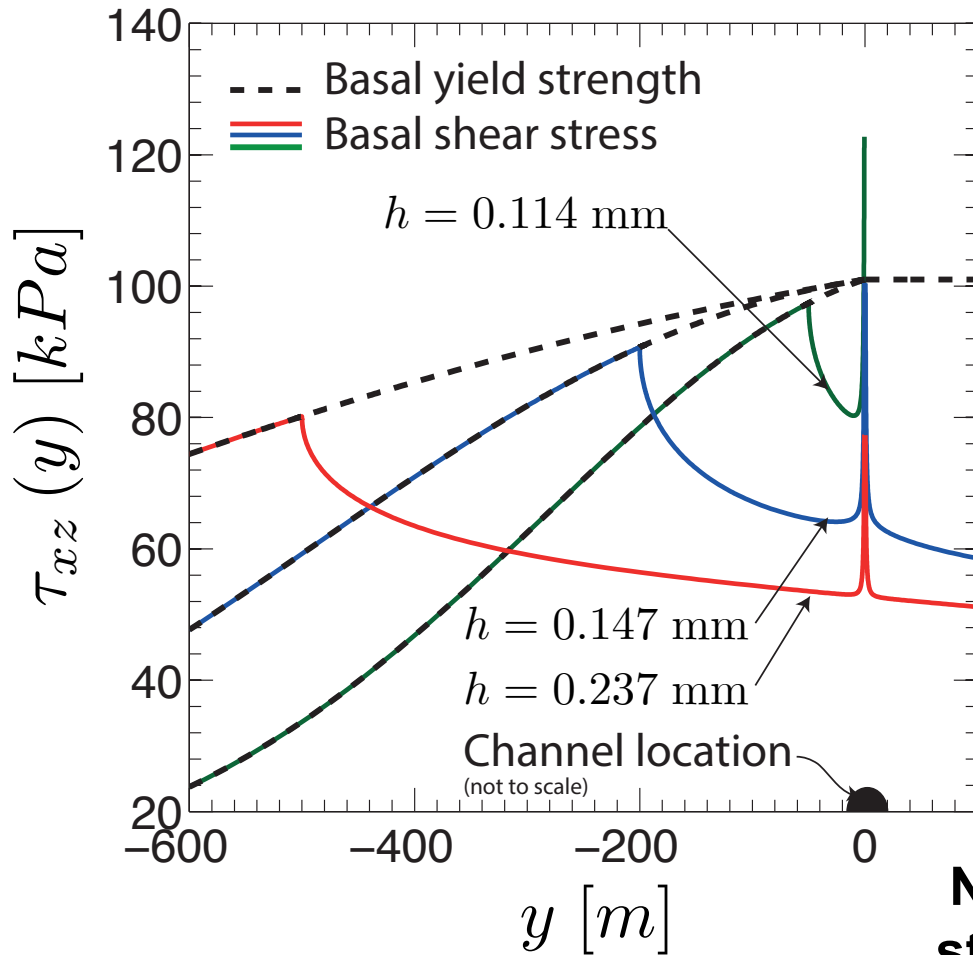
Influence of channel size

- The channel size also influences the maximum stress on the bed.

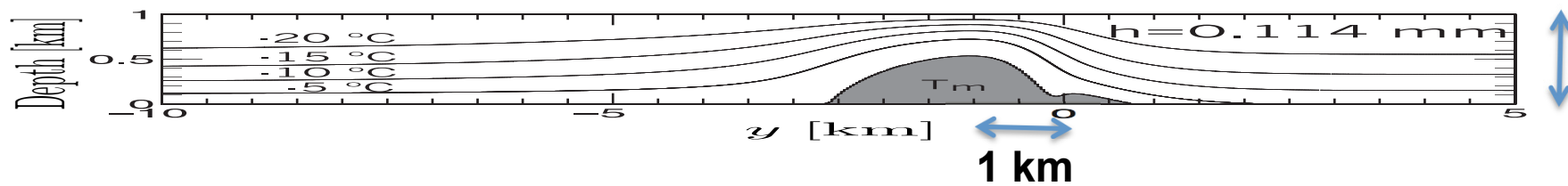
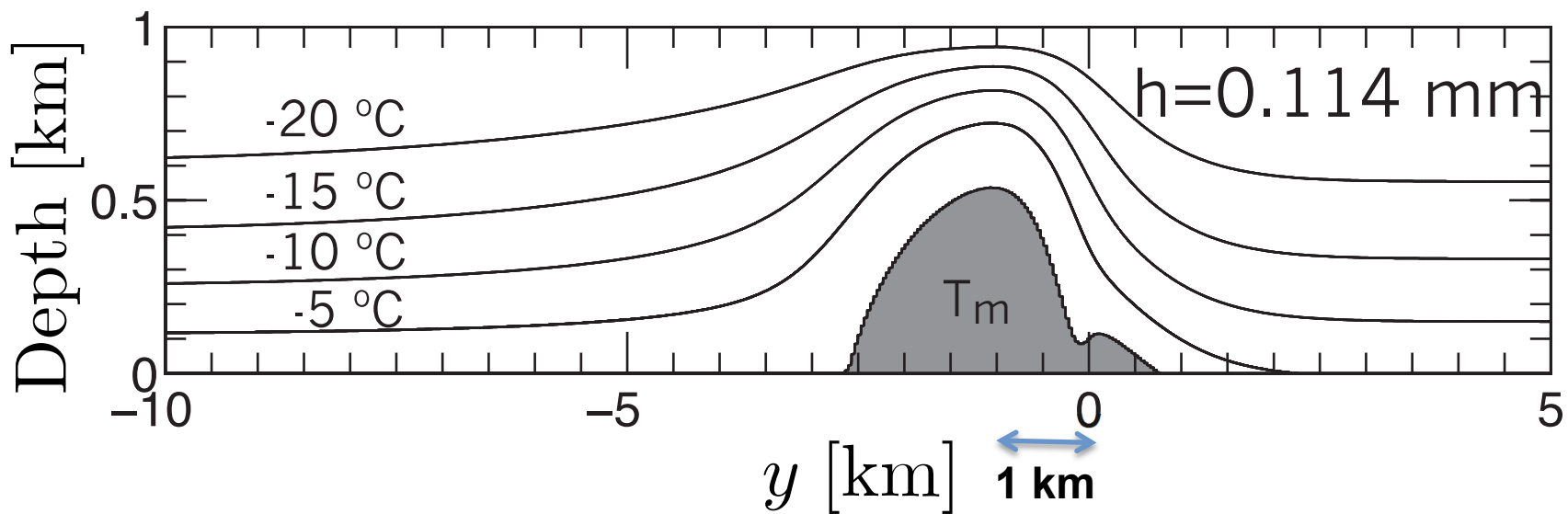


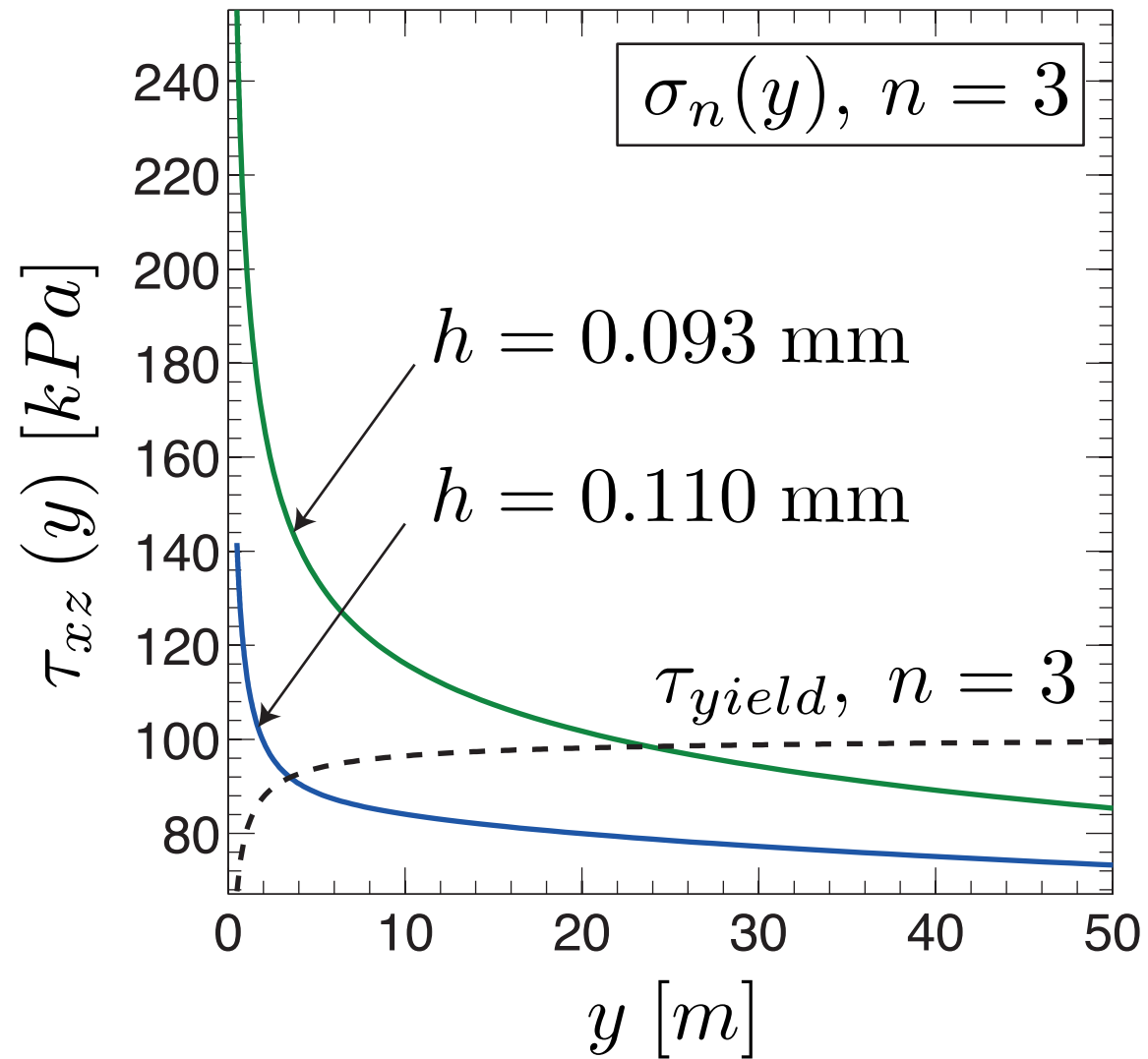
- A larger channel size leads to a lower maximum stress on the bed and a larger strength of the ice-bed interface.
- Even if the the stress is larger than the strength the channel may still facilitate locking through a cohesive zone (Dugdale [1960]; Barenblatt [1962]; Schoof [2012]).

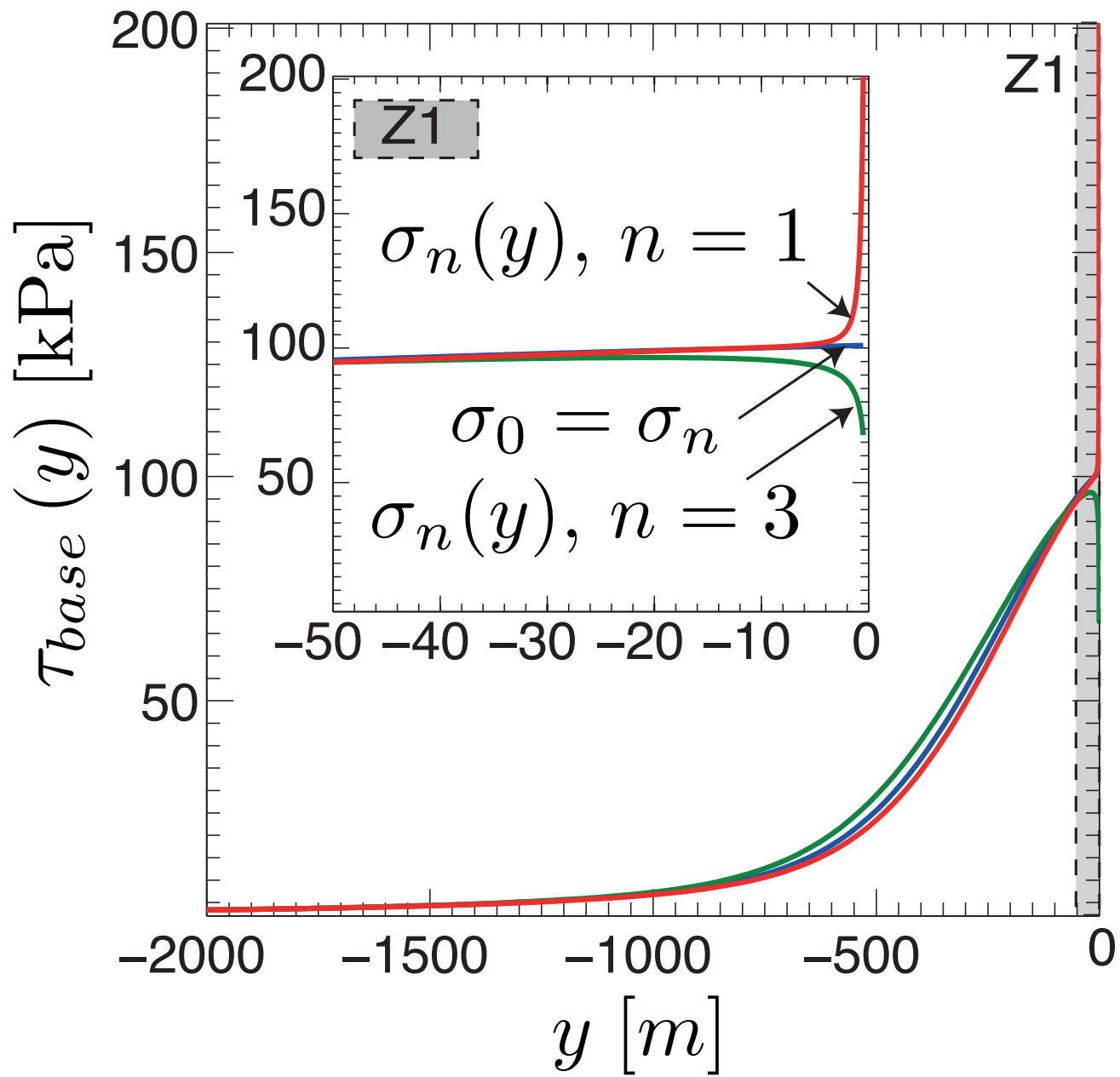
How subglacial hydrology can select the location of the margin



Note that the basal shear stress, and strength, near the channel is far larger than the average $\tau_{base} \approx 4$ kPa.







Mass rate of melt production per unit volume in temperate zone:

$$\dot{m} = \frac{\tau \dot{\gamma}}{L}, \quad \tau = \left(\frac{\dot{\gamma}}{2A_{melt}} \right)^{1/3} F(n) \quad (\text{where } F(n) \leq 1), \quad \dot{m} = \frac{\dot{\gamma}^{4/3} F(n)}{(2A_{melt})^{1/3} L}$$

Latent heat per unit mass Porosity Strength reduction due to porosity (not yet quantified)

Darcy seepage flux of melt water:

$$\vec{\nabla} \cdot (\rho_w \vec{q}) = \dot{m} \quad \Rightarrow \quad \frac{dq_z}{dz} = \frac{\dot{m}}{\rho_w} = \frac{\dot{\gamma}^{4/3} F(n)}{(2A_{melt})^{1/3} L \rho_w} \quad [\text{assumes } \vec{q} = (0, 0, q_z)]$$

Assuming $F(n) \approx 1$ because $n \ll 1$, and that $\dot{\gamma}$ is approximately uniform in z (like in the 1D model)

$$q_z \approx - \dot{\gamma}^{4/3} (H' - z) / [(2A_{melt})^{1/3} L \rho_w],$$

where H' is the height of the temperate interval at the location considered.

Water permeation through the partially melted ice:

J. F. Nye and F. C. Frank,
 [J. Glac., 1973], building on
 Frank's [Nat., 1968]
 analysis of melt convection
 in Earth's mantle:

Permeability

$$k = \alpha n^2 d_g^2$$

n = porosity,

d_g = grain size (1-10 mm),

$\alpha \approx 1/2000$ to $1/1500$

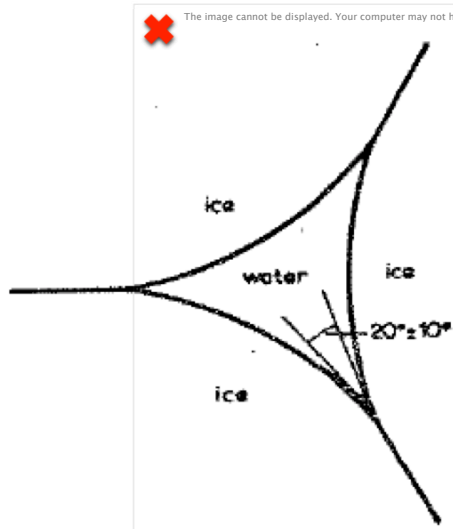


Fig. 2. Cross-section of a vein of liquid situated at a grain edge, where three grain boundaries meet. The figure is drawn for a dihedral angle φ equal to 20° , as measured for ice—water by Ketcham and Hobbs (1969).

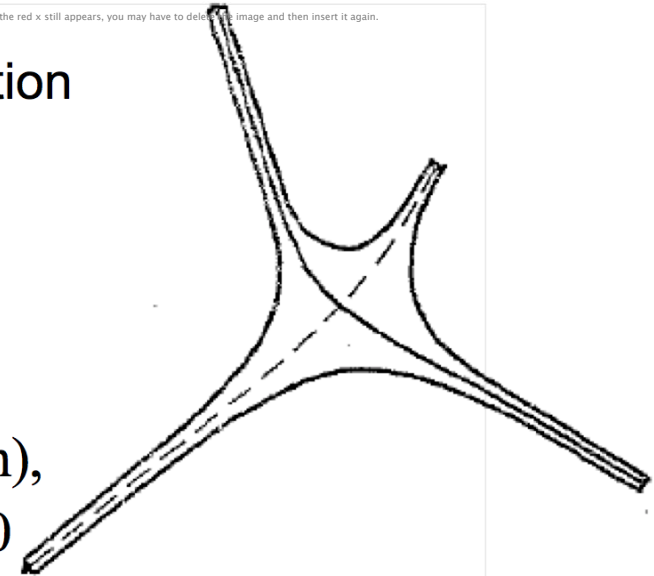


Fig. 3. A junction between four water veins in polycrystalline ice. The figure is a tetrahedron with non-spherical faces and with open corners.

Water permeation through the partially melted ice:

J. F. Nye and F. C. Frank,
 [J. Glac., 1973], building on
 Frank's [Nat., 1968]
 analysis of melt convection
 in Earth's mantle:

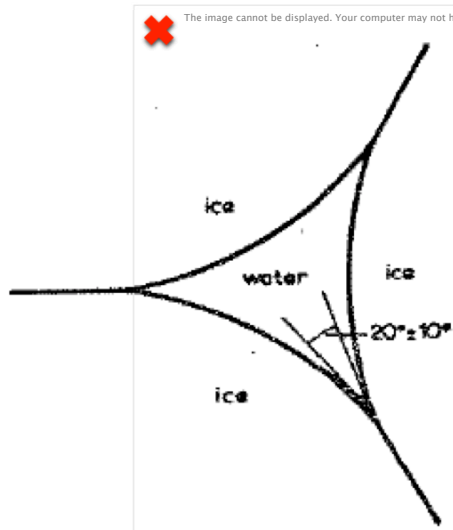


Fig. 2. Cross-section of a vein of liquid situated at a grain edge, where three grain boundaries meet. The figure is drawn for a dihedral angle φ equal to 20° , as measured for ice—water by Ketcham and Hobbs (1969).

$$k = \alpha n^2 d_g^2$$

$n =$ porosity,
 $d_g =$ grain size (1-10 mm),
 $\alpha \approx 1/2000$ to $1/1500$

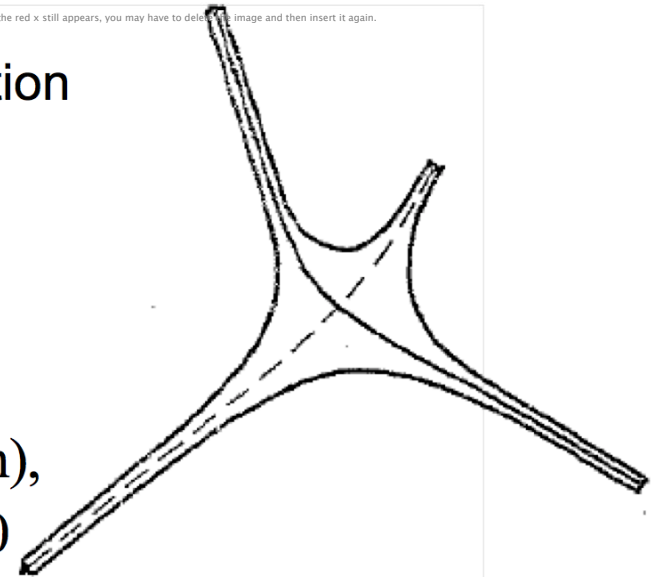


Fig. 3. A junction between four water veins in polycrystalline ice. The figure is a tetrahedron with non-spherical faces and with open corners.

$$q_z \approx - \frac{\langle \dot{\gamma}^{4/3} \rangle (H' - z)}{(2A_{melt})^{1/3} L \rho_w} = - \frac{k}{\mu_w} \left(\frac{dp}{dz} + \rho_w g \right) = - \frac{k}{\mu_w} (\rho_w - \rho_{ice}) g$$

if $p =$ ice overburden pressure $= \rho_{ice} g (H - z)$
 \Rightarrow porosity $n \leq 5 \times 10^{-4} \text{ mm} / d_g \leq 5 \times 10^{-4}$

Table 2. Ice streams and their tributaries gravitational driving stress as measured at profiles located in Figure 2 and calculated temperate ice height fraction, lateral stress, basal shear stress, and ratio of basal stress to driving stress, neglecting the gradient in net axial force. Profiles beginning with the letter T are made at the tributaries.

Ice Stream	Profile	τ_{grav}^a (kPa)	H'/H (%)	$\bar{\tau}_{lat}$ (kPa)	$\bar{\tau}_{base}$ (kPa)	$\bar{\tau}_{base}/\tau_{grav}$ (%)
Mercer	A	14.9	9	112.3	7.7	52
Whillans	WB1	12.5	39	113.4	5.0	38
	WB2	10.8	39	124.2	3.6	33
	W Narrows	7.6	45	135.0	2.8	37
	W Plain	3	0	97.0	1.8	61
	TWB1	47.5	50	89.0	32.0	67
	TWB2	40.9	26	101.6	28.4	69
Kamb	C	16.7	0	50.6	14.1	84
	TC1	40.1	0	64.5	26.4	66
	TC2	89.7	0	51.5	84.4	94
Bindschadler	D	10.0	0 ^c	125.1	6.0	60
	TD1	67.8	16	94.1	52.5	77
	TD2	29.0	37	105.5	20.5	71
	TD3	31.0	0	67.4	23.8	77
MacAyeal	E	15.3	26	126.1	12.3	81
	TE	44.9	23	113.7	30.9	69

^c The ratio increases to $\sim 53\%$ when evaluated 30 km downstream

